APPLICATIONS AND MECHANISMS OF INTRAVASCULAR DRAG REDUCING POLYMERS

by

Philip Justin Marascalco

B.S. in Biomedical Engineering, Wright State University, 2000

Submitted to the Graduate Faculty of

Swanson School of Engineering in partial fulfillment

of the requirements for the degree of

Doctor of Philosophy

University of Pittsburgh

2008

UNIVERSITY OF PITTSBURGH

SWANSON SCHOOL OF ENGINEERING

This dissertation was presented

by

Philip Justin Marascalco

It was defended on

April 10th, 2008

and approved by

James F. Antaki, Ph.D.
Professor, Departments of Biomedical Engineering & Computer Science, Carnegie Mellon University; Professor, Departments of Bioengineering & Surgery, University of Pittsburgh

Harry C. Blair, M.D.
Professor, Departments of Pathology & Cell Biology and Physiology

Harvey S. Borovetz, Ph.D.
Professor & Chair, Department of Bioengineering; Robert L. Hardesty Professor, Department of Surgery; Professor, Department of Chemical & Petroleum Engineering

Richard R. Koepsel, Ph.D.
Research Associate Professor, Department of Chemical Engineering

Dissertation Director: Marina V. Kameneva, Ph.D.
Research Professor, Departments of Bioengineering & Surgery

APPLICATIONS AND MECHANISMS OF INTRAVASCULAR DRAG REDUCING POLYMERS

Philip Justin Marascalco, Ph.D.

University of Pittsburgh, 2008

Blood soluble drag reducing polymers (DRPs) represent a potential novel treatment of hypoperfusion and other disorders. Injections of these high molecular weight viscoelastic molecules into the blood of experimental animals at sub-nanomolar concentrations were shown to increase cardiac output with no changes in blood pressure (a reduction of vascular resistance) and enhance tissue perfusion and oxygenation. The DRP intravascular phenomena have been successfully utilized in animal models of various pathologies including hemorrhagic shock, hypobaric hypoxia, coronary stenosis, and diabetes. Chronic injections of DRPs demonstrated the reduction/prevention of atherosclerosis. Two reported potential mechanisms behind the DRP intravascular effects were a decrease in flow separations at vascular bifurcations and a reduction/elimination of the Fåhraeus effect (cell-free plasma layer existing in the near-vessel-wall space) in microvessels. The latter effect may enhance blood transport efficiency and selectively implement an increased shear stress on the endothelial cells in microvessels.

This work was aimed to expand the knowledge on the mechanisms behind the phenomenological effects of DRPs in the cardiovascular system and to study new biomedical applications.

A rodent model of chemically-induced diabetes illustrated the potential utility of DRPs for the improvement of microcirculation impaired by disease development and implicated as an etiology of its complications. Additional rodent experiments tested and proved the absence of

acute and chronic deleterious effects of hemodynamically effective concentrations of DRPs on hematological, serum chemistry, blood gas and blood coagulation parameters. Further experiments were performed to determine the DRP concentration thresholds which could be safely used intravenously.

A hypothesis that DRPs affect RBC deformability was tested using bulk blood filtration and viscoelastometry techniques. The filterability of RBC suspensions with DRPs was found to be slightly increased reflecting a potential increase in RBC deformability. It was also shown that DRPs slightly decreased RBC viscoelasticity which was increased due to diabetes in rodents which also reflects a potential increase in RBC deformability.

Finally, DRPs were explored in tissue engineering, demonstrating that this new microhemodynamic phenomena could be employed to retard the inflammatory response to implanted biodegradable synthetic scaffolds. This resulted in enhanced collagen structure and production in tissues that replaced the scaffold material.

TABLE OF CONTENTS

LIST OF TABLES

LIST OF FIGURES

NOMENCLATURE

ACD	Anticoagulant citrate dextrose
ANOVA	Analysis of variance
ATCC	American Type Culture Collection
BG	Blood glucose
CBC	Complete blood count
DMEM	Dulbecco's modified eagle medium
DPBS	Dulbecco's phosphate buffered saline
DRP	Drag reducing polymer
EDTA	Ethylenediamine tetraacetic acid
FBS	Fetal Bovine Serum
HA	Hyaluronic Acid
HSI	Hue-Saturation-Intensity
Ht	Hematocrit
IC	Intracardiac
IM	Intramuscular
IV	Intravenous
kDa	kilo Dalton
MAP	Mean arterial pressure
MW	Molecular Weight

MWCO	Molecular Weight Cutoff
P/S	Penicillin/Streptomycin
PEO	Poly(ethylene oxide)
PEO-200	Poly(ethylene oxide) molecular weight 200 kDa
PEO-4500	Poly(ethylene oxide) molecular weight 4500 kDa
PMNN	Poly(mannan)
POD	Post operative day
PT	Prothrombin time
PTT	Partial thromboplastin time
RBC	Red blood cell
RCA	RBC aggregation
SBP	Systolic blood pressure
SD	Standard deviation
SEM	Standard error of the mean
SEM	Scanning electron microscope
SQ	Subcutaneous
STZ	Streptozotocin
TP	Tissue perfusion

ACKNOWLEDGEMENTS

I would like to start by thanking my advisor, Dr. Marina Kameneva, to whom I am extremely grateful for her support and guidance in my research efforts at the University of Pittsburgh and for her never-ending patience. She has dedicated countless hours to teach and help me with experimental design, data analysis, grant, abstract and manuscript writing and presentation preparation, all of which form the basis of this dissertation. She has truly taught me what it takes to be a good scientist. And of course, I cannot thank her enough for the bottomless supply of chocolate!

Along with my advisor, I would also like to express my gratitude to Drs. James Antaki, Harry Blair, Harvey Borovetz and Richard Koepsel for agreeing to be members of my committee. I thank them for their invaluable time, expertise, and advice; all of which helped me to complete this dissertation. Special thanks go to Dr. Blair for his assistance with the histological analyses. Lastly, I cannot express my gratefulness to Dr. Borovetz for his unwavering support of graduate students. I was lucky enough to be one.

I would also like to thank Dr. Robert Kormos, Steve Winowich, Dr. Rick Schaub and Don Severyn for affording me the opportunity to work for the Artificial Heart Program and to be a member of the clinical transport team. I am sincerely appreciative for the time Don gave me while I was an undergrad to visit with him at the hospital. That tour helped guide my future and make my decision to come to the University of Pittsburgh for graduate school. The experiences

and opportunities given by the program will forever be cherished and have taught me much about selflessness and compassion. I have gained many friends and colleagues through the program and have many fond memories. Lastly, to the many patients and their families, you have touched my life in so many ways. You have taught me to truly appreciate my family, my friends and every day I have on this earth.

I would like to acknowledge the sources of funding that allowed me to pursue and complete my doctorate: American Diabetes Association, Commonwealth of Pennsylvania and the Pennsylvania Department of Health, Department of Bioengineering University of Pittsburgh, and National Tissue Engineering Center. In addition, the staff and facilities of the McGowan Institute for Regenerative Medicine (MIRM) at the University of Pittsburgh provided help and resources which enabled the completion of this dissertation. Specifically, I would like to thank Jennifer Debarr for her assistance in preparing all the histology slides, Alex Nieponice for his initial interpretation of the histology preparations, and Lisa Gordon, Joe Hanke, Aaron Dean, and Shawn Bengston for always letting me borrow something I forgot to bring to the animal facility.

To the members, past and present, of the Hemodynamics, Hemorheology, and Artificial Blood Laboratory, I could not have done all this work without you and I am forever grateful. I am thankful to Dr. Arkady Uryash for teaching me the techniques necessary to perform animal experiments and teaching me how to manage all the related equipment. I cannot thank Mary Watach enough for convincing Drs. Litwak and Kameneva to let an undergrad from the animal facility spend a few months in our laboratory. It was in those months that I met my true love who is now my wife. Special thanks are due to Dr. Joie Marhefka, for her willingness to lend a hand in my experiments and to stay late to proofread a grant or report, for her moral support and for her friendship. I cannot forget the help provided to me by all my lab interns: Kim Sturk, Garrett

Smith, Dorian Arnold, Nitin Narayana, Stephanie Shaulis, Sean Ritchie, Elaine Blyskun, Tina Mornak, Dan Albano, Bailey Roche, Salim Olia. My apologies to anyone I may have forgotten. To the members of the Federspiel and Russell laboratories, you made those long days in the lab and office much more enjoyable and kept me sane throughout these many years. I cannot thank you enough for your friendship.

During this journey, I have gained many wonderful friends and made lots of lasting memories. I cannot possibly name all of you here, but I thank all of you for your help, support, and friendship over the last eight years. I would especially like to thank Eric Chen and Drs. Thomas Payne, Karin Corsi Payne, Jon VandeGeest, and Dan Debrah.

Finally, none of this would have ever been possible without the support of my family and my wife. To my parents, to whom I am eternally grateful for their sacrifices to get me here, you have always believed in me and provided unconditional support. You encouraged me to chase my dreams and taught me perseverance. To my extended family: thank you for your love and support. And to my loving wife, Dr. Tara Cotroneo, you deserve the most credit of all. Even during your own stressful times of veterinary school, you were always willing to do anything and everything to be there for me. You provided the moral support and motivation for me to overlook my frustrations and trudge along to the finish line to complete this dissertation. Without your love, patience and sacrifice, I don't know how I could have done it all. I thank you for being so understanding for all these years. I love you so much. This is the end of this chapter of our lives. It has been wonderful but I cannot wait to write the rest.

1.0 INTRODUCTION

Blood is a living tissue that is transported throughout the circulation to deliver oxygen, nutritive metabolites (e.g., glucose), electrolytes (e.g., Na^+), vitamins and hormones and heat to all the living cells while removing carbon dioxide and other waste products (e.g., urea). Millions of patients suffer from conditions and diseases which disrupt the flow of blood causing a state of hypoperfusion which results in dysfunction and damage of tissues through tissue ischemia. These conditions and diseases include cardiovascular disease (hypertension, arteriosclerosis, myocardial infarction, etc.), cerebrovascular disease (thrombosis, embolism, stroke, etc.), peripheral vascular disease, diabetes, sickle cell disease, trauma, hypovolemic shock and other severe illnesses. Treatment of tissue perfusion includes a wide array of modalities aimed at restoring blood flow and oxygenation to the ischemic tissues. Standard therapies available today for treatment of tissue hypoperfusion include administration of vasopressive agents to enhance pressure and administration of inotropic agents to enhance myocardial contractility and cardiac output, hyperbaric oxygenation, clot-dissolving drugs, and surgical intervention. In spite of significant progress in the treatment of these diseases and some decline in morbidity and mortality due to these diseases, they still represent major killers in the United States and other developed countries. Health care costs associated with current treatments continue to increase. Tissue engineering and regenerative medicine promise future treatments but are not yet readily

available. Therefore, it is imperative that novel methods for the treatment of impaired microcirculation continue to be developed.

A novel bioengineering approach for the treatment of hypoperfusion is being developed using special blood-soluble drag reducing polymers (DRPs). These long-chain viscoelastic molecules, when injected into blood of experimental animals at nanomolar concentrations, were shown to increase cardiac output with no changes in arterial blood pressure and enhance tissue perfusion and oxygenation [1-10]. The DRP intravascular phenomena have been successfully utilized in animal models of various pathologies including hemorrhagic shock, hypobaric hypoxia, coronary stenosis, and diabetes [11-17]. Chronic injections of DRPs were demonstrated to reduce/prevent development of atherosclerosis [5, 18-21]. The reported major hemodynamic effect produced by the intravenous injection of a small concentration of the DRPs was a significant reduction of flow resistance in the vascular system with no effect on vascular tone [10].

The exact mechanisms behind the beneficial effects of DRPs on blood circulation still remain to be identified. However, some hemodynamic and rheological hypotheses regarding the DRP intravascular action have been tested. Briefly, it was demonstrated *in vitro* that under flow conditions corresponding to realistic vascular hemodynamics ($1 \leq Re \leq 400$) DRPs reduced the size and delayed the development of flow separations at vessel bifurcations [22]. *In vivo*, this mechanism may reduce pressure loss in arterial vessels and thus increase precapillary pressure thereby promoting an increase microcirculatory blood flow. It was also demonstrated that DRPs had a significant impact on red blood cell (RBC) flow behavior in microvessels. Experiments on the flow of an RBC suspension in 100-micron diameter channels showed a significant decrease in the near-wall cell-free layer thickness due to the presence of DRPs (5 – 10 μg/ml (1.25 – 2.5

nM)) in suspensions [11]. However, it is plausible that several other mechanisms exist through which DRPs enact their beneficial effects.

The goals of the studies presented in this dissertation were to expand the knowledge on the mechanisms behind the phenomenological effects of DRPs in the cardiovascular system and to study several potential new biomedical applications of these effects. This was achieved by completing the following **specific aims**:

(1) Determine whether the DRP additives have a rheological effect on red blood cells to establish additional mechanisms behind the DRP microrheological phenomena using several techniques to study animal blood hemorheology

One proposed mechanism behind the intravascular effect of DRPs is a direct enhancement of the mechanical properties of the red blood cells, i.e. their deformability. This hypothesis was investigated using two techniques: (i) a filtration technique and (ii) measurements of viscoelasticity. The filtration of RBC suspensions is an established method used to study RBC deformability. The second method was first validated with a series of experiments that tested whether measurements of bulk fluid rheological properties could indeed discriminate differences in RBC deformability. After this step, this method was used to study the effects of DRPs on blood incubated *in vitro* and *in vivo* with glucose (in diabetic rats). This mechanism would provide insight into the unique ability of DRPs to increase the number of functioning capillaries especially in a model of diabetes.

(2) Demonstrate that the intravenous administration of DRP preparations in rats with streptozotocin-induced diabetes enhances impaired microcirculatory perfusion.

It was hypothesized that the intravascular injection of DRPs, which have the unique ability to enhance microcirculatory blood flow, can improve the microcirculation in the situation of progressive microangiopathies associated with diabetes. This hypothesis is based on the extensive body of work on the hemodynamic and hemorheological effects of DRPs in experimental animal models of hypoperfusion caused by severe hemorrhage and hypoxia and have defined DRP preparations that may serve as an innovative approach to modulate and enhance microcirculatory blood flow and improve oxygen delivery in diabetic microangiopathies. The hypothesis was tested through chronic and acute hemodynamic studies in which the microcirculatory blood flow in diabetic rats was monitored and after diabetes caused impairment of hemodynamics was established, minute concentrations of DRPs were infused to examine their efficacy in restoring perfusion. Additional rodent experiments tested and proved the absence of acute and chronic deleterious effects of hemodynamically effective concentrations of DRP preparations on hematological, serum chemistry blood gas and blood coagulation parameters. Further experiments were performed to determine the thresholds of DRP concentrations which could be safely used for intravenous infusions.

(3) Demonstrate the potential applications of DRPs in the field of tissue engineering by studying the ability of DRPs to improve cell proliferation and tissue in growth and facilitate angiogenesis in synthetic scaffolds.

DRPs were recently shown to regulate the axial distribution of flowing RBCs in *in vitro* models of microvessels with diameters below 300 μm which lead to a significant increase

in wall shear stress via an increase in the near-wall viscosity [11]. This effect might facilitate gas transport and waste removal through the vessel wall and promote angiogenesis via mechanotransduction mechanisms that translate these additional mechanical forces into biological responses of endothelial cells. Based on this recently discovered microrheological phenomenon, we tested the hypothesis that the chronic intravascular injection of DRPs would improve tissue infiltration and structure, facilitate blood vessel formation and decrease inflammatory response to a synthetic scaffold implanted subcutaneously in rat.

Experiments were carried out in which porous polymeric scaffolds were implanted subcutaneously and the animals were infused twice weekly for 7 weeks post scaffold implantation with DRPs (saline as Control). Assessment of tissue infiltration and growth and collagen deposition as well as blood vessel growth inside the scaffold matrix were made after scaffold explant using histological and digital analysis techniques.

2.0 BACKGROUND

2.1 DRAG REDUCING POLYMERS

Shortly after the end of World War II, a British scientist named B.A. Toms described the ability of soluble high molecular weight (MW > 1000 kiloDaltons (kDa) polymers, so-called drag-reducing polymers (DRPs), to reduce resistance to turbulent flow in a pipe [23]. It was demonstrated that the addition of a minute amount of soluble polymers with long chains, relatively linear structure, and unique elastic properties to flowing fluid significantly increased the flow rate under a constant driving pressure or decreased the pressure under constant flow conditions. The polymers had no effect on flow resistance at laminar flow conditions in a pipe, nor did they change the fluid viscosity at the effective concentrations. It was also found that DRP additives reduced hydrodynamic resistance in systems with nonturbulent (disturbed laminar) flow, such as pulsating flow in straight and spiral pipes or Couette flow with Taylor vortices at low Reynolds numbers [24, 25]. The Toms effect has been intensively investigated for decades and has been utilized for various industrial applications [26-30]. However, the exact mechanism underlying Toms phenomenon is still unknown.

Based on the extraordinary hemodynamic effects which were shown in various acute and chronic animal models, blood-soluble drag-reducing polymers may have potential in multiple biomedical applications [1, 3-6, 8-10, 17-19, 21, 31-35]. Kameneva et al. recently reviewed the

intravascular effects of DRPs which have been demonstrated in these various animal models [11]. Nanomolar concentrations of these polymers injected intravenously caused an increase in aortic and arterial blood flow and a decrease in blood pressure and in peripheral vascular resistance with no effect on blood viscosity or blood vessel tone [1, 3-6, 8-10, 32]. Briefly, DRPs were shown to significantly increase collateral blood flow [31] and the number of functioning capillaries in normal and diabetic rats [17]. In canine models, DRPs were shown to reduce poststenotic separation flows and flow disturbances in models of a subcritical stenosis in the aorta [34, 36] and carotid artery [33], to increase blood flow through stenosis in iliac arteries [35], to redistribute wall shear stresses in the area of stenosis in the aorta [21] and most recently, in a model of flow-limiting coronary artery stenosis, DRPs reduced microvascular resistance increased capillary volume and improved myocardial perfusion [37]. Beneficial effects of DRPs on myocardial perfusion were also demonstrated in the rodent model of acute myocardial ischemia [38]. Chronic intravenous injections of DRPs were shown to diminish the development of atherosclerosis in several atherogenic animal models [18-20]. These experiments, which included regular intravenous injections of DRPs into rabbits and pigeons at concentrations significantly (50-100 times) exceeding those deemed hemodynamic effectively, demonstrated no chronic toxicity. Additionally, Nokes et al. demonstrated the absence of acute toxicity to DRPs in studies of DRP-based perfusion of isolated feline hearts [39]. In models of hemorrhagic shock, it was demonstrated that the intravenous infusion of DRPs significantly increased tissue perfusion and oxygenation and reduced lethality in rats [11, 12]. DRPs were previously applied in rats with alloxan-induced diabetes [17] to test the hypothesis that these polymers could improve the microcirculation in progressive microangiopathies associated with diabetes. The hypothesis that DRPs could improve the microcirculation in progressive microangiopathies

associated with diabetes was tested. The study yielded two major results. First, it was shown that alloxan diabetes caused a significant reduction in the number of functioning capillaries and the capillary blood flow velocity. After a single injection of the DRP (polyethylene glycol with MW of ~ 4000 kDa) at the concentration of the polymer in blood as low as 1 μg/ml (0.25 nM), the number of functioning capillaries increased by nearly 50%, and the linear velocity of capillary flow increased by over 50%. It was hypothesized that the results were attributed to both a reduction in vascular resistance and an improvement in deformability of red blood cells.

Four long chain polymers were applied in previous studies of the DRP effects on blood circulation: polyacrylamide, polyethylene oxide (or polyethylene glycol), a polysaccharide extracted from okra and characterized as a rhamnogalactogalacturonan (RGGu) [3], and calf thymus DNA [32]. Our laboratory added to this list a new natural DRP, which we discovered in the inner matter of aloe vera leaves [11]. The polymer was purified, partially characterized in our laboratory, and proven to have a very high drag-reducing efficiency *in vitro* and hemodynamic and hemorheological efficiency *in vivo* in normal rats and in animals subjected to hemorrhage. We recently added to this list a synthetic polymer, poly(N-vinylformamide) (PNVF) with a molecular weight of 4500 kDa which we found to significantly reduce resistance to turbulent flow in a pipe and thus to presents a DRP. PNVF is known to have low toxicity. Our pilot *in vivo* study showed that PNVF had acceptable biocompatibility and hemodynamic effectiveness and thus could be considered as a DRP candidate for potential biomedical applications [40]. Of significant importance is the fact that although these polymers are chemically dissimilar, they all possess the ability to reduce drag in turbulent flow and have a proven efficiency *in vivo* owing this behavior to their high molecular weights and long linear structures.

As previously mentioned, the exact mechanisms behind the beneficial effects of DRPs on blood circulation remain to be identified. It was demonstrated *in vitro* that under flow conditions corresponding to realistic vascular hemodynamics ($1 \leq Re \leq 400$), DRPs reduce the size and delay the development of flow separations at vessel bifurcations [22]. *In vivo,* this mechanism may reduce pressure loss in arterial vessels and thus increase precapillary pressure thereby promoting an increase in the density of functioning capillaries and in tissue perfusion, both of which were observed in animal experiments. **Figure 2.1** demonstrates a hypothetical distribution of mean arterial blood pressure along the vascular system at normal blood pressure levels, and after an injection of DRP into the blood. One can see that a decrease in pressure drop in small arteries and arterioles caused a significant increase in precapillary pressure.

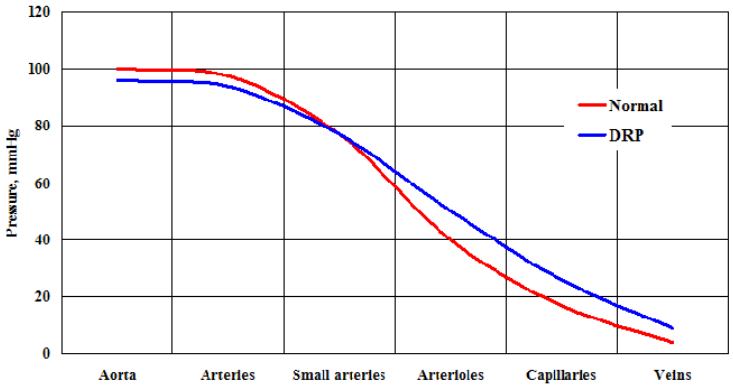

Figure 2.1. Hypothetical distribution of mean arterial blood pressure along the vascular system at normal blood pressure levels and after a hypothetical injection of DRPs into the blood.

2.2 HEMORHEOLOGY

Blood is a living tissue that is transported throughout the circulation to deliver oxygen, nutritive metabolites (e.g., glucose), electrolytes (e.g., Na+), vitamins and hormones and heat to all the living cells while removing carbon dioxide and other waste products (e.g., urea). It also serves as the organism's defense against infections and foreign materials and as a clotting mechanism to prevent fluid loss when blood vessels are ruptured. Its flow is highly regulated in order to maintain the function of the cells it serves, and disturbances in flow can result in serious complications.

Blood is a two-phase fluid consisting of a suspension of solid cellular elements (red and white blood cells and platelets) in an aqueous solution known as plasma. Red blood cells (RBCs), responsible for delivering oxygen and removing carbon dioxide from cells, constitute 99% of the cellular elements. The typical hematocrit (volume fraction of red cells in whole blood) in humans is between 40-45%. Therefore, these cells strongly influence the flow behavior of blood. Red cells are the shape of a biconcave disk (concavity of each face) with a diameter of ~8 μm and thickness ~2 μm. The red cell is filled with an incompressible, viscous hemoglobin solution which is surrounded by a flexible viscoelastic membrane consisting of a lipid bilayer and a cytoskeleton [41].

The last few decades have had considerable attention placed on the study of the behavior of blood flow, hemorheology. However, it was earlier in the 20th century when Fåhraeus began to explore the flow properties of blood and modernize the understanding of circulatory physiology. In his work, he discovered alterations in the suspension stability and flow of blood in disease processes [42]. Further work would uncover the dependence of whole blood viscosity on plasma viscosity [43, 44], hematocrit [45-47], temperature [48], and shear rate (making blood a

non-Newtonian fluid). The shear rate dependence was found to be a function of red cell aggregation at low shear rates [44, 49] and red cell deformation at high shear rates [50-52]. Alterations in any of these parameters, which occur in certain disease states, would change the flow behavior of blood thus raising clinical interest in blood rheology. A decrease in RBC deformability results in an increase in whole blood viscosity at high shear rates. Blood viscoelasticity as a function of shear rate was presented by Thurston in 1972 using oscillatory flow at a known frequency in a cylindrical tube [53]. This established that blood not only behaved as a fluid but also as a solid. Therefore, RBC deformability significantly impacts the viscoelasticity of whole blood at high shear rates and a decrease in deformability would result in an increase in whole blood viscosity and elasticity.

Our laboratory research is concerned of the hemorheological effects of blood soluble drag-reducing polymer additives in normal and pathological blood. One hypothesis behind the intravascular drag reducing phenomena is their effect on RBC deformability.

The smallest capillaries are ~3-5 μm; therefore the cells must deform a substantial amount to be able to pass throughout the microcirculation. Consequently, a small reduction in RBC deformability can significantly compromise the number of functioning capillaries and hence oxygen delivery, extraction of products of metabolism from the tissue, etc. Diabetes Mellitus is associated with hemorheological abnormalities. Rheological studies of blood obtained from patients with diabetes have shown increased blood viscosity [54, 55] and reduced RBC deformability [56-58].

2.3 DETERMINATION OF BLOOD VISCOSITY AND VISCOELASTICITY AND RBC DEFORMABILITY

Viscosity is typically measured with either a capillary or rotational viscometer. Capillary or tube viscometers are the oldest and most popular method of measuring viscosity due to their extreme simplicity. This method is based on the Poiseuille flow relationship for steady flow in a long circular cylindrical tube and thus with knowledge of flow, applied pressure and tube dimensions, viscosity can be determined. These viscometers lend themselves quite useful to measurements of Newtonian fluids such as plasma but there are several constraints that limit their use for viscosity measurements of the non-Newtonian fluid, whole blood, including measurements at fixed shear rates. A summary of these limitations are given in a review on clinical blood rheology [59]. Reasonable measurements of the asymptotic viscosity of blood can be obtained using these instruments.

Measurements of the viscosity of non-Newtonian fluids are better accomplished with rotational viscometers which consist of radially symmetrical cylindrical/conical elements (one fixed and one moving) separated by the test fluid since these devices allow viscosity measurements over a wide shear rate range and since blood viscosity is shear dependent. The torque resulting from shearing the test sample is recorded and shear stress is calculated based on torque measurement and the cylindrical geometry. The three basic types are: (1) cone-plate, (2) cone-in-cone, and (3) coaxial cylinder (Couette). The first commercially available rotational viscometer to measure blood rheology was Wells-Brookfield cone and plate rheometer. The cone-plate and cone-in-cone rheometers are limited due to RBC sedimentation [60]. Couette viscometers are made to be extremely sensitive at low shear rates and are reproducible at both low and relatively high shears making them an appropriate choice for measurements of blood

rheological properties [59, 61]. Conventional rheometers (rotational cone/plate and Couette) provided most of the initial data on the effects of temperature, shear rate, hematocrit, and level of plasma proteins on human adult blood viscosity.

Thurston proposed to use oscillatory tube flow measurements to show that viscoelasticity was a basic rheological property of blood. With this device, Thurston demonstrated that aggregation, deformability, and flow-induced cell organization are the factors that make human blood viscoelastic, non-Newtonian, thixotropic, and dilatant [62, 63].

A comparison of conventional rheometers (rotational cone/plate and Couette) where viscosity is measured under steady flow conditions to a rheometer capable of making oscillatory flow measurements shows that in steady flow the strain is increasing continuously whereas in oscillatory flow it reverses periodically thus allowing measurements of minimal microstructural changes to blood. In steady flow, the relative displacement of neighboring cell groups increases without limit and blood structure is modified from its quiescent state. At higher shear rates these changes become similar between steady and oscillatory flow [64]. Thurston's viscoelasticity analyzer is capable of making oscillatory measurements with high precision and sensitivity where conventional rotational rheometers cannot meet these requirements, operates at frequencies near the pulse rate and requires small sample volumes [65].

Measurements of bulk viscosity and viscoelasticity at high shears (>100 s^{-1}) provide an indirect measurement of RBC deformability. A Vilastic Scientific viscoelasticity analyzer and a Brookfield cone-plate rheometer were used in the studies performed in this dissertation to study the rheological effects of DRPs on blood obtained from normal and diabetic rats to further elucidate potential mechanisms behind the beneficial intravascular effects of DRPs.

Other techniques have been developed and used to directly measure the deformability of RBCs. Bulk filtration has been the most widely used method for clinical studies of RBC deformability. This technique, developed in 1976 by Reid and Dormandy [66], involves the filtration of RBC suspensions through a 5 micron filter by constant negative pressure of 20 cmH_2O. This method has several technical challenges which affect RBC filtration including contaminating particles such as platelet aggregates and white blood cells in the suspension media which may clog the filter pores or the effects of storage in suspension media. A complete list of *in vivo* and *in vitro* factors that influence RBC filtration measurements has been reviewed [59]. Commercially available instruments have been designed around this concept. Other techniques available for measurement of RBC deformability include micropipette aspiration which directly measures the intrinsic deformability of the cell membrane. This method is advantageous in that it directly measures the individual RBC deformability independent of other cells. However, only a small number of RBCs can be sampled out of an entire population and this method is extremely time consuming limiting its use in clinical studies. Another method, ektacytometry, measures RBC elongation under a constant shear stress using laser diffractrometry. This instrument is particularly versatile even being able to measure the deformability of RBC ghosts [67]. This method has the same limitation as ektacytometers characterizing only small population of RBCs which may not represent the whole blood rheological behavior.

The bulk filtration method described above was also used in this dissertation to further study and complement the work in which measurements of bulk viscosity and viscoelasticity were applied to indirectly measure RBC deformability in the presence of DRPs.

2.4 DRP FOR THE TREATMENT OF DIABETES MELLITUS

Twenty-one million people in the United States have diabetes mellitus. The costs associated with their health care and disability are over $132 billion annually [68]. Diabetes is associated with high levels of glucose in the blood, hyperglycemia, due to defects in insulin production, insulin action, or both. The cumulative effects of hyperglycemia in diabetic patients lead to two types of vascular damage: a nonocclusive microcirculatory dysfunction involving the capillaries and arterioles of the kidneys, retina, and peripheral nerves, and macroangiopathies characterized by atherosclerotic lesions of the coronary and peripheral arterial circulation [69]. The micro- and macrovascular damage places diabetic patients at high risk for heart disease and stroke, high blood pressure, blindness, dental, kidney and nervous system disease, and delayed wound healing and limb amputation. The damage to the microcirculation is a multi-step process ultimately ending in microvascular hypoperfusion resulting in cellular damage and eventually damage to organs, systems (i.e., nervous), or processes (i.e., wound healing) [70].

The treatment of poor tissue and organ circulation is extremely important for millions of patients suffering from diabetic complications. Standard therapies available today for the treatment of low blood flow, i.e. low oxygen delivery to tissue and organs, include administration of vasopressive agents to enhance pressure and the administration of inotropic agents to enhance cardiac output (flow) [71]. More advanced treatments include the newly developed antihypertensive drugs called ACE (angiotensin-converting enzyme) inhibitors to prevent or delay kidney failure; laser treatment for diabetic retinopathies; and the transplantation of kidneys and pancreases in patients with kidney failure due to diabetes. Insulin therapy has provided significant improvement in capillary perfusion [72]; however, it can cause complications such as hypoglycemia, lipoatrophy, allergic reactions, insulin resistance, and

insulin edema, especially in children [73, 74]. Although novel drugs possessing radical scavenging ability, such as Troglitazone, are expected to improve impaired microcirculation in diabetes [75], the maintenance of normoglycemia continues to be the most successful means of prevention of diabetes-related complications. This is reflected in the most recent advances in the management and treatment of diabetes including the development of a quick-acting insulin analog; improved methods to monitor blood glucose; and the development of external insulin pumps to replace daily injections. This largely overlooks the hemorheological component and the serious damage that altered mechanical properties of RBCs and increased flow resistance may cause in microcirculation. This is of particular interest to our laboratory since a potential treatment of the diminished blood flow and reduced red blood cell (RBC) deformability [56, 57], both of which have been implemented in diabetic complications, may be the intravascular injection of DRPs as we described above as having the unique ability to increase microcirculatory blood flow and may possess the ability to enhance RBC deformability. Previous attempts to address this problem using drugs that improve the deformability of RBCs (Trental®) were used in healing of ischemic wounds and showed some improvement [76]. Therefore, the need for new therapeutics to treat and prevent these diabetic complications is still crucial for the reduction of mortality and morbidity due to diabetes.

Currently there is no truly effective prevention regimen or treatment for diabetes-related microcirculation impairment. In this dissertation, an experimental evaluation of a novel therapy for the restoration and maintenance of impaired microcirculation in tissue and organs, which is significantly reduced due to diabetes based on the ability DRPs to provide blood with exceptionally low resistance to flow in the microcirculatory system which increases functional

capillary density and markedly improve blood flow in microcirculatory disorders associated with diabetes was performed.

2.5 DRP IN TISSUE ENGINEERING AND REGENERATIVE MEDICINE

Angiogenesis plays a very important role in many normal and pathological conditions and it is strongly involved in the process of wound healing and tissue regeneration. Angiogenesis is required to supply new tissue with oxygen metabolites and to remove waste products of metabolism. When angiogenesis is impaired due to a variety of causes (physical, chemical, aging, etc.), the gas transport is diminished and the tissue growth is weakened. While inhibition of angiogenesis is crucial for suppression of the tumor growth, inducing angiogenesis is a vital issue in regenerative therapy, especially in the biointegration and biocompatibility of biomaterials and healing of wounds. It was previously shown that a sustained hemodynamic wall shear stress stimulates neovascularization and damaged tissue repair *in vivo* [77].

It was long believed that increased blood flow improves wound healing [78], and that blood flow acceleration is essential for wound healing angiogenesis [77]. Hemodynamic forces produced by flowing blood are strong and important regulators of cell and organ function. Flow induced wall shear stresses are known to play an important role in the activation of many signal transduction pathways in vascular endothelial cells [79, 80]. Application of a shear stress to the surface of blood vessels wall causes deformation of endothelial cells with rearrangement of the cytoskeleton which triggers endothelial mechanotransduction. Hemodynamically induced wall shear stresses influence vascular function and adaptation affecting vessel tone and the vascular remodeling generated during the vasculo- and angiogenesis associated with vascular

physiological adaptation or disease [81, 82]. More recently, Van Gieson at al. studied the *in vivo* adaptation of microvessels in the presence of elevated pressure and circumferential wall stress and found an enhanced coverage of fully differentiated mature smooth muscle cells in mesenteric microvessels related to sustained elevated pressure and wall strain [83]. Therefore, hemodynamic stresses are important angiogenic stimuli along with hypoxia, inflammation and other factors, and growth of new microvessels is essential for uncompromised wound healing and tissue regeneration [82]. Unfortunately, there are very limited possibilities to increase blood flow in microvessels to stimulate angiogenesis. In animal models, powerful vasorelaxants are used to increase peripheral circulation [77]

Hemodynamic forces applied to a vessel wall can be estimated by using a force balance in the vessel segment schematically shown in **Figure 2.2**,

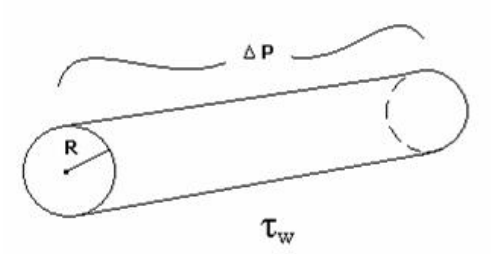

Figure 2.2: Schematic of forces on blood vessel segment

$$\tau_w \times 2\pi R \times L = \Delta P \times \pi R^2, \quad (1)$$

where τ_w is the wall shear stress, **ΔP** is the pressure gradient across the vessel, **R** is the vessel radius and **L** is the segment length. Therefore,

$$\tau_w = \Delta P \times R/2L. \quad (2)$$

Using the Poiseuille equation

$$\Delta P = Q \times 8L \times \mu/\pi R^4, \quad (3)$$

we obtain $\tau_w = 4Q \times \mu/\pi R^3$, (4)

Substituting **Q** with the formula $Q = v \times \pi R^2$, where **v** is velocity of blood flow, we obtain a final formula for calculation of the wall shear stress.

$\tau_w = 4 \times v \times \mu/R$ or $\tau_w = f(v, \mu, R)$. (5)

From this equation one can see that the vessel wall shear stress depends on three parameters: velocity of blood flow through the vessel, viscosity of blood and the vessel radius. Therefore to increase wall shear stress, one should increase velocity of flow as it was done by Ichioka et al. [77] or decrease vessel radius. Blood viscosity is usually considered to be a constant. However, in small vessels with a size below 200 μm, the near wall viscosity is much lower than the whole blood viscosity, since there is a cell free layer of plasma present there which has a lower viscosity. Therefore, to increase wall shear stress via an increase in viscosity, one should consider infusion of substances which would increase plasma viscosity such as dextran or starch solutions which would significantly increase the whole blood viscosity. Another method could be a reduction or elimination of the near wall plasma layer.

One further hypothesis regarding the mechanisms of the DRP intravascular effects was related to the potential impact of the DRPs on RBC flow behavior in microvessels. Experiments on the flow of an RBC suspension in 100 μm diameter channels showed a significant decrease in the near-wall cell-free layer thickness in the presence of minute concentrations (5 – 10 μg/ml (1.25 – 2.5 nM)) of DRPs in suspensions **(Figure 2.3)**.

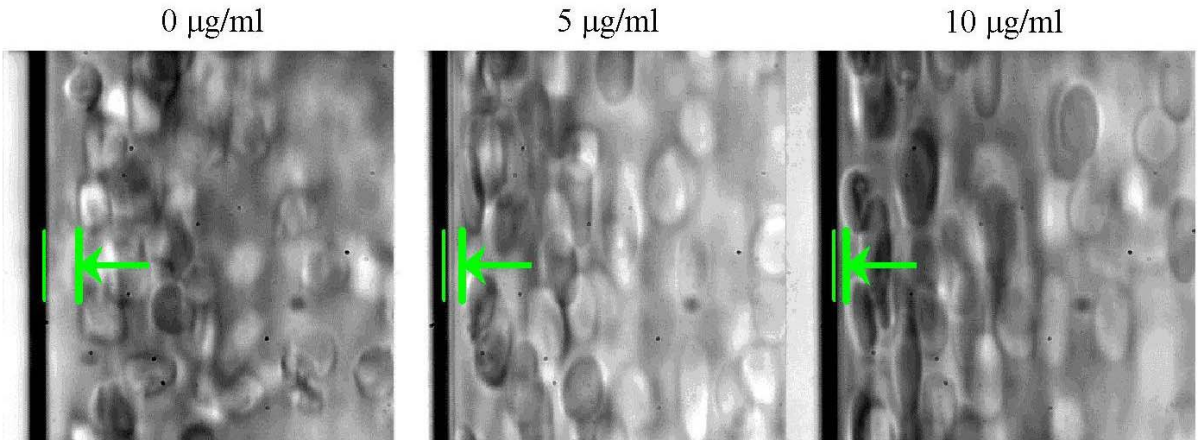

Figure 2.3: Effect of DRPs on the near-wall plasma layer in a 100 μm channel

A decrease in the size of the near-wall plasma layer in a 100 micron channel was demonstrated after the addition of DRPs. An increase in the DRP concentration causes a decrease in the near-wall plasma layer (photo by Dr. ZJ Wu [84]).

The same polymers with lower molecular weight and with no ability to produce the Toms effect did not change flow behavior of RBCs in the microchannels. In the vascular system, this rheological effect can attenuate the plasma "skimming" and both Fåhraeus and Fåhraeus-Lindquist effects in small vessels and, thus, increase local hematocrit, apparent viscosity and wall shear stress in microvessels and capillaries. *In vivo* this effect may facilitate gas exchange in arterioles and capillaries due to relocation of some RBCs to the near-wall space. In addition, due to an increase in the microvessel hematocrit caused by attenuation of the plasma-skimming effect, DRPs would produce an increase in local blood viscosity and wall shear stress potentially promoting the release of vasodilators in microvessels, and an increase in collateral flow and number of functioning capillaries. The decrease in the near wall cell-free layer associated with the DRPs is a new phenomenon which has yet to be investigated in detail and explained. We speculate that the alignment and stretch of the polymers along the flow paths may diminish RBC rotation. RBC rotation is an important contributor to the formation of a near-wall plasma layer in microvessels. In addition, an increase in blood viscoelasticity due to the presence of DRPs may

strengthen non-Newtonian patterns of the axial velocity profile in vessels (increasing the profile bluntness, decreasing the velocity near the central axis and increasing the velocity near channel/vessel wall). This would change the RBC distribution in the axial core and shift their mean velocity closer to the mean velocity of blood.

The presence of the DRPs in blood, which selectively increase near wall viscosity and thus wall shear stress in microvessels, might promote angiogenesis and change the cellular response to biomaterials via the mechanotransduction mechanisms that translate mechanical forces into biological responses of endothelial cells (**Figure 2.4**).

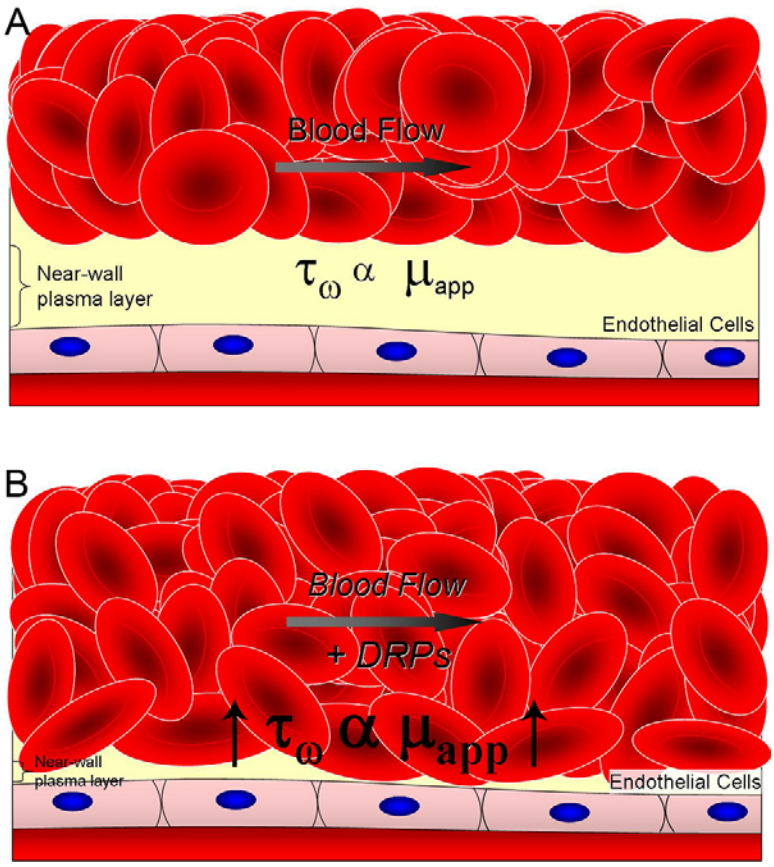

Figure 2.4: Schematic of DRP action in microvessels

(A) Pre-DRP: RBCs flowing in small vessels (diameter < 0.3 mm) move radially toward the vessel center producing a near-wall plasma layer and reducing the apparent viscosity at the vessel wall and the shear stress on the endothelium (Fåhraeus-Lindquist effect). (B) Post-DRP: The presence of DRPs in blood moves RBCs axially toward the vessel wall, reducing the near-wall plasma layer and increasing the local hematocrit. The effective viscosity at the vessel wall and the shear stress on the endothelium also rise, possibly stimulating cytokine production or limiting leukocyte extravasation.

A study was performed in this dissertation to investigate this innovative hemodynamic approach for the enhancement of biointegration of a polymeric scaffold by increasing blood circulation in microvessels and stimulating local angiogenesis related to increased shear forces applied to endothelial cells.

3.0 STUDY OF THE POTENTIAL MECHANISMS BEHIND THE MICRORHEOLOGICAL PHENOMENA OF DRPS: A VALIDATION OF TECHNIQUES AND THE RHEOLOGICAL EFFECT OF DRP ADDITIVES ON BLOOD

3.1 INTRODUCTION

Microcirculatory blood flow is dependent on the ability of red blood cells (RBCs) to deform. A reduction in RBC deformability can have significant consequences on the number of functioning capillaries, oxygen delivery, extraction of products of metabolism from the tissue, etc. The filterability and viscoelasticity of blood significantly depends on RBC deformability and both a decrease in filterability and an increase in blood viscosity and elasticity without changes in hematocrit and plasma viscosity signify a decrease in RBC deformability. It has been suggested, that decreased RBC deformability may be responsible for the pathogenesis of some of the complications in diseases such as diabetes. One hypothesis of the mechanism behind the intravascular effect of DRPs, in which these blood soluble macromolecules greatly enhance blood flow in the microcirculation, is a direct enhancement of the mechanical properties of the red blood cells. The exploration of this hypothesis is described in this chapter.

3.2 DRP EFFECT ON RED BLOOD CELL (RBC) FILTERABILITY

3.2.1 Introduction

The filtration of RBCs through polycarbonate sieves has been extensively investigated and used as a method for determining the deformability of RBCs. In this part of the chapter, a study to investigate the effect of DRPs on the filterability of RBC suspensions using this technique is discussed.

3.2.2 Methods

3.2.2.1 Drag-reducing polymer preparation

Three drag-reducing polymers were used in the *in vivo* and *in vitro* experiments outlined in this dissertation and include: a synthetic DRP, PEO-4500 (Sentry™ Polyox WSR-301-NF grade, MW = 4500 kDa, Dow Chemical, Midland, MI) and two natural DRPs, an aloe vera-based DRP, Poly(mannan) (PMNN; MW = ~4000-6000 kDa) which was discovered in our laboratory and a hyaluronic acid-based DRP, Hyvisc® (HA; MW = ~2000 kDa, Anika Therapeutic, Bedford, MA). An additional polymer, PEO-200 (MW = 200 kDa, Aldrich Chemical, Milwaukee, WI) was prepared and used in some experiments as a control. PEO-200 has the same chemical structure as PEO-4500 but due to its lower molecular weight, it does not possess drag reducing ability (molecular weight must be greater than 1000 kDa to produce drag reduction). The preparation of the DRP solutions used in this and all subsequent chapters is provided below to forgo repetitiveness in further chapters.

PEO-4500 was prepared weekly by dissolving PEO-4500 powder in pyrogen-free sterile normal saline (Baxter, Deerfield, IL) at a concentration of 1.5 mg/ml (0.33 μM). The PEO solution was slowly mixed by a magnetic stirrer for 2-4 hours until the solution was thoroughly homogenized. The solution was then placed in plastic-walled conical centrifuge tube and slowly rocked on a laboratory rocker (Type M79700 Platform Vari-Mix Rocker, Barnstead Thermolyne Corp., Dubuque, IA) for 16 hours to ensure mixing and homogeneity. Any low molecular weight polymer and/or other low molecular weight impurities were removed by subsequent dialysis against saline for 48 h using a dialysis membrane with a 50 kDa molecular weight cutoff (Spectra/Por membrane; MWCO: 50 kDa, Spectrum Laboratories, Rancho Dominguez, CA). The preparation was then centrifuged at 2200 x g for 30 minutes (CR412; Jouan, Winchester, VA) to remove the silicate particles, which were added into the PEO powder during manufacturing as a desiccant, and stored at 4°C until use. The polymer was dissolved in saline to the desired concentration (50 – 100 μg/ml (1.1 – 2.2 nM)) and mixed 4-6 hours prior to use. PEO-200 was prepared when needed using the same technique.

Poly(mannan) (PMNN) was prepared based on the methods previously described by Kameneva et al. [85]. PMNN is a naturally occurring DRP that was extracted and purified from the viscous mucilage of the aloe vera (*Aloe Barbadensis Miller*) of the Lily plant family. The drag reducing properties of the PMNN polymer were first discovered and reported by Kameneva et al. [11, 85]. After the extraction process was completed, PMNN was dissolved in pyrogen-free sterile normal saline at a concentration of 2.5 mg/ml (0.42 μM) and stored at -20°C. On the day of an experiment, PMNN was thawed at room temperature, centrifuged at 2200 x g for 30 minutes (CR412; Jouan) to remove any potential precipitates and further dissolved in saline to the desired concentration (50 – 1250 μg/ml (8.3 – 208 nM)) and mixed 4-6 hours prior to use.

The hyaluronic acid-based DRP, Hyvisc® (HA) was purchased from a veterinary supply vendor (NLS Animal Health, Owings Mills, MD). Hyvisc®, a readily available formulation of HA, is currently used by veterinarians used to treat joint dysfunction in horses associated with equine osteoarthritis. HA was stored as recommended by the manufacturer until use. On the day of an experiment, HA was diluted from its supplied concentration of 11 mg/ml (3.7 μM) in saline to the desired concentration (50 – 3000 μg/ml (16 – 1000 nM)) and mixed 4-6 hours prior to use.

All procedures for the preparation and manipulation of the polymer solutions were done aseptically to maintain sterility of the solutions. The polymer preparations were tested in an *in vitro* circulating flow loop prior to *in vivo* experiments to ensure the reproducibility of the desired drag reducing ability.

3.2.2.2 Blood collection and sample preparation

Since our animal tests with DRPs were performed in rats, we proposed to test the effects of DRP of blood *in vitro* using donor rat blood. Arterial blood was collected from the right carotid artery of male Sprague-Dawley rats weighing ~350-500 grams. A surgical plane of anesthesia was induced and maintained by an intramuscular (IM) injection of ketamine (90 mg/kg; KetaJect®; Phoenix Pharmaceutical; St. Joseph, MO) and xylazine (10 mg/kg; Xyla-Ject®; Phoenix Pharmaceutical). A thermistor probe (Yellow Springs Instruments) was inserted into the rectum and the animal placed on a heating pad in dorsal recumbency to maintain a body temperature of 37 °C. The ventral surface of the neck was shaved and a midline incision from the caudal end of the larynx to the suprasternal notch was made. To gain access to the right carotid artery, the sternothyroideus and omohyoideus muscles were separated from the sternocleidomastoideus using blunt dissection and the carotid artery located by direct palpation. The sheath was incised

to expose the carotid artery and the vagus nerve. The carotid artery was then carefully dissected free from the vagus, ligated distally with 3-0 silk surgical suture (Surgical Specialties, Reading, PA), and cannulated with a 22 gauge IV catheter (ProtectIV Plus; Medex, Carlsbad, CA). Approximately 50-75% of an animal's blood volume (3-4% of the lean body weight) was obtainable through exsanguination (total blood volume can be approximated as 6% of the lean body weight) [86]. The average blood volume collected from the rats ranged from 10-12 ml. Blood was allowed to freely flow from the catheter into glass K_3EDTA Vacutainer® tubes (BD, Franklin Lakes, NJ) for collection. The animals were sacrificed by a bolus of potassium chloride (2 mmol/kg).

Experiments were performed using whole blood dilutions since blood sample volumes were small and washing the cells would have diminished the amount of available blood further. Suspensions of erythrocytes were prepared by diluting fresh whole blood forty times with phosphate buffered saline (PBS; pH 7.4, osmolality 290 mOsm/kg; Sigma-Aldrich, St. Louis, MO) containing 1% bovine serum albumin (BSA; Sigma-Aldrich), which served as the suspension medium. The erythrocyte suspension was then aliquoted into three equal volumes and PEO-4500 (1.5 mg/ml (0.33 μM)) was added to two of the aliquots to yield final DRP concentrations of 1 (0.22 nM) and 10 μg/ml (2.2 nM), respectively. The 1.5 mg/ml (0.33 μM) PEO-4500 solution was diluted accordingly to allow equivalent volumes of the DRP to be added. An equal volume of the original suspension medium was added to the third aliquot to serve as a control. In an additional set of experiments, the erythrocyte suspension was aliquoted into two equal volumes and PEO-200 (1.5 mg/ml (7.5 μM)) was added to one of the aliquots to yield a final polymer concentration of 10 μg/ml (50 nM). The second aliquot received an equal volume of the original suspension medium. PEO-200 has an identical chemical structure to PEO-4500

but because its molecular weight is below 1000 kDa, it possesses no drag reducing ability and therefore serves as another control to exclude chemical effects on the cells. After the 40x dilution, the blood suspensions' hematocrits were in the order of 1%. The micro-centrifugation/micro-capillary method commonly employed to measure Ht was not used to determine the final RBC concentration of the suspensions since it is moderately insensitive at such very low Ht values.

Pathological RBCs or RBCs which exhibit a reduced deformability, as previously reported in diabetic patients [56-58], were simulated by incubating the RBCs with 0.015% glutaraldehyde for 30 minutes. After the incubation period, the RBC suspension was centrifuged and the excess glutaraldehyde was removed. The samples were then washed three times with PBS. In between PBS washes, the RBC suspension was centrifuged at 2200 x g for 10 minutes (CR412; Jouan) and the PBS was exchanged. A final RBC suspension of glutaraldehyde-hardened cells was prepared by dilution with PBS + 1% BSA to a final hematocrit of 1%. The suspension was then aliquoted into two equal volumes and PEO-4500 (1.5 mg/ml (0.33 μM)) was added to one of the aliquots to yield a final polymer concentration of 10 μg/ml (2.2 nM). The second aliquot received an equal volume of the original suspension medium. Rigidified RBCs are commonly employed in determining the utility of specific techniques to distinguish the differences between normal and pathological cells.

3.2.2.3 Filtration apparatus and experimental procedure

Filtration experiments were performed using a filtration apparatus, as shown in **Figure 3.1**, based on the system originally described by Reid and Dormandy [66]. The system was comprised of a 10 ml disposable syringe barrel (BD) attached to the female luer-lock inlet of a 13mm Swinnex®

filter holder (Millipore Ireland BV, Tullagreen, Carrigtwohill, County Cork, Ireland) containing a straight channel 5-μm pore polycarbonate filter (Isopore; Millipore Ireland BV). According to the manufacturer, the filters had a diameter of 13 mm, a maximum thickness of 10 μm and a mean pore density of $4x10^5$ pores/cm^2. Each filter was used only once, to avoid any potential clogging of the filter. The male slip-tip outlet of the Swinnex® filter holder was fit into a 2-way stopcock which was subsequently attached to a luer-lock fitting that was tightly secured in one of the holes of a two-hole rubber stopper. The two-hole rubber stopper was positioned into the top of a 6-liter Pyrex® Erlenmeyer flask (Corning Life Sciences, Acton, MA). The Erlenmeyer flask acted as both the filtrate and vacuum reservoir. A piece of ¼" Tygon® tubing (Cole-Palmer Instrument Company, Vernon Hills, IL) connected the second hole of the rubber stopper in the filtrate/vacuum flask to a water column and to a pipette bulb. The water column's base was submerged in a beaker of water and it served to measure the negative pressure in the system that was applied to the bottom of the filter. With the stopcock closed, the pipet filler was used to evacuate the air in the system and create a vacuum pressure of -20 cmH_2O. This pressure was maintained constant after the stopcock was opened by slowly releasing the pipette bulb at a rate that corresponded to the flow rate of the filtrate entering the system.

RBC suspensions, as described above (Control (no polymer), 1 (0.22 nM) and 10 μg/ml (2.2 nM) PEO-4500 and 10 μg/ml (50 nM) PEO-200) and the suspension media (Control (no polymer), 1 (0.22 nM) and 10 μg/ml (2.2 nM) PEO-4500 and 10 μg/ml (50 nM) PEO-200) were loaded into the 10 ml syringe barrel and drawn through the 5 μm filter under the constant -20 cm H_2O pressure. The efflux time required for 1 ml of the cell suspensions or 4 ml suspension media to pass through the filter channels was recorded and the flow rate was calculated by dividing the filtrate volume by its efflux time. Two different filtrate volumes were chosen in order to have

efflux times that were in the same order between cell suspensions and suspension media. Flow rates were standardized to a constant temperature of 24°C by slightly raising or lowering the value using linear interpolation. Recorded temperature values were ±1°C. The relative RBC filtration index (RFI) was determined to be the ratio of the flow rates of cell suspension (Q) and the corresponding suspension medium (Q_0): RFI = Q / Q_0. An increase in RFI signified an increase in RBC filterability.

In addition, the RBC suspensions were observed using a light microscope (Labophot-2, Nikon Instruments, Melville, NY) before and after filtration through the 5 μm filter pores to study whether the filtration process had any direct effect on the RBCs shape.

Results are expressed as the Mean ± SE. Individual data points that were greater than two standard deviations from the mean of the remaining data were discarded. Data analysis was performed using GraphPad Prism 5 (GraphPad Software, San Diego, CA). A one-way ANOVA with Tukey post hoc test was used to compare the means of the experimental groups to that of the control group. A $p < 0.05$ was considered to be statistically significant.

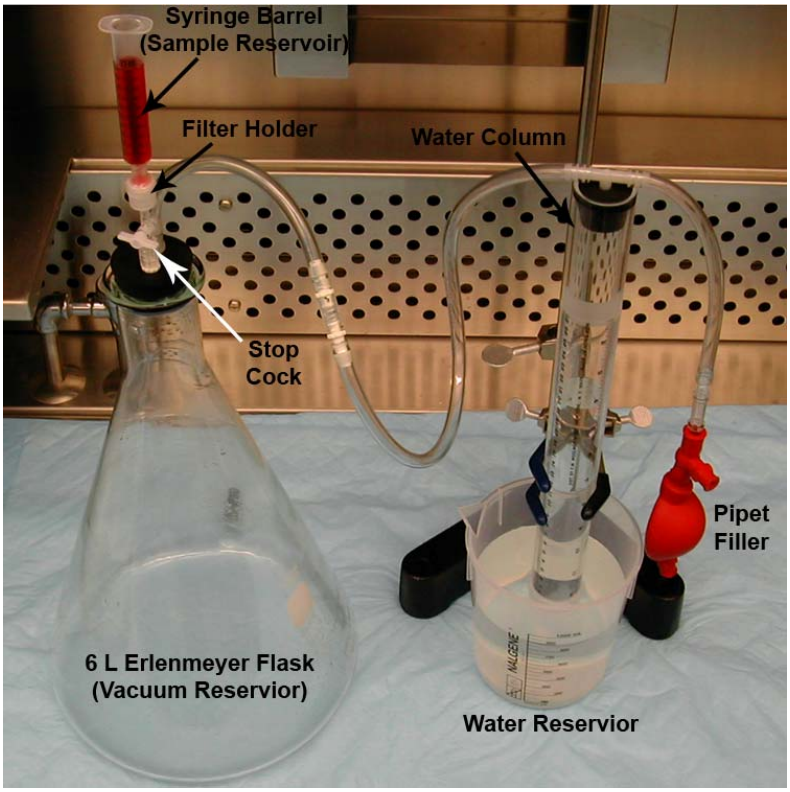

Figure 3.1: Experimental setup used in filtration experiments

3.2.3 Results and Discussion

3.2.3.1 Microscopic evaluation of RBC properties

Visual observation of RBC suspensions revealed cells with a normal biconcave shape and no presence of aggregation as shown in **Figure 3.2 (A and B)**. RBC aggregation, although weak, is commonly observed in the whole blood of rats due to the presence of the macromolecule fibrinogen [87]. However, the suspension media used in these filtration experiments lacked fibrinogen and thus RBC aggregation was not expected. **Figure 3.2 (C)** shows the 5 μm pores of the filter membrane.

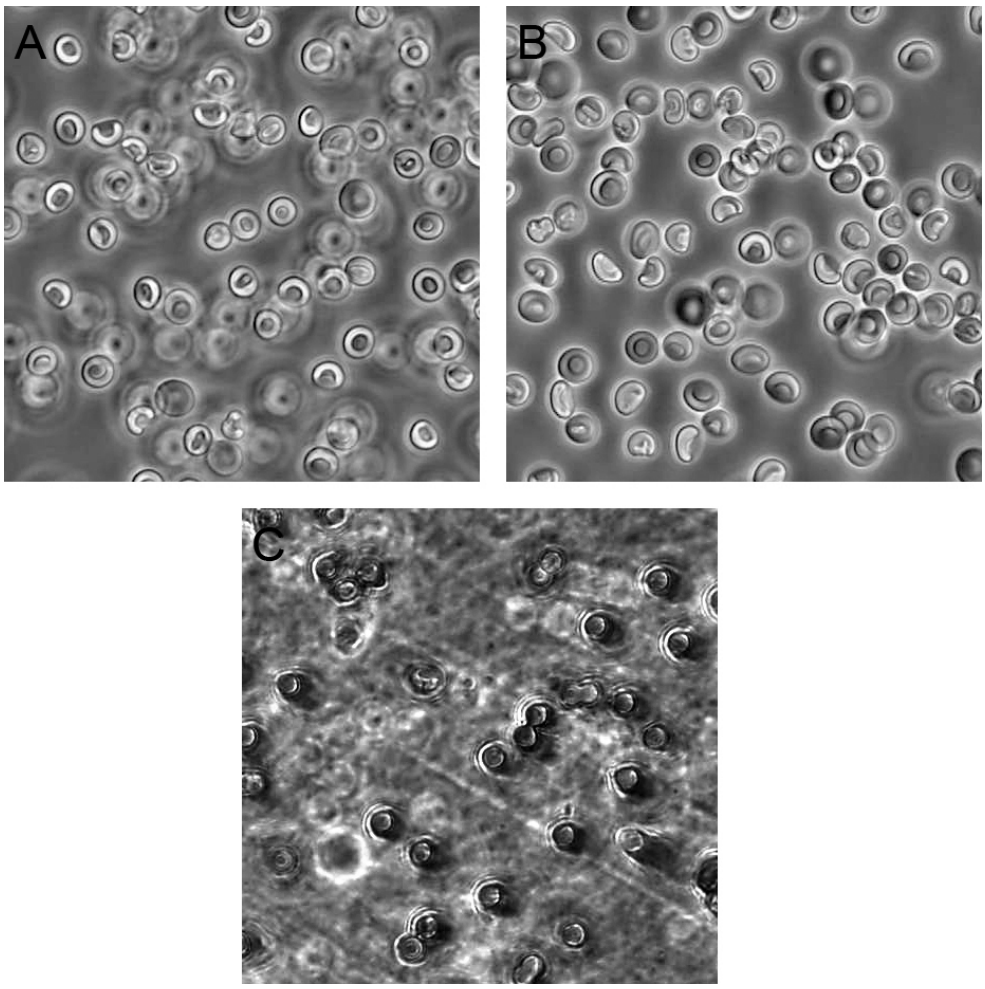

Figure 3.2: Rat red blood cells (before and after filtration) and polycarbonate membrane used in filtration experiments

Photomicrographs show rat RBCs before (A) and after (B) passage through the 5 μm pores of the filter membrane (C) demonstrating that this process did not alter RBC shape.

3.2.3.2 RBC Filtration experiments

Bulk filtration of red blood cell suspensions was performed to study the effects of DRPs on the filterability of RBCs through 5 μm pores. This technique has been previously been employed to investigate the effects of disease [88-90] and various pharmaceuticals [91-93] on the filterability of RBCs.

In this study, dilute RBC suspensions were prepared from fresh whole blood and the effect of a DRP (PEO-4500 at a final concentration of 1 (0.22 nM) and 10 μg/ml (2.2 nM) on the filterability of RBCs was investigated. The RBC suspensions and their corresponding suspension media were drawn through a 5 micron filter under 20 cm H_2O of negative pressure. A RBC Relative Filtration Index (RFI) was determined to be the ratio of the flow rates of a cell suspension (Q) to its corresponding suspension medium (Q_0). A statistically significant increase in RFI was found in normal RBC suspensions containing PEO-4500 (by 13%, $p<0.01$, 1 μg/ml (0.22 nM), n = 24 and 29%, $p<0.001$, 10 μg/ml (2.2 nM), n = 25) when compared to RBCs suspended in the buffer solution (n = 24) (**Figure 3.3**). No difference in RFI was observed in normal blood suspensions containing PEO-200 (10 μg/ml (50 nM), n = 14) compared to RBCs suspended in buffer (**Figure 3.3**). An increase in RFI signifies an increase in RBC filterability. A lack of an effect of PEO-200 on RFI suggests that the increase observed in RFI after the addition PEO-4500 was unlikely related to a chemical effect on the RBCs since PEO-200 and PEO-4500 are built from the same monomer and thus chemically similar except in molecular weight. The increase in RFI of the RBC suspensions observed after the addition of PEO-4500 is most likely related to a change in the extensional flow of the suspensions through the 5 μm pores of filter membrane. The flow of both the RBCs and the viscoelastic polymers through these constrictions

is highly dependent on both the viscous and elastic forces imparted on the fluid as they pass through the constriction. Leyrat-Maurin et al. [94] demonstrated theoretically that as a RBC passes through a filter membrane pore, it recoils due to the elastic properties of its membrane and effectively aspirates fluid downstream of the pore. As the elastic modulus increases, this aspiration becomes more efficient. It may be likely that the same phenomenon occurred through the addition of PEO-4500. Although at low concentrations, the addition of these viscoelastic macromolecules would bring to a strictly viscous fluid (isotonic saline) some elasticity. As with the RBC model, the aspiration of fluid through the constrictions would increase and become more efficient. This would effectively help to aspirate the RBCs through the filter pores as well. This is confirmed through the increase in RFI by increasing the polymer concentration and thus the elasticity of the suspension fluid. Since PEO-200 is not viscoelastic, there was observed effect. It may also be possible that this phenomenon lead to better organization or better trafficking of RBCs as they passed through the 5 μm pores of the filter membrane.

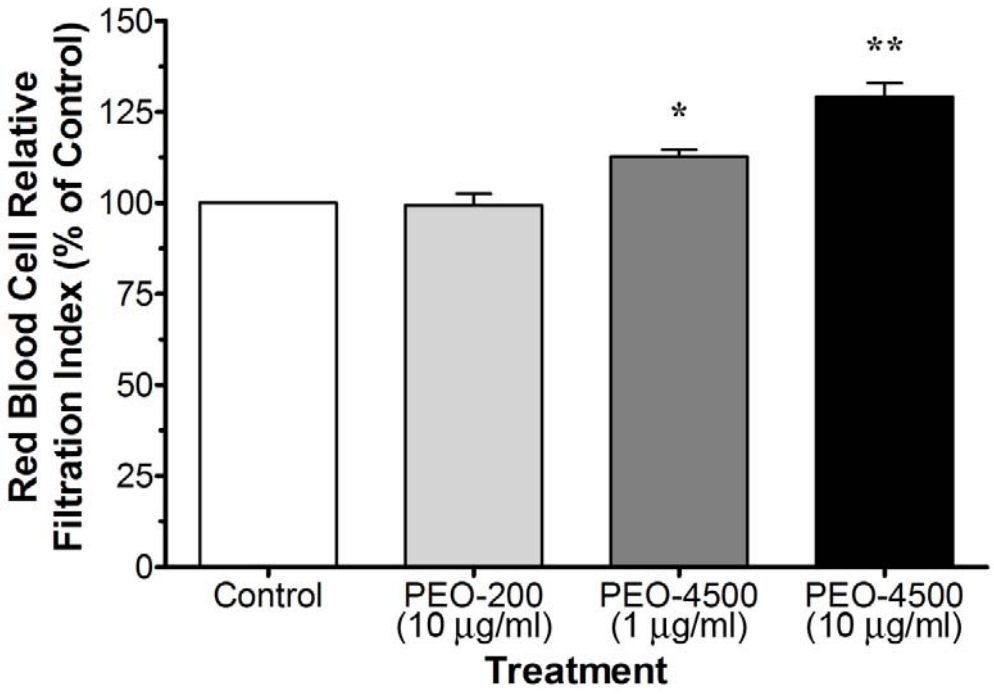

Figure 3.3: DRP effect on red blood cell filterability

Observed increase in the Red Blood Cell RFI of normal RBC suspensions containing PEO-4500 (by 13%, * - $p<0.01$, 1 µg/ml (0.22 nM), n = 24 and 29%, ** - $p<0.001$, 10 µg/ml (2.2 nM), n = 25) when compared to RBCs suspended in buffer solution alone (PBS + 1% BSA, n = 24). No difference in RFI was observed in normal blood suspensions containing PEO-200 (10 µg/ml (50 nM), n = 14) compared to RBCs suspended in buffer. Results expressed as Mean ± SE. An increase in RFI signifies an increase in RBC filterability.

The sensitivity of the filtration technique employed in these experiments was further tested by examining the filterability of RBCs rigidified by incubation with glutaraldehyde. These experiments also tested the ability of DRPs to enhance the filterability of RBCs whose deformability was decreased artificially in order to mimic the RBCs seen in some diseases where deformability is impaired. The feasibility of measurement techniques for distinguishing differences in RBC deformability is sometimes evaluated using glutaraldehyde fixed cells [95, 96]. **Figure 3.4** shows that the RFI of glutaraldehyde-treated RBC suspensions was 25% lower ($p < 0.001$, n = 14) than the RFI of normal (un-treated, n = 24) RBCs. The addition of PEO-4500 (10 µg/ml (2.2 nM)) to the hardened RBC suspensions caused a 34% increase ($p < 0.001$, n = 14)

in the RFI of glutaraldehyde-hardened RBCs which brought the RFI of these suspensions to within 1% of the RFI of the normal RBC suspensions prior to the addition of PEO-4500 (**Figure 3.4**). The 34% increase in RFI that was observed after the addition of PEO-4500 (10 μg/ml (2.2 nM)) to the hardened RBC suspensions was very similar to the 29% increase in RFI that was observed after the addition of the same concentration of PEO-4500 to the normal (un-treated) RBC suspensions.

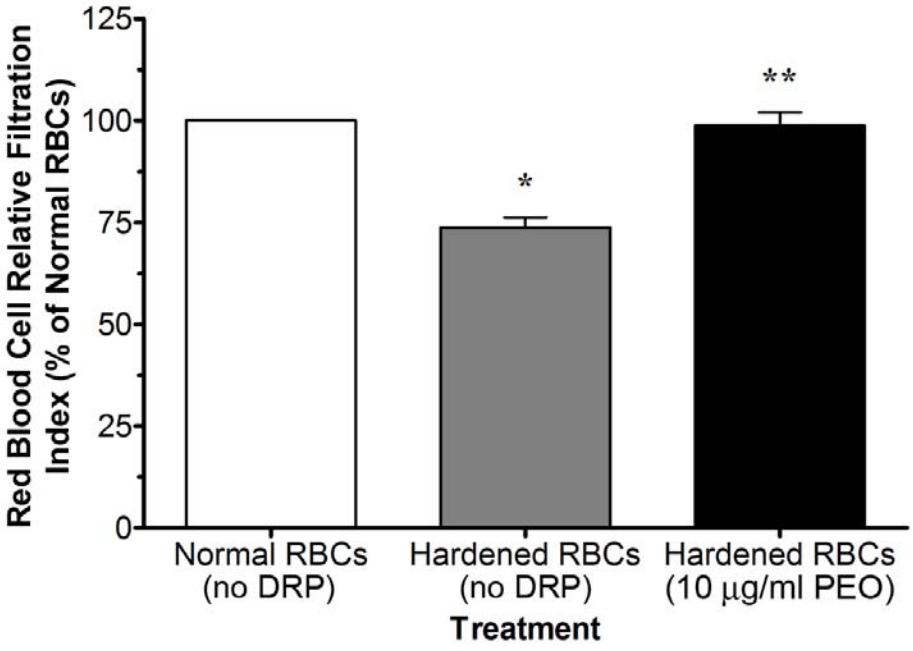

Figure 3.4: DRP effect on the filterability of glutaraldehyde-hardened RBCs

Hardening of RBCs with glutaraldehyde (0.015%) resulted in a 25% decrease (* - $p < 0.001$ vs. Control, n = 14) in RFI compared to the RFI of normal (un-treated, n = 24) RBCs. The addition of PEO-4500 (10 μg/ml (2.2 nM)) to the hardened RBC suspensions caused a 34% increase (** - $p < 0.001$ vs. Hardened RBCs without DRP, n = 14) in the RFI of glutaraldehyde-hardened RBCs. Results expressed as Mean ± SE. An increase in RFI signifies an increase in RBC filterability.

In these filtration experiments, the rat RBCs with an average diameter of 7.0 μm had to deform to be able to pass through the straight channel pores with a diameter of 5.0 μm. This process is very similar to a normal RBC passing through the smallest capillaries in the vascular

system. Our results signify that the PEO-4500 slightly increased the filterability of RBCs and facilitated their flow through the filter channels by some unknown mechanism which may include in part the direct DRP effect on the RBC deformability. The filtration technique provides insight into the possible mechanisms of DRPs in the circulation system. However, this interpretation does not go without its limitations. The results of the filtration technique can be significantly affected by the presence of white blood cells and platelet aggregates which can clog the filter pores. In this study, this potential artifact was minimized by preparing RBC suspensions with a significantly lower hematocrit. To further study the ability of DRPs to enhance RBC deformability, a state of the art viscoelastometer to directly measure the elasticity of RBCs along with the whole blood viscosity was employed.

3.3 VALIDATION OF USING A VISCOELASTICITY ANALYZER TO DETERMINE DISSIMILARITIES AND ALTERATIONS IN THE RHEOLOGICAL PROPERTIES OF ANIMAL BLOOD

3.3.1 Introduction

The results of Section 3.2 suggest that DRPs have some effect on enhancing the filterability of RBCs where cells with an average diameter of 7.0 μm had to deform to be able to pass through the straight channel pores with a diameter of 5.0 μm. The mechanism behind DRPs ability to enhance RBC filterability still remains unknown. Further tests were performed to examine the effects of DRPs on the viscoelasticity of blood from which we may infer if DRPs have an effect of the deformability of RBCs and further explain the results obtained in Section 3.2. In this

section, we tested the feasibility of using measurements of viscoelasticity of animal blood as a sensitive standard method of evaluation of changes in RBC deformability. This evaluation was based on the fact that both viscosity and elasticity of blood significantly depend on RBC deformability. Portions of this work have been previously published elsewhere [97].

3.3.2 Methods

3.3.2.1 Study populations

Bovine:

Bovine blood was collected at slaughter from healthy cows after transection of the carotid and jugular vessels into plastic bottles containing 10 IU sodium heparin/ml blood. Blood was also drawn from the jugular vein of donor animals by sterile venipuncture into plastic blood collection bags (Baxter, Deerfield, IL) with 10% anticoagulant citrate dextrose (ACD; Gambro BCT, Lakewood, CO). All blood was twice filtered through 40 μm pore size filters (Pall Biomedical, SQ40S, Fajardo PR) on the day of collection to remove any large white blood cell (WBC) and platelet aggregates or other material, and gentamicin (0.25 g/L (0.52 mM); American Pharmaceutical Partners, Schaumburg, IL) was added to prevent bacterial growth.

Ovine and Porcine:

Samples of ovine and porcine blood were obtained via sterile venipuncture and collected into plastic K_2EDTA tubes (Becton Dickinson, La Jolla, CA). Samples of ovine blood anticoagulated with sodium citrate were also obtained from Cleveland Scientific Inc. (Bath, OH).

RBCs were observed using a light microscope to examine their morphology and confirm the absence or presence of RBC aggregation. Due to the multiple origins of these blood samples, all samples were stored at 4°C overnight and tests were conducted the day following blood collection.

3.3.2.2 Hematocrit measurement and standardization

The whole blood hematocrit (Ht) was measured by micro-hematocrit centrifugation (IEC MB Centrifuge, International Equipment Company, Needham Heights, MA) at 13,000 x g for 5 minutes and adjusted by the addition and removal of autologous plasma. Autologous plasma was obtained by centrifuging a separate sample tube at 2200 x g for 15 minutes (CR412, Jouan, Winchester, VA) and added to blood samples to lower Ht. Ht was increased by centrifuging whole blood at 500 x g for 15 minutes, aspirating a calculated volume of plasma and then gently mixing the sample to resuspend the RBCs. Ht was adjusted to a standard level of 45-48% except in experiments in which the dependence of viscoelasticity on Ht was investigated. In these experiments, the Ht in bovine blood was adjusted to 20, 30, 40, 45 and 50%. Ovine and porcine blood viscoelasticity was measured at Ht values of 30, 45, 50 and 55% and 30, 40 and 50%, respectively.

3.3.2.3 RBC deformability modification methods

RBC deformability was altered using methods of fluid shear and heat exposure. The aim of these studies was to demonstrate, using common procedures applied for the modification of RBC deformability (heat treatment or cell modification by shearing blood), that measurements of changes in bovine blood viscoelasticity are detectable and that this method may have applicability in assessing changes in RBC deformability.

Heat exposure:

Using a modified method of that previously described by Nash and Meiselman, RBC deformability was altered by heat exposure [98]. After adjustment to the standard Ht value of 46.2 ± 1.3% , bovine blood was placed in a plastic-walled conical centrifuge tube, immersed in a water bath at a temperature of 50°C for 30 minutes, after which the tubes were then removed and allowed to cool prior to measurement of viscoelasticity.

Shear exposure:

A Wells-Brookfield Cone/Plate viscometer (DVIII+, Middleboro, MA) with CPE-41 cone (cone radius = 2.4 cm, cone angle = 3°) was used to expose a 2 ml bovine blood sample to a uniform mechanical shear stress of 2.3 Pa for 60 minutes at 25°C. Blood Ht was adjusted to 46.4±1.9%. Following shear exposure, samples were collected for viscoelasticity measurement.

3.3.2.4 Measurement of viscoelasticity

Whole blood viscoelasticity was determined using a Vilastic-3 Viscoelasticity Analyzer (Vilastic Scientific Inc., Austin, TX) with a stainless steel capillary measurement tube (0.0512 cm inner radius, 6.179 cm length) at a constant temperature of 25°C. The blood samples were exposed to sinusoidally oscillating flow at a fixed frequency of 2 Hz at logarithmically spaced shear strains ranging from 2 to 20. These strains were chosen to reflect the transition from disaggregation to deformability effects [62]. Due to the lack of aggregation in bovine and ovine blood [99], the viscoelasticity of bovine and ovine blood was not studied at shear strains less than 2. All blood samples were gently mixed for 5-10 seconds before being placed in the device's sample cup (0.5 ml) to allow for adequate mixing. The sample was then loaded in the capillary measurement tube

and the blood was allowed to equilibrate for 30 seconds before testing commenced. Measurements of viscoelasticity were also performed at various temperatures of 15, 20, 25, 30, 35 and 45°C for investigation of the dependence of bovine blood (Ht=45.9±1.5%) viscoelasticity on temperature. Since the blood was exposed to a 45°C temperature for at most 2 min, we did not anticipate any detrimental effects of this relatively high temperature on RBC deformability. As mentioned above, an increase in both blood viscosity and elasticity without changes in Ht and plasma viscosity would signify a decrease in RBC deformability and vice versa.

3.3.2.5 Data Analysis

Results are expressed as the Mean ± standard error of the mean (SE). Any elasticity value which fell below 1/60th of the viscosity value at the same shear rate was disregarded as recommended by the device manufacturer as data which was outside the device's acceptable range of error. Viscoelasticity measurements of blood subjected to thermal and shear exposure were normalized to the viscoelasticity of blood prior to exposure on the corresponding day the experiment was performed. A regression analysis for the data on the viscoelastic dependence on Ht and temperature in bovine blood was performed at strains of 2.4, 5.6 and 13.0 using Microsoft Excel XP (Microsoft Corp., Seattle, WA). Student's un-paired t test was used to compare normalized blood data before and after heat and shear exposure. A $p < 0.05$ was considered to be statistically significant.

3.3.3 Results and Discussion

3.3.3.1 Findings of microscopic observation

Visual observation of bovine and ovine RBCs using a light microscope revealed cells with a normal biconcave shape and no presence of aggregation while porcine RBCs had a normal biconcave shape with the presence of cell aggregation. These are typical findings of blood from these species [99, 100].

3.3.3.2 Comparison of viscoelasticity of bovine, ovine and porcine blood at 30% hematocrit

A comparison of the viscosity (**Figure 3.5, top**) and elasticity (**Figure 3.5, bottom**) of bovine (n=5), ovine (n=7) and porcine (n=5) blood samples at 30.2±0.4%, 29.7±0.5% and 29.6±0.2% Ht was performed at shear rates from 40 to 220 s^{-1}. The percent decrease in viscosity between a shear rate of 40 and 160 s^{-1} was 2.9% for bovine blood, 4.5% for ovine blood, and 14.7% for porcine blood. The percent decrease in elasticity between these shear rates was 51.1% for bovine blood, 69.9% for ovine blood, and 77.9% for porcine blood.

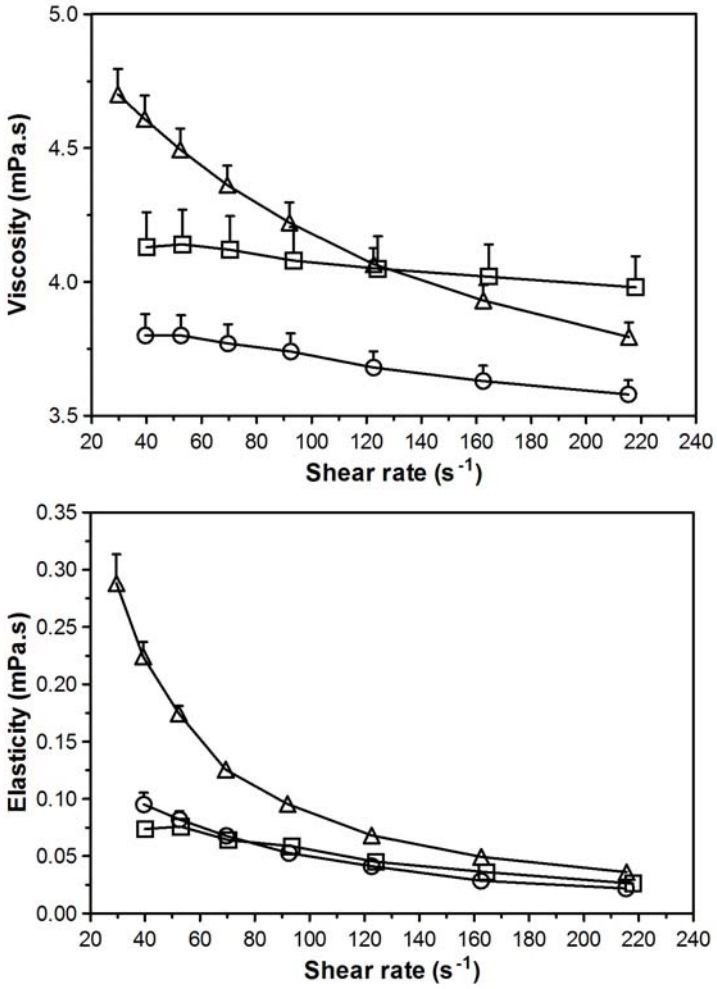

Figure 3.5. Dependence of viscosity and elasticity of bovine, ovine and porcine on shear rate at 30% hematocrit

Comparison of viscosity (top) and elasticity (bottom) of bovine (square, n=5), ovine (circle, n=7) and porcine (triangle, n=5) whole blood samples at 30% hematocrit at shear rates ranging from 40 to 220 s^{-1}

3.3.3.3 Bovine blood viscoelasticity at multiple hematocrit values

Viscosity and elasticity (**Figure 3.6, top** and **bottom,** respectively) measurements were performed at shear rates ranging from 30 to 220 s^{-1} using bovine blood at Ht values of 20.2±0.3% (n=6), 30.2±0.4% (n=5), 41.2±0.5% (n=6), 46.2±0.4% (n=9) and 49.7±0.3% (n=7). The dependence of viscosity and elasticity on shear rate became more evident with increasing values of Ht with viscosity and elasticity being almost independent of shear rate at a Ht of 20% while at the highest Ht, 50%, bovine blood viscosity decreased 18.5% from 8.1±0.3 mPa·s at the lowest shear rate of 30 s^{-1} to 6.6±0.2 mPa·s at the highest shear rate of 220 s^{-1} and bovine blood elasticity decreased 80.0% from 0.5±0.02 mPa·s at 30 s^{-1} to 0.1±0.01 mPa·s at 220 s^{-1}.

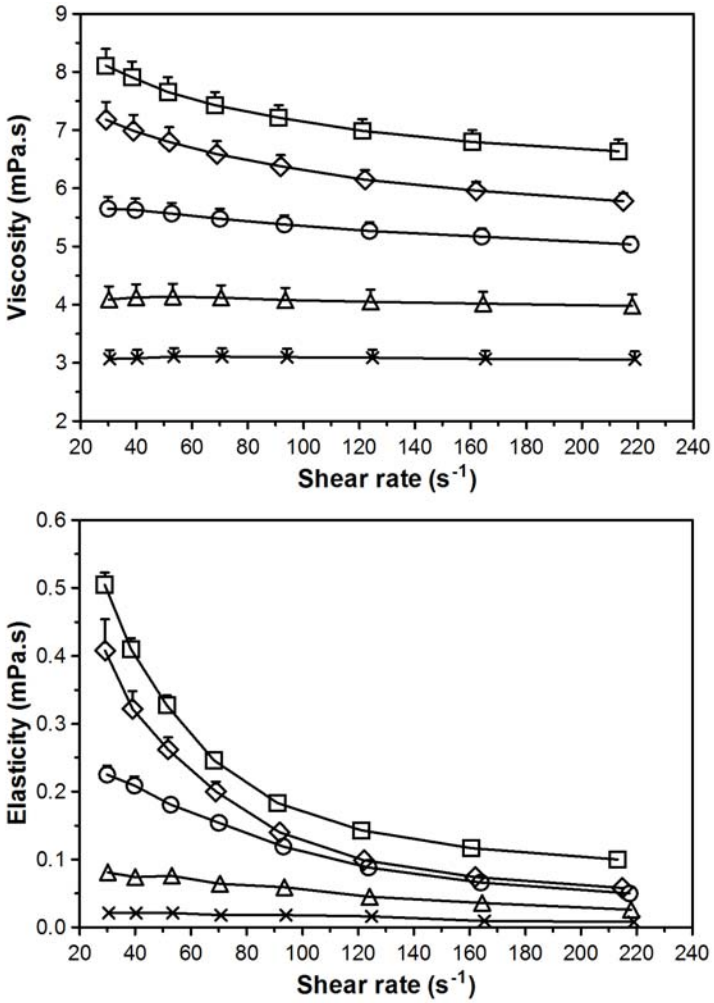

Figure 3.6. Effect of bovine blood hematocrit on the dependence of viscosity and elasticity on shear rate

Viscosity (top) and elasticity (bottom) of bovine blood as a function of shear rate at hematocrit values of 20 (cross, n=6), 30 (triangle, n=5), 40 (circle, n=6), 45(diamond, n=9), and 50% (square, n=7).

Equations obtained from a non-linear regression analysis of viscosity and elasticity values as functions of Ht at three shear strains (2.4, 5.6, and 13.0) which represent low, middle and high shear rate regions are shown in **Table 3.1**. These equations allow recalculating blood viscosity and elasticity of blood samples to a standard Ht and thus determining changes in these parameters which are not related the changes in the concentration of RBCs.

Table 3.1: Equations for viscosity (η′) and elasticity (η") of bovine blood as functions of hematocrit at Strains of 2.4, 5.6 and 13

Strain	Viscosity and Elasticity (mPa•s)	Correlation coefficient
2.4	$\eta' = 1.67e^{3.1H}$	$R^2 = 0.996$
	$\eta'' = 4.91\ H^3 - 0.189\ H^2 - 9.43E\text{-}2\ H + 1E\text{-}3$	$R^2 = 0.989$
5.6	$\eta' = 1.72e^{2.9H}$	$R^2 = 0.999$
	$\eta'' = 1.36\ H^2 - 0.174\ H + 9E\text{-}4$	$R^2 = 0.998$
13	$\eta' = 1.75e^{2.7H}$	$R^2 = 0.999$
	$\eta'' = 0.572\ H^2 - 0.067\ H + 4E\text{-}4$	$R^2 = 0.977$

H is hematocrit as a fraction

3.3.3.4 Ovine blood viscoelasticity at multiple hematocrit values

The dependence of viscosity and elasticity (**Figure 3.7, top** and **bottom,** respectively) on shear rate of ovine blood was compared at Ht values of 29.7±0.5% (n=5), 45.0±0.0% (n=4) and 55.5±0.5% (n=3) at shear rates of 30 to 220 s^{-1}. Ovine blood also demonstrated an increase in the dependency of viscosity and elasticity on shear rate with increasing Ht values. At a Ht of 30%, viscosity and elasticity are almost independent of shear rate while at a Ht of 55%, ovine blood viscosity decreased 20.6% from 10.7±1.1 mPa·s at the lowest shear rate of 30 s^{-1} to 8.5±0.8 mPa·s at the highest shear rate of 220 s^{-1} and ovine blood elasticity decreased 83.6% from 1.22±0.3 mPa·s at 30 s^{-1} to 0.2±0.03 mPa·s at 220 s^{-1}.

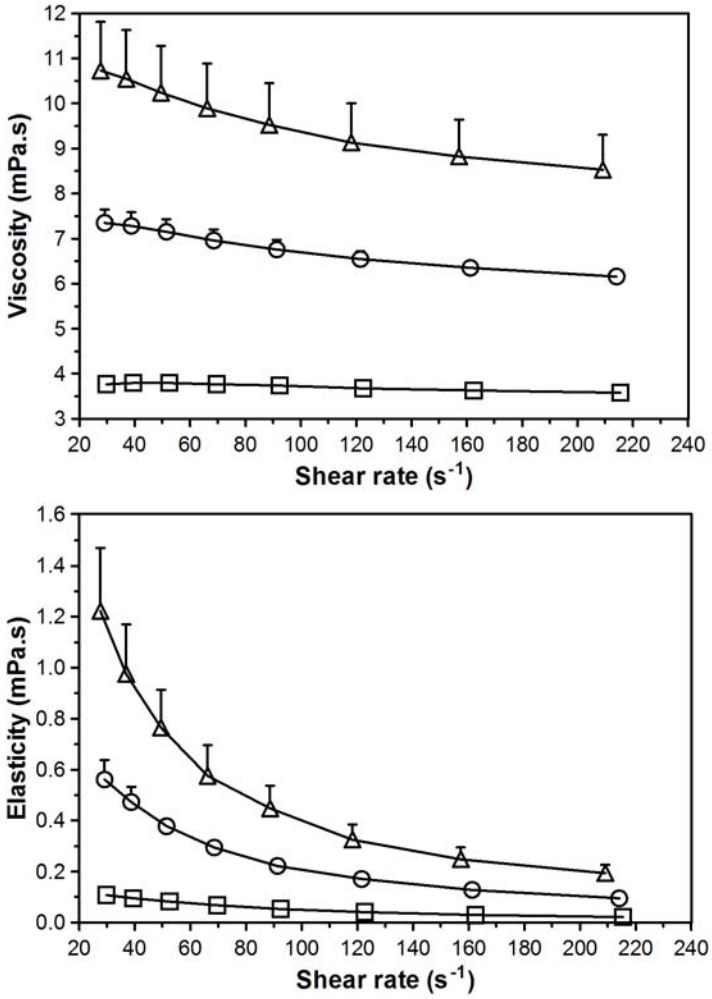

Figure 3.7: Effect of ovine blood hematocrit on the dependence of viscosity and elasticity on shear rate

Viscosity (top) and elasticity (bottom) of ovine blood as a function of shear rate at hematocrit values of 30 (square, n=7), 45 (circle, n=4) and 55% (triangle, n=3).

3.3.3.5 Comparison of viscoelasticity of bovine and porcine blood at ~50% hematocrit

Viscosity (**Figure 3.8, top**) and elasticity (**Figure 3.8, bottom**) of bovine (n=7), ovine (n=4) and porcine (n=4) blood samples at 49.7±0.3%, 50.0±0.0% and 49.8±0.3% Ht, respectively, were compared at shear rates from 20 to 220 s^{-1}. At this Ht, there is a more pronounced non-Newtonian behavior in all blood samples. Bovine blood demonstrated a 14.0% decrease in viscosity between shear rates of 40 and 160 s^{-1}, ovine blood exhibited a 13.6% decline and porcine blood exhibited a 34.0% decline. The percent change in elasticity at these shear rates was 71.4% for bovine blood, 75.9% for ovine blood and 90.3% for porcine blood.

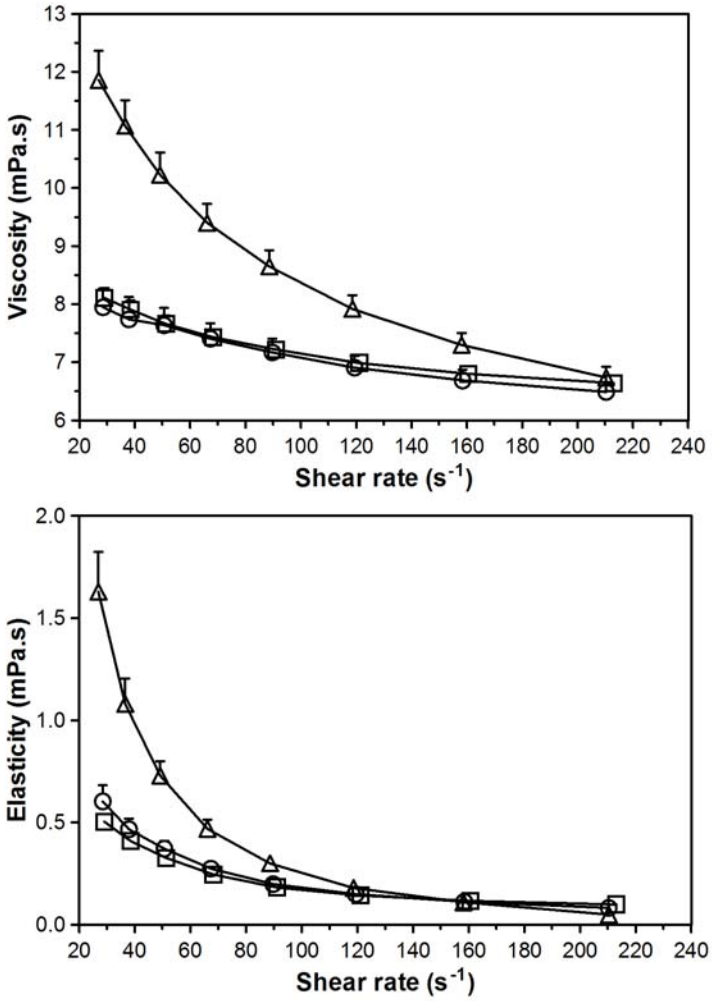

Figure 3.8. Dependence of viscosity and elasticity of bovine, ovine and porcine on shear rate at 50% hematocrit

Comparison of viscosity (top) and elasticity (bottom) of bovine (square, n=7), ovine (circle, n=4) and porcine (triangle, n=4) whole blood samples at 50% hematocrit at shear rates ranging from 40 to 220 s^{-1}.

3.3.3.6 Bovine blood viscoelasticity measured at multiple temperatures

Viscosity (**Figure 3.9, top**) and elasticity (**Figure 3.9, bottom**) of bovine blood at Ht 45.9±0.5% were measured at temperatures of 15 (n=2), 20 (n=2), 25 (n=10), 30 (n=2), 35 (n=2), and 45°C (n=1) at shear rates ranging from 30 to 220 s^{-1}. **Figure 3.9** shows the dependence of viscosity (**top**) and elasticity (**bottom**) values on both shear rate and the temperature. At low shear rates (30 s^{-1}), the viscosity of blood measured at 15°C was over 96% higher than the viscosity of blood measured at 45°C while the difference between elasticity values was about 79%. At high shear rates (220 s^{-1}), the viscosity of blood measured at 15°C was 144% higher than the viscosity of blood measured at 45°C while elasticity was 350% higher which points to a significant increase in rigidity of RBCs with a decrease in temperature.

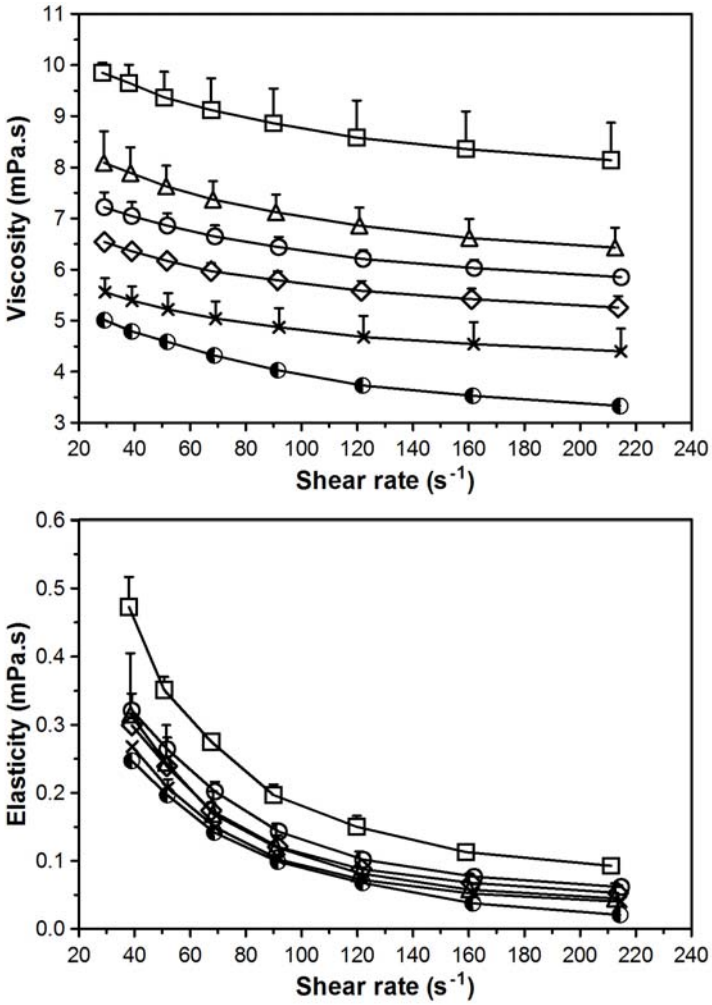

Figure 3.9. Effect of temperature on the dependence of viscosity and elasticity on shear rate

Viscosity (top) and elasticity (bottom) of bovine blood as a function of shear rate at temperatures of 15 (square, n=2), 20 (triangle, n=2), 25(empty circle, n=10), 30 (diamond, n=2), 35 (cross, n=2) and 45° C (half-circle, n=1).

Equations obtained using a non-linear regression analysis of viscosity and elasticity as functions of temperature at three shear strains (2.3, 5.5, and 13.0) are presented in **Table 3.2**. Both blood viscosity and elasticity are dependent on temperature, therefore these equations may be used to recalculate these parameters based on a standard temperature and will allow determination of differences in these parameters unrelated to temperature.

Table 3.2. Equations for viscosity (η′) and elasticity (η") of bovine blood as functions of temperature at Strains of 2.3, 5.5 and 13

Strain	Viscosity and Elasticity (mPa•s)	Correlation coefficient
2.3	$\eta' = 53.18\ T^{-0.624}$	$R^2 = 0.991$
	$\eta'' = 2.38\ T^{-0.538}$	$R^2 = 0.851$
5.5	$\eta' = 56.94\ T^{-0.675}$	$R^2 = 0.990$
	$\eta'' = 1.03\ T^{-0.530}$	$R^2 = 0.753$
13	$\eta' = 65.23\ T^{-0.752}$	$R^2 = 0.976$
	$\eta'' = 0.926\ T^{-0.815}$	$R^2 = 0.753$

T is blood temperature in Centigrade

3.3.3.7 Bovine blood viscoelastic shear rate dependence following heat and shear-induced damage

The viscoelastic properties of bovine blood with Ht (45.9±0.5%) were evaluated before and after exposure to heat and shear stress. The results of the viscosity and elasticity of blood samples after exposure to thermal (n=7) and mechanical stress (n=5) were normalized to the viscosity and elasticity of blood before exposure (**Figure 3.10, top** and **bottom,** respectively). After heat exposure, the average increase in blood viscosity was 11.7±0.4% and the average increase in blood elasticity was 47.7±10.9% from baseline. The increase in viscosity was statistically significant at shear rates of 70 to 220 sec^{-1} ($p<0.05$) and the increase in elasticity was statistically significant at shear rates of 50 to 160 sec^{-1} ($p<0.05$). In blood exposed to mechanical stress, the

average increases in the viscosity and elasticity were 4.9±0.4% and 6.6±2.8%, respectively. The viscosity increase observed in the sheared blood was statistically significant at shear rates of 50 to 220 sec^{-1}. The sheared blood elasticity was statistically significantly higher at shear rates of 90 to 120 sec^{-1}. **Figure 3.11** (**top**) shows an example of the typical dependence of viscosity on shear rate of blood with Ht 47.5% before and after exposure to thermal and mechanical stress. In this experiment, the viscosity and elasticity of blood after shear exposure increased 4.6±0.3% and 10.0±2.0% respectively. After heat exposure, the average increase in viscosity and elasticity of this blood was 26.6±0.8% and 54.9±8.3%, respectively. **Figure 3.11** (**bottom**) shows the changes in blood elasticity at the highest shear rates.

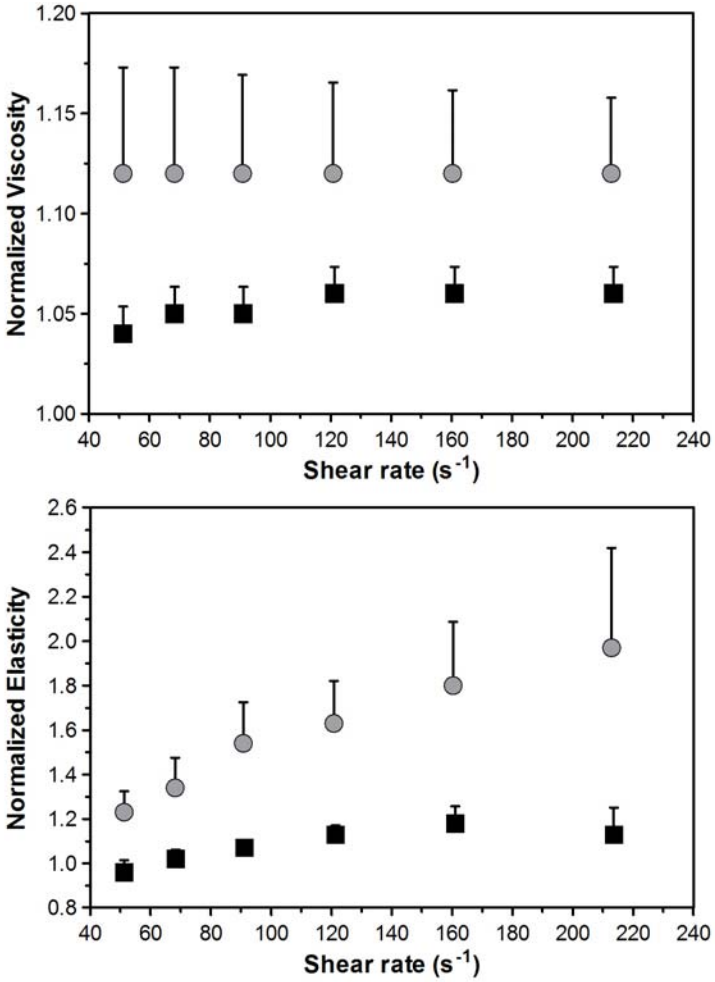

Figure 3.10. Viscosity and elasticity of bovine blood after heat and shear exposure normalized to control

Viscosity (top) and elasticity (bottom) of bovine blood normalized to the viscosity and elasticity of blood prior to exposure to heat (circles, n=7) and mechanical stress (squares, n=5) on the day the experiment was performed.

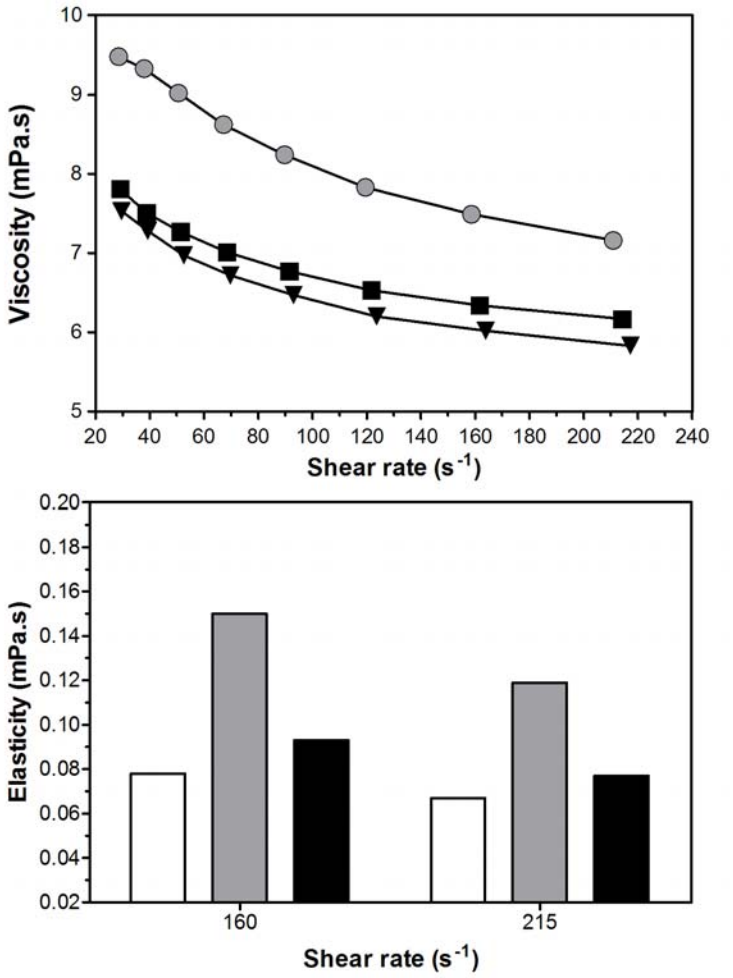

Figure 3.11. Effect of heat and shear exposure on the viscosity and elasticity of bovine blood

The viscosity (top) and elasticity (bottom) of bovine blood before (triangle (top), white bar (bottom)) and after exposure to heat at 50°C for 30 minutes (circle (top), gray bar (bottom)) and after exposure to a 2.3 Pa shear stress for 60 minutes (square (top), black bar (bottom)). Since the difference in the elasticity values is an order of 10, this parameter is shown at two the highest applied shear rates to clarify the dissimilarity in elasticity values before and after exposure.

3.3.4 Discussion

In these studies we tested whether measurements of viscoelasticity of animal blood would provide a sensitive standard method of evaluation of changes in RBC deformability. The ultimate goal was to use this technique to examine the hypothesis that the intravascular action of DRPs is directly related to an effect on RBC deformability. The use of this technique was based on the fact that both viscosity and elasticity of blood significantly depend on RBC deformability. The deformability of erythrocytes was previously shown to be impaired in many pathological states. Therefore, measurements of blood viscoelasticity could provide quantitative and fast assessment of RBC deformability status.

Previous studies have investigated and reviewed the effects of hematocrit, temperature, plasma proteins and shear rate on the viscosity [45-48, 51, 59, 61, 100-108] and viscoelasticity [53, 62, 98, 104, 109-120] of human adult and pediatric blood as well as that of several other mammalian species including some of those studied herein. These studies demonstrated a varying degree of non-linear dependence of both blood viscosity and elasticity on hematocrit, temperature, plasma protein concentration and shear rate in all species studied. Conventional rheometers (rotational cone/plate and Couette) provided most of the initial data on the effects of temperature, shear rate, hematocrit and level of plasma proteins on human adult blood viscosity. These classical studies are typically assembled in comprehensive reviews such as one on normal and pathological human and animal blood viscosity and RBC aggregation and deformability [59]. Blood viscoelasticity as a function of shear rate was first presented by Thurston in 1972 using oscillatory flow at a known frequency in a cylindrical tube [53]. Measurements of flow rate and pressure throughout the cycle allowed calculation of shear rate and shear stress. Since shear

stress and shear rate are out-of-phase in viscoelastic fluids such as blood, a complex viscosity can be written as: $\eta = \eta' - i\eta''$ where η' is viscosity and η'' is elasticity. In a subsequent work, the non-linear dependence of viscoelasticity on hematocrit was studied and a set of equations allowing for recalculation of measured viscoelasticity values to a standard hematocrit were developed for human blood [112]. Long et al. [120] have recently demonstrated the strong dependence of pediatric blood viscoelasticity on hematocrit and found that no correlation existed between patient age and blood viscoelasticity. Most importantly, no statistically significant difference was found between pediatric and adult blood viscosity. A set of viscoelasticity equations was also developed to predict the viscosity and elasticity of pediatric blood given a known hematocrit. In a study of other mammalian species, differences in the viscoelasticity of bovine, ovine and porcine blood have been found but were attributed to a lack of standardization of hematocrit between species [118]. However, this study did demonstrate the overall dependence of these species blood viscoelasticity on shear rate. This work compared viscoelastic properties of bovine, ovine and porcine blood obtained from healthy animals. Blood from these species is readily obtainable in large quantities making them useful for investigating the hypothesis on the DRP effect on RBC deformability. More importantly, although many studies look at the applicability of using DRPs for the treatment of pathologies in rats, pre-clinical studies for these uses would most likely be conducted in large animal models such as those studied here, i.e. porcine. Therefore, rheological characterization of the blood of these species with and without DRPs would play an important role in understanding the mechanisms of the intravascular action of DRPs in these species.

Porcine blood was included in our studies since this blood better simulates human blood due to the ability of porcine RBCs to aggregate and their larger size compared to those of bovine

and ovine blood. This study tested the effect of hematocrit, temperature and heat and shear stress exposure on the viscoelasticity of bovine blood. The latter study demonstrated a statistically significant increase in both viscosity and elasticity in blood after exposure to both mechanical and thermal stresses. Even after exposure of blood to a very low shear stress (2.3 Pa) over 60 min, some changes in RBC deformability, which caused a measurable increase in whole blood viscosity and elasticity, were observed. Therefore, these results confirm that at relatively high levels of hematocrit (~46-47%), bovine blood can provide sensitive measurements of changes in deformability.

The comparative study of blood from three species revealed that at relatively low Ht (30%) both bovine and ovine blood demonstrated an almost Newtonian behavior with little change in viscosity and elasticity over a wide shear rate range (**Figure 3.5 top** and **bottom**). A 30% Ht was chosen for analysis because it represents the standard physiological hematocrit value for these species [100]. As anticipated, due to the lack of RBC aggregation, bovine and ovine blood viscoelasticity is almost independent of shear rate. Therefore, it seems that measurements of changes in blood viscoelasticity at low Ht values are not practical for evaluation of changes in RBC deformability using bovine or ovine blood. However, even a moderate increase in Ht makes these measurements meaningful and applicable by demonstrating a pronounced dependence of both viscosity and elasticity on shear rate (**Figure 3.6** and **Figure 3.7**). In general, a very significant transition from almost Newtonian to a pronounced non-Newtonian rheological behavior due to an increase in blood Ht was shown in bovine and ovine blood. Porcine blood, however, exhibited non-Newtonian flow behavior even at low Ht values of 29-30% making blood from this species more appropriate for the testing of changes in RBC deformability. Obviously, this difference in rheological behavior between bovine, ovine and

porcine blood is mostly related to the ability of porcine RBCs to aggregate and to the larger porcine RBC diameter (~7 μm) compared to bovine (~5.5 μm) or ovine (4.5 μm) RBCs. These differences result in porcine blood producing a significant increase in the magnitude of change between low and high shear rate viscosity and elasticity compared to that in bovine and ovine blood as seen in **Figure 3.5**. Brookshier and Tarbell previously demonstrated that porcine blood viscoelasticity was quite similar to that of human blood at a broad range of shear rates (1-1000 s^{-1}) and Ht values (20%-80%) [121]. Despite these advantages, bovine blood tended to be more readily available and was used more extensively in the rheological studies performed in this dissertation. Based on the studies in this section, the samples of bovine blood collected for use in viscoelasticity studies were adjusted to a standard Ht of 40% or higher.

Another benefit of using the Vilastic-3 viscoelastometer used in these studies is the very small sample volume required for the measurement of viscoelasticity; an important factor when working with blood samples from rats. These tests require at most 0.7 ml of blood (0.05 ml for hematocrit, 0.5 ml for the test sample, and about a 0.2 ml loss to the walls of sample tube and transfer pipette).

Therefore, assessment of changes in RBC deformability by measurement of blood viscoelasticity would be possible using this technique.

3.4 *IN VITRO* DRP EFFECT ON THE VISCOELASTICITY OF WHOLE BLOOD OF NORMAL AND DIABETIC ANIMALS

3.4.1 Introduction

In Section 3.3, experiments were performed which confirmed the ability of using measurements of viscoelasticity of animal blood as a sensitive standard method of evaluation of changes in RBC deformability. This evaluation was based on the fact that both viscosity and elasticity of blood significantly depend on RBC deformability.

Diabetes mellitus has been associated with several hemorheological abnormalities. Rheological studies of blood from patients with diabetes have shown increased blood viscosity [54, 55] and reduced RBC deformability [56-58]. Since RBCs are roughly 8 μm in diameter and the smallest capillaries are ~3-5 μm, the cells must deform a substantial amount to be able to pass throughout the microcirculation. Consequently, a small reduction in RBC deformability can significantly compromise the number of functioning capillaries and hence oxygen delivery, extraction of products of metabolism from the tissue, etc. Diamantopoulos et al reported that the deformability of rat RBCs was significantly impaired in a streptozotocin (STZ)-induced experimental model of diabetes and preceded the manifestation of diabetic microangiopathy [122]. Golub et al. demonstrated that the intravenous injection of DRPs into rats with alloxan-diabetes increased the number of functioning capillaries to an order close to that of normal animals [17]. It is possible that this phenomenon occurred through the enhancement of RBC deformability. The results of Section 3.2 suggested that the addition of DRPs to normal and glutaraldehyde-treated RBC suspensions enhanced their filterability from which it may be inferred that the deformability of RBCs was increased. Using measurements of viscoelasticity,

studies were performed to evaluate the hypothesis that the presence of DRPs in diabetic whole blood samples would demonstrate enhanced deformability. This work is presented in this section.

3.4.2 Methods

These experiments were completed in two stages. The first stage was the development and maintenance of a rat model of experimental diabetes. The second stage involved the collection of blood samples from the animals with subsequent measurement of their viscoelasticity with and without the addition of DRPs.

3.4.2.1 Animal Care Compliance

The surgical procedures and animal treatments performed in this study were approved by the Institutional Animal Care and Use Committee of the University of Pittsburgh (protocols #0408443, #0108461). All animal care and procedures conformed to the National Institutes of Health Guidelines for the Care and Use of Laboratory Animals.

3.4.2.2 Animals

Male Sprague-Dawley rats (250-300 g, SASCO; Charles River Laboratories, Wilmington, MA) were housed in solid bottom micro-isolator containers and fed rat chow and water *ad libitum* except during fasting periods, 2 hours prior to blood glucose measurements. The animals were allowed a 6-day acclimatization period after delivery before experimental procedures commenced. Animals were housed in plastic animal containers under constant conditions of temperature and light cycling (12 h light-12 h darkness). Bedding was changed daily in order to keep the animals clean and dry.

3.4.2.3 Development and care of a rodent model of diabetes.

Baseline measurements of blood glucose concentration and weight were attained. Subsequently, experimental diabetes mellitus was induced through an intraperitoneal injection of streptozotocin (STZ; 65 mg/kg, freshly dissolved in 0.1 M citrate buffer, pH 4.5) after an ~18 hour fasting period and confirmed by sustained blood glucose levels of 300 mg/dl (16.7 mM) or greater. The age and weight-matched control group received the citrate buffer only. The injectant was sterilized via filter sterilization using a 0.22 μm syringe filter (Millipore).

Blood glucose levels were monitored twice weekly using a OneTouch® FastTake® glucometer (LifeScan, Milpitas, CA) from blood (10 μl) obtained by pricking the tip of the tail with a fine point lancet. Blood glucose measurements were timed so that they occurred several hours after the start of the 12 hour light cycle. Insulin (3-5 IU/day; Humulin® U; Eli Lilly, Indianapolis, IN) treatment was initiated ~4 weeks after STZ administration and continued throughout the study to reduce mortality and the potential of the animal's developing ketoacidosis. This dose was not enough to normalize blood glucose levels. Body weight was measured several times per week to monitor the health of the animals.

3.4.2.4 Blood collection and sample preparation.

Approximately 4-8 weeks after STZ administration (buffer in control), blood was collected from ten diabetic animals and ten normal animals (non-diabetic) based on the methods described in Section 3.2.2.2. The whole blood hematocrit was measured and adjusted to a standard level of ~40% as previously described in Section 3.3.2.2. The blood samples were then aliquoted into three equal volumes and either PEO-4500 (2.5 mg/ml (0.56 μM)), PMNN (2.5 mg/ml (0.42 μM))

or saline (control) was added in equal volumes to an aliquots to yield final concentrations of 10 μg/ml (1.7 – 2.2 nM) of the DRP.

3.4.2.5 Measurement of viscoelasticity.

Viscoelasticity was measured according to the protocol outlined in Section 3.3.2.4 at shear rates ranging from 20-180 s^{-1} at 24°C.

3.4.2.6 Statistical methods

Results are expressed as the mean ± SD. A repeated measures two-way ANOVA with Bonferroni post hoc test was used to compare the viscosity and elasticity of whole blood of diabetic animals to that of normal animals at each shear rate. The same statistical test was also used to compare the viscosity and elasticity of whole blood of diabetic and normal animals before and after the addition of DRPs. A $p < 0.05$ was considered to be statistically significant.

3.4.3 Results and Discussion

3.4.3.1 Outcomes of development of experimental diabetes in rodents

The development of experimental diabetes was without adverse events. Two days after animals were injected with STZ, blood glucose levels increased to above 300 mg/dl (16.7 mM) and remained at this level until blood was taken and the animals were sacrificed. The animals exhibited the polyuria, polydipsia and polyphagia commonly associated with diabetes mellitus.

3.4.3.2 Results of viscoelasticity measurements

Whole blood was collected from diabetic (n = 10) and non-diabetic (normal; n = 10) rats after a minimum of 4 weeks of diabetes. It has been previously reported that reductions in RBC deformability are seen in as little as 5 days after diabetes inception and that this reduction reaches its lowest value by 15 days [122]. In this study, the viscoelasticity of diabetic and non-diabetic rat blood was measured with and without the addition of DRPs. Both the viscosity and elasticity of the whole blood of diabetic rats was found to be higher than that of non-diabetic rats signifying a decrease in RBC deformability (**Figure 3.12**). Although no statistical significance was found, the viscosity and elasticity of the diabetic rat blood was roughly 20.2 ± 3.0% and 43.4 ± 9.0%, respectively, higher than that of non-diabetic rat blood over a shear rate range of 20 to 180 s^{-1}.

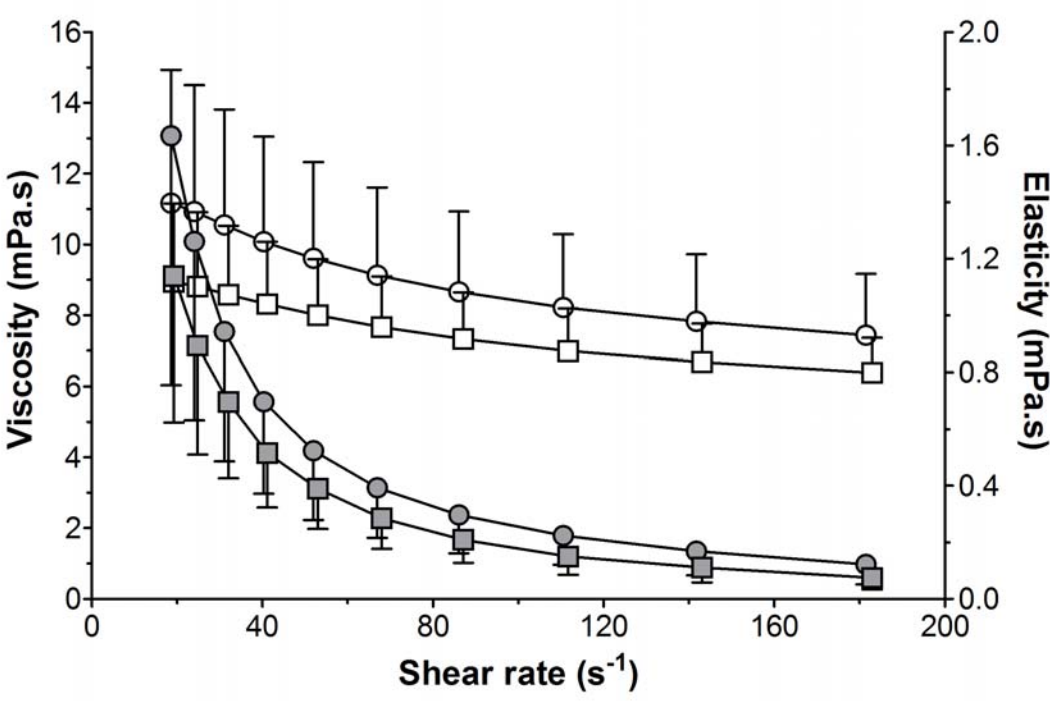

Figure 3.12: Viscosity and elasticity shear rate dependence of diabetic and non-diabetic rat whole blood

The viscosity (open circles) and elasticity (gray circles) of the diabetic rat blood were roughly 20.2 ± 3.0% and 43.4 ± 9.0%, respectively, higher than viscosity (open squares) and elasticity (gray squares) of non-diabetic rat blood over a shear rate range of 20 to 180 s^{-1} signifying a decrease in RBC deformability.

The addition of PEO and PMNN to the diabetic whole blood samples, which showed a moderate increase in viscosity compared to that of the control, resulted in a slight decrease in viscosity. The viscosity of the blood samples at three different shear rates (50, 100 and 150 s^{-1}) is shown in **Figure 3.13**. This suggests that the deformability of the diabetic RBCs was reduced after polymer addition. No noticeable difference was observed in the viscosity of the blood of normal animals after the addition of the two DRPs or in the elasticity of the blood of both the diabetic and normal animals after polymer addition. The absence of measurable DRP effects on the viscosity of normal animals and the elasticity of both diabetic and normal animals is most likely related to the sensitivity of the measurements of the bulk viscosity and elasticity in the whole blood. Additionally, it may also be possible that the effects of DRPs on viscosity and elasticity of

blood in normal and diabetic rats were undeterminable due to artifacts of exposure of rat RBCs to *in vitro* conditions. Rat RBCs are extremely sensitive to their environment. It is well known that the collection of rat blood into sample vials such as Vacutainer® tubes (BD) can result in RBC crenation and undoubtedly introduces error into viscoelasticity measurements. Finally, it is possible that DRPs do not directly affect RBC deformability and all the changes which we have observed (filtration, etc.), were related to their effect on the RBC flow environment. Studies with measurements of single cell deformation using ektacytometry will possibly help to elucidate whether DRPs directly affect RBC deformability.

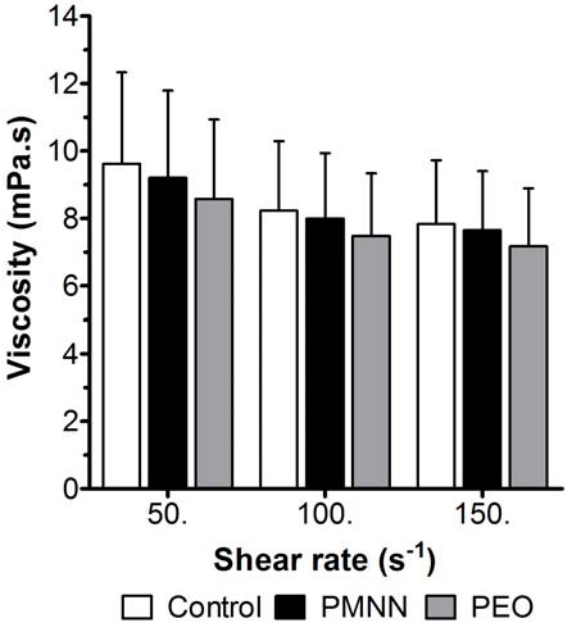

Figure 3.13: Viscosity of whole blood of diabetic animals after the *in vitro* addition of two DRPs

A decrease in blood viscosity is attributed to an increase in the deformability of RBCs after the addition of DRPs to blood. Further studies are necessary to completely understand the beneficial effects of DRPs on RBC flow through capillaries. These results suggest that DRPs may be beneficial in enhancing the deformability of RBCs which has been shown previously to be

markedly decreased in diabetes mellitus. The results of these experiments are significant because the increased blood viscosity, decreased capillary perfusion, and reduced RBC lifespan due to increased splenic sequestration and the pathogenesis of microangiopathy associated with diabetes mellitus may be attributed to impaired RBC deformability. Several therapies have been investigated for the treatment of decreased RBC deformability such as the use of Pentoxifylline (Trental®) [123-125]. However, still no effective standardized treatment exists. Direct management of the clinical conditions causing the reduction in RBC deformability remains to be the effective treatment/prevention. These results suggest that drag-reducing polymers may represent a novel treatment for impaired RBC deformability and the conditions to which it's attributed.

3.5 *IN-VITRO* EFFECT OF D- AND L-GLUCOSE ON BLOOD VISCOELASTICITY BEFORE AND AFTER THE ADDITION OF DRPS

3.5.1 Introduction

In Sections 3.2 and 3.4, we demonstrated that DRPs had the ability to increase RBC filterability and decrease whole blood viscosity, respectively. These results support the hypothesis that the intravascular DRP phenomena are related to a direct effect of DRPs on RBC deformability. The objective of this study was to mimic the reported *in-vivo* reduction in RBC deformability that has been observed in the blood of diabetic patients and which was shown in the studies of Section 3.4, *in-vitro,* by incubating RBC suspensions with varying concentrations of D-glucose and examining the effect of DRP additives on the viscoelasticity of these RBC suspensions. D-

glucose represents a naturally occurring enantiomer of glucose which is used in all cells as energy and a metabolic intermediate. However, during hyperglycemia when high levels of D-glucose are present in the blood, increased non-enzymatic glycosylation of the RBC membranes and intracellular hemoglobin can occur affecting the deformability of the cell and physicochemical properties of the hemoglobin. In turn, this can lead to reduced RBC deformability and increased blood viscosity and elasticity.

3.5.2 Methods

3.5.2.1 Blood collection

Rat (n = 2) and bovine (n = 14) blood samples were collected based on the methods described in Sections 3.2.2.2 and 3.3.2.1, respectively. Additionally, human blood samples (n = 2) were collected. The first sample was banked blood obtained from a volunteer donor that had been collected in ACD (Gambro BCT). IRB approval was not required since informed consent for the use of the blood was obtained at the time of collection. The second sample was drawn from a healthy adult blood donor into glass K_3EDTA Vacutainer® tubes (BD). The rat blood samples and the first human sample were only used to test the effect of increasing D-glucose concentration on hematocrit. The bovine blood samples and the second human blood sample were used to test the effect of increasing D-glucose concentration on hematocrit and on the viscoelasticity of the samples.

3.5.2.2 Blood sample preparation

Bovine blood was centrifuged at 500 x g for 15 minutes after which the plasma and buffy coat were removed. RBCs were then washed two times with PBS with further removal of any residual

buffy coat. RBCs were then resuspended in PBS at a hematocrit of 49 ± 3% (n = 14). It was found in Section 3.3.3.3 that measurements of viscoelasticity of bovine blood were more meaningful at higher hematocrit values due to its small RBC diameter and lack of aggregation. The hematocrit of rat and human whole blood samples was not adjusted. A more detailed explanation for the adjustment and standardization of blood hematocrit is given in Section 3.3.2.2.

Stock solutions of 16 g/dl (0.8 M) D- and L-glucose (Sigma Aldrich) in PBS were prepared and added to the bovine RBC suspensions and to rat and human whole blood to yield final D- and L-glucose concentrations of 200 (11 mM), 400 (22 mM), and 800 mg/dl (44 mM) (saline in control – 0 mg/dl) and incubated at 25 °C for 1 hour. The effect of incubation time and temperature was also investigated with one of the bovine RBC suspension samples. In this experiment, the RBC suspension was incubated for 0, 1 and 24 hours and at incubation temperatures of 4, 25 and 37°C. After the selected time point, the hematocrit of the samples was measured. Osmolality of the suspension media or plasma was obtained by centrifuging the samples at 20,000 x g (5417R: Eppendorf, Westbury, NY), removing the supernatant and then measuring the osmolality by freezing-point depression (Osmette micro-osmometer, Precision Systems, Inc., Natick, Massachusetts, USA). Changes in hematocrit (up – cell swelling, down – cell shrinkage) were used to determine if D-glucose was entering the cells since facilitated diffusion of D-glucose should give way to an iso-osmotic condition. The RBC deformability in a sample of the human whole blood that was used for viscoelasticity measurements was altered by heat exposure using the methods described in Section 3.3.2.3. However, in this experiment the time of heat exposure was 3 minutes.

3.5.2.3 Measurement of viscoelasticity and viscosity.

After a 1 hour incubation of the bovine RBC suspensions (n = 4) and one of the human whole samples with D-glucose at ~25°C, the samples' viscoelasticity was measured according to the protocol outlined in Section 3.3.2.4. An increase in both blood viscosity and elasticity without changes in Ht and plasma viscosity would signify a decrease in RBC deformability and vice versa. After viscoelasticity measurements were performed, the hematocrit and suspension media or plasma osmolality were measured.

3.5.2.4 Statistical methods

Results are expressed as the mean ± SD except for the results on the effect of D-glucose concentration on bovine blood hematocrit and suspension media osmolality in which case they are expressed as mean ± SEM. A repeated measures two-way ANOVA with Bonferroni post hoc test was used to compare the viscosity and elasticity of bovine RBC suspensions with D-glucose to samples without D-glucose. The same statistical test was also used to compare the change in the hematocrit of human, rat, and bovine blood after the addition of D-glucose. A repeated measures one-way ANOVA with Tukey post hoc test was used to compare the change in the bovine RBC suspensions hematocrit before and after the addition of D-glucose as well as the change in the osmolality of the suspension media. A $p < 0.05$ was considered to be statistically significant.

3.5.3 Results and Discussion

In Sections 3.2 and 3.4, DRPs were demonstrated to have the ability to increase RBC filterability and decrease whole blood viscosity, respectively. It was suggested that the intravascular DRP

phenomena was related to a DRP effect on RBC deformability. These experiments were intended to emulate, *in-vitro,* the previously reported alterations in RBC deformability of blood of diabetic patients and that which was demonstrated in rat blood in Section 3.4, by incubating RBC suspensions with varying concentrations of D-glucose. Secondly, they were intended to study the effect of DRP additives on the viscoelasticity of these less deformable RBC preparations.

The effect of D-glucose concentration on the viscoelasticity and viscosity of bovine RBC suspensions (Ht = 51 ± 1%) was measured with a Vilastic-3 viscoelastometer and Wells-Brookfield Cone/Plate rheometer, respectively. The viscosities of the RBC suspensions (n = 4) with (200 (11 mM), 400 (22 mM) and 800 mg/dl (44 mM)) and without (0 mg/dl) D-glucose, measured with the viscoelastometer, are shown in **Figure 3.14 (A)**. At shear rates ranging from 70-285 s^{-1}, the viscosity of the bovine RBC suspensions was statistically significantly higher after increasing the D-glucose concentration to 400 mg/dl (22 mM) ($p < 0.05$ at 70 s^{-1}; $p < 0.01$ from 90-285 s^{-1}; vs. 0 mg/dl). Increasing the D-glucose concentration to 800 mg/dl (44 mM) lead to a further statistically significant increase in viscosity of the suspensions at shear rates ranging from 40-380 s^{-1} ($p < 0.001$; vs. 0 mg/dl). A slight increase in the viscosity of the RBC suspensions was observed at a D-glucose concentration of 200 mg/dl (11 mM). A comparable increase in the viscosity, after the addition of D-glucose at concentrations of 400 (22 mM) and 800 mg/dl (44 mM) to the RBC suspensions, was obtained from the rotational cone/plate viscometer **Figure 3.14(C)**. These results were obtained from a single sample that was used in the viscoelasticity measurements. The slightly higher viscosities acquired from the cone/plate viscometer are due to the fundamental differences between steady flow and oscillatory flow viscosity measurements. In oscillatory flow, minimal microstructural changes occur at the very small strains required to invoke a blood response. In steady flow, the blood's structure is

modified from its resting state due to a continuously increasing strain that increases the relative displacement of neighboring cell groups [64]. No discernible difference was observed in the elasticity of the RBC suspensions after the addition of 200 (22 mM) and 400 mg/dl (44 mM) D-glucose. However, after the addition of 800 mg/dl (44 mM) D-glucose, a statistically significant increase in elasticity was detected at shear rates ranging from 40 to 120 s^{-1} ($p < 0.001$ from 40-50 s^{-1}; $p < 0.01$ from 70-90 s^{-1}; $p < 0.05$ at 120 s^{-1}; vs. 0 mg/dl) (**Figure 3.14 (B)**). The viscosity of the 800 mg/dl (44 mM) D-glucose incubated sample was on average, over shear rates from 40-375 s^{-1}, 12.0 ± 2.3% higher than that of the normal blood sample (0 mg/dl D-glucose). As mentioned above, an increase in both blood viscosity and elasticity without changes in Ht and plasma viscosity would signify a decrease in RBC deformability and vice versa. Therefore, the results on the increase in the viscosity and elasticity presented in this study may be indicative of a decrease in deformability of the RBCs.

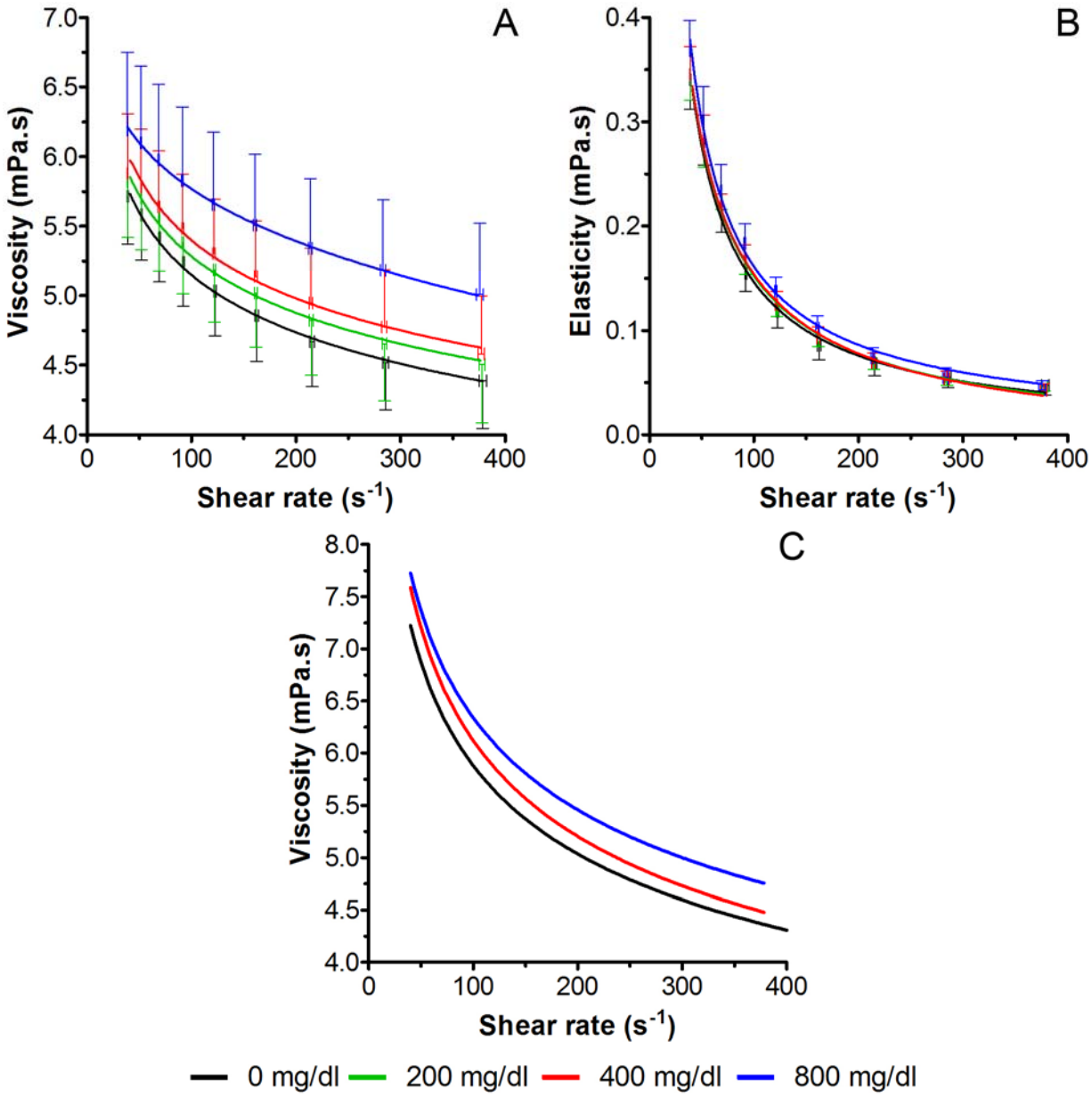

Figure 3.14: Effect of D-glucose concentration on the viscosity and elasticity of bovine RBC suspensions

The effect of D-glucose concentration (0-800 mg/dl (0-44 mM)) on the rigidity of bovine RBCs suspended in PBS (Ht = 51 ± 1%) was determined by measuring the viscosity (A) and elasticity (B) of bovine RBC suspensions containing D-glucose at concentrations of 0 (n = 4), 200 (11 mM) (n = 4), 400 (22 mM) (n = 4) and 800 mg/dl (44 mM) (n = 4) at shear rates ranging from ~40 to 375 s^{-1} with a Vilastic-3 viscoelasticity analyzer. This effect was also examined by measuring the viscosity (C) of a bovine blood sample at shear rates ranging ~40 to 400 s^{-1} with a Wells-Brookfield Cone/Plate rheometer. Results in A and B are presented as mean ± SEM. The results in C were obtained from a single blood preparation that was used in the experiments from A and B.

The effect of increasing D-glucose concentration on the viscoelasticity and viscosity of human whole blood (Ht = 42%) was also measured. The viscosity and elasticity of the human whole blood with (200 (11 mM), 400 (22 mM) and 800 mg/dl (44 mM) and without D-glucose (0 mg/dl), measured with a Vilastic-3 viscoelastometer, is shown in **Figure 3.15 (A)** and **(B)**. The addition of D-glucose appeared to have little effect on the deformability of human RBCs as evidenced by the lack of an increase in viscosity and elasticity of the sample. The observations made with the cone/plate rheometer also demonstrated a lack of increase in viscosity. A sample of this blood was heated to 50 °C for several minutes; a process shown to reduce the deformability of bovine RBCs in Section 3.3.3.7. The result of the heat hardening process on the RBCs deformability is evident in **Figure 3.15 (A) and (C)** where the viscosity of the heated sample is moderately higher than those samples with and without D-glucose. The viscosity of the heated blood sample was on average, over shear rates from 10-375 s^{-1}, 6.5 ± 1.2% higher than the normal blood sample (0 mg/dl D-glucose) and 5.2 ± 1% higher than the blood sample containing 800 mg/dl (44 mM) D-glucose. It is apparent that the deformability of the human RBCs was reduced after the heat hardening procedure based on the viscosity measurements. It is not completely clear why a change in the elasticity was not observed. However, it may possible that the decrease in RBC deformability was small enough that a change was not observable due to the accuracy of the measurements. The alteration of bovine RBC deformability by heat exposure was shown in Section 3.3.3.7 to increase the viscosity and elasticity of the RBC suspensions by approximately 12% and between 20 and 100%, respectively. However, those RBC suspensions were heated for 30 minutes instead of the 3 minutes used in the protocol for the human whole blood. Therefore, the moderate decrease in human RBC deformability was caused by a lesser effect of the heat exposure process on the RBC membrane proteins.

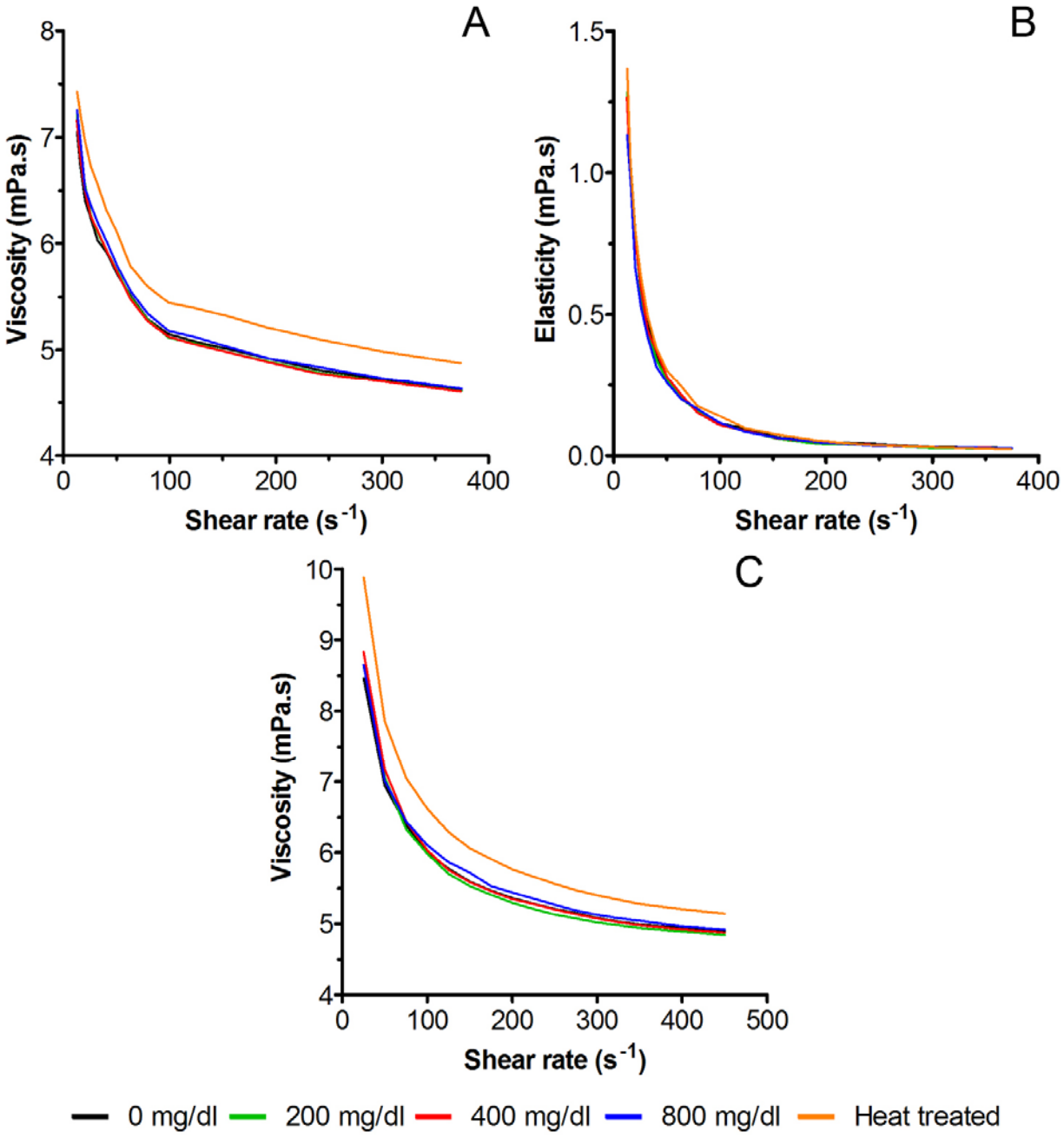

Figure 3.15: Effect of D-glucose concentration and heat rigidification on the viscosity and elasticity of human whole blood

The effect of D-glucose concentration (0-800 mg/dl (0-44 mM)) and heat on the rigidity of human RBCs was determined by measuring the viscosity (A) and elasticity (B) of a human whole blood samples (hematocrit = 42%) containing multiple D-glucose concentrations (0, 200 (11 mM), 400 (22 mM) and 800 mg/dl (44 mM)) at shear rates ranging from ~10 to 375 s^{-1} with a Vilastic-3 viscoelasticity analyzer. This effect was also examined by measuring the viscosities (C) of the same samples at shear rates ranging ~25 to 450 s^{-1} with a Wells-Brookfield Cone/Plate rheometer. Results obtained from single sample.

It was interesting that the addition of D-glucose to bovine blood RBC suspensions produced a decrease in RBC deformability but when the same concentrations were added to the human RBCs and incubated at the same temperatures and time periods, the deformability did not change. Hence, these results agree with previous reports that have shown that the rheological properties of human blood were not altered by short-term *in vitro* hyperglycemia [126].

RBCs in hypertonic solutions are known to shrink which causes a decrease in RBC deformability [127]. The addition of D-glucose raises solution osmolality leading to RBC shrinkage and a reduction in cell volume, i.e. reduction in the centrifuged hematocrit. However, D-glucose represents a naturally occurring enantiomer of glucose which can rapidly pass through the mammalian RBC membrane via facilitated diffusion by the erythrocytic glucose transporter GLUT-1 resulting in an iso-osmotic condition in and outside of the cell [128]. Therefore, hematocrit should remain unchanged.

Studies were performed to investigate whether the addition of D-glucose would result in an osmotically active condition in bovine, human and rat blood. The effects of D-glucose concentration on bovine blood hematocrit (n = 14) and suspension media osmolality (n = 8) are shown as a percent change from the 0 mg/dl condition in **Figure 3.16**. The addition of 200 (11 mM), 400 (22 mM) and 800 mg/dl (44 mM) D-glucose to the suspension media resulted in statistically significant ($p < 0.001$ vs. 0 mg/dl) increases in osmolality of 4.5 ± 0.6, 8.7 ± 0.6 and 16.7 ± 0.6%, respectively. Each consecutive increase in solution osmolality resulted in a statistically significant ($p < 0.001$ vs. 0 mg/dl) decrease in the hematocrit of the RBC suspensions. The addition of 200 (11 mM), 400 (22 mM) and 800 mg/dl (44 mM) D-glucose to the suspension media resulted in decreases in hematocrit of 2.3 ± 0.2, 4.8 ± 0.4 and 8.4 ± 0.7%, respectively indicating a lack of D-glucose transmembrane transport and an osmotically active

state. The effect of D-glucose concentration on bovine (n = 14), human (n = 2) and rat (n = 2) blood hematocrit was then compared and is shown in **Figure 3.17**. The rat whole blood demonstrated the same tendency as the bovine RBCs in suspension. The addition of 400 (22 mM) and 800 mg/dl (44 mM) D-glucose to the rat whole blood resulted in statistically significant ($p < 0.05$) decreases in hematocrit of 5.3 ± 1.2 and 8.3 ± 1.2%, respectively. The addition of 200 mg/dl (11 mM) D-glucose resulted in a moderate 3.0 ± 1.0% decrease in hematocrit. The osmotic effects of D-glucose on rat blood compared very closely with those on bovine blood. However, when examining the effect of D-glucose on human blood, there was no significant effect present. In fact, at a concentration of 200 (11 mM) and 400 mg/dl (22 mM) D-glucose, no change in hematocrit was observed. The 0.7 ± 0.9% decrease that occurred at 800 mg/dl (44 mM) was the result of a 0.5% decrease in the actual hematocrit value. Bühler et al. previously reported that the addition of D-glucose at concentrations upwards of 1440 mg/dl (80 mM) had no effect on the hematocrit of human blood and was attributed to the osmotically inactive state that is produced by the facilitated diffusion of glucose [126]. Therefore, it is very unlikely that the slight decrease observed in the 800 mg/dl (44 mM) sample was due to hyperosmolality of the plasma. The slight reduction may be simply attributed to an error in reading of the hematocrit.

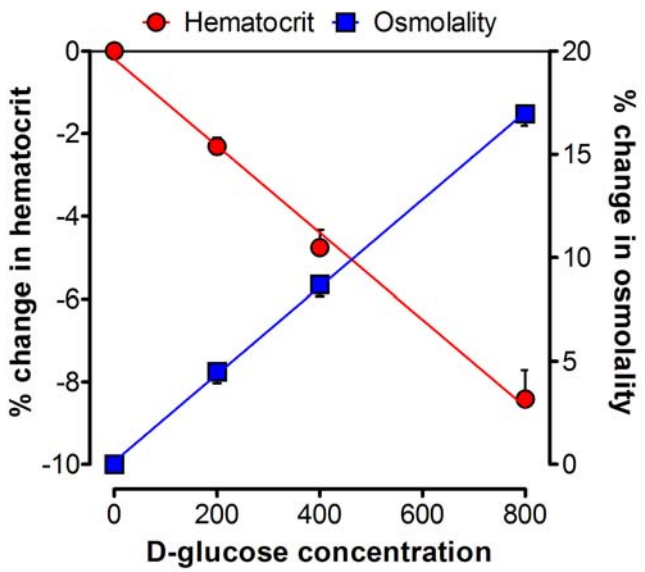

Figure 3.16: Percent change in the hematocrit bovine RBC suspensions and in the osmolality of suspension media

Effect of D-glucose concentration on bovine blood hematocrit (circles; n = 14) and plasma osmolality (squares; n = 8). Results are presented as mean ± SEM.

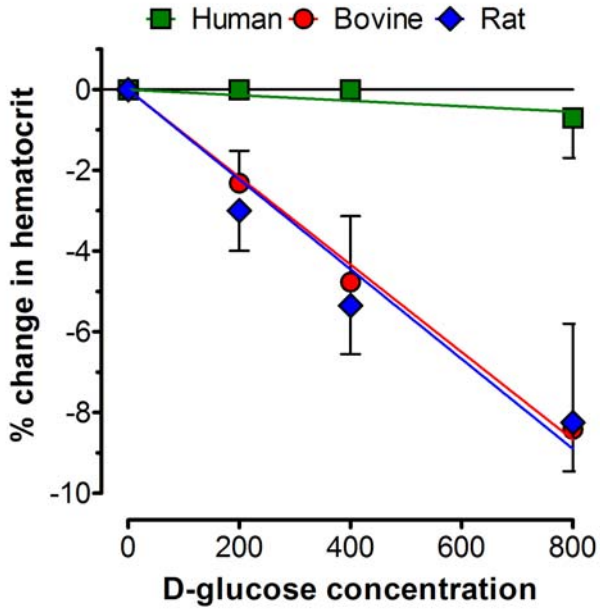

Figure 3.17: Percent change in hematocrit of bovine, human and rat blood after the addition of D-glucose

Effect of D-glucose concentration on the hematocrit of bovine (n = 14), human (n = 2) and rat blood (n = 2). Results are presented as mean ± SD.

The feeding habits of mammalian species can vary greatly and so can the regulatory mechanism of glucose utilization. Herbivorous cattle have lower blood glucose concentrations than omnivorous animals such as dogs. The D-glucose transport activities in erythrocytes of canines were reported to be similar to the values of those found in humans or rats [129]. This same study also demonstrated that the D-glucose transport in bovine blood was approximately one-third of that shown in canine blood. Therefore, a study was performed to examine whether incubation time (0, 1 and 24 hours) had a role in the osmotically inactive state of bovine blood. A study on the effect of incubation temperature (4, 25 (room temp) and 37°C) was conducted at the same time. Bovine blood was incubated in 0 and 800 mg/dl (44 mM) D- and L-glucose using these conditions. L-glucose represents an optical isomer of D-glucose that lacks stereospecificity with the GLUT-1 protein and therefore the ability to enter the cell thus creating an osmotically active condition which would result in cell shrinkage. At all three temperatures, immediately following and one hour after D- and L-glucose addition the hematocrit decreased roughly 8%, from a value of 48% to 44%, compared to baseline. After 24 hours at all three temperatures, the hematocrit in control tubes (0 mg/dl) had decreased slightly from a value of 48 to 47%, which is expected due to RBC loss of intracellular constituents. The additions of D- and L-glucose again reduced the hematocrit 8% compared to control. The results of this study are shown in **Figure 3.18 (A-C).** Therefore, it is evident, that the incubation temperature and time were not contributing factors to the absence of an iso-osmotic condition in the bovine blood suspensions. In general, standard laboratory practice dictates that viscoelasticity measurements be performed within a few hours of blood withdrawal since alterations in the its rheological properties occur with time [59]. Therefore, had a longer incubation time period proved to be effective in

preventing cell shrinkage, it would have been impractical from a rheological standpoint due to confounding alterations in cell deformability due to storage.

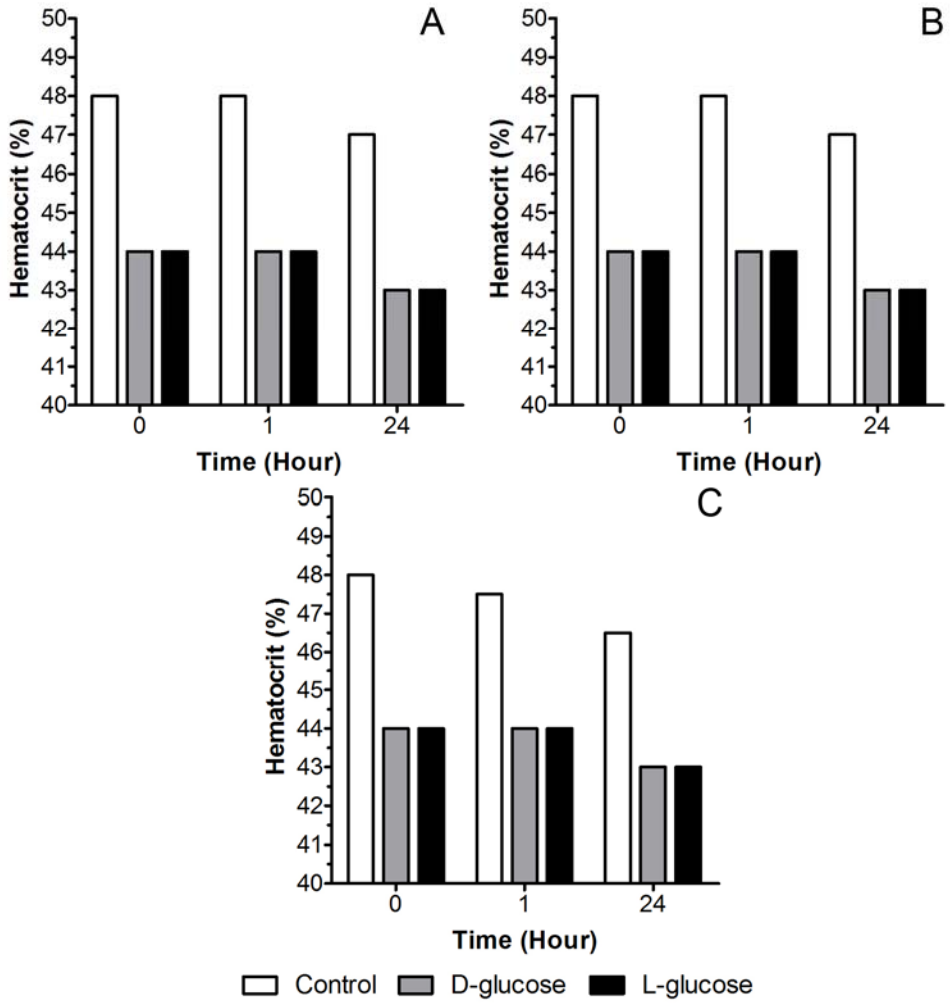

Figure 3.18: Effect of incubation time and temperature on D-glucose transport in bovine RBCs

Bovine blood hematocrit is shown after incubation with D- (grey bar) and L-glucose (black bar) at a concentration of 800 mg/dl (44 mM) for 0, 1 or 24 hours at temperatures of (A) 4 °C, (B) 25 °C and (C) 37 °C. A reduction in hematocrit indicates RBC shrinkage due to an osmotic activity.

It may be that osmotically inert conditions do not present in all species [130]. For instance, D-glucose demonstrated a noticeable effect on RBC deformability in the diabetic ob/ob mouse due to osmotic stress [131]. Therefore, the changes in the hematocrit of bovine and rat blood observed in this study are likely due to the osmotic stress of the D-glucose additive. The adaptation of the cells in these two species to uptake glucose based on different feeding habits may prohibit high levels of glucose from entering the cells. In this case, the GLUT-1 transporter may become overwhelmed by seemingly small concentrations of D-glucose resulting in an osmotically active state and cell shrinkage.

The results of these experiments thus suggest that the increases in viscoelasticity and viscosity shown in **Figure 3.14** after the addition of D-glucose were due to hyperosmolality of the suspension media due to D-glucose addition causing RBC shrinkage and not due to the effects of glycosylation of the cell membrane and hemoglobin. This was further confirmed by the study on human blood where hematocrit remained unchanged and likewise the viscoelasticity. The overall objective of this study was to replicate the decrease in the deformability of RBCs which was shown in the blood of diabetic rats in Section 3.4 and to evaluate the DRP effect on blood with reduced deformability. Due to the complications of the osmotic conditions that existed in the bovine and rat blood, the glycosylation of the RBCs by glucose was not detectable because the effect on cell deformability from cell shrinkage dominated. Therefore, experiments testing the DRP effect on the deformability of RBCs incubated with glucose should be included in future studies. These studies may be performed by equalizing the osmolality of the suspension media and re-evaluating the effects of D-glucose on the viscoelasticity of the samples.

4.0 ENHANCEMENT OF IMPAIRED MICROCIRCULATION IN RATS WITH STREPTOZOTOCIN-INDUCED DIABETES VIA INTRAVENOUS ADMINISTRATION OF DRP PREPARATIONS

4.1 INTRODUCTION

Previous experimental animal studies have demonstrated the potential clinical applicability of the intravenous delivery of DRPs for the treatment of hemorrhagic shock, hypobaric hypoxia, coronary stenosis and atherosclerosis. One acute animal study using rats with alloxan-induced diabetes mellitus demonstrated a significant increase in the density of functioning capillaries after the injection of a DRP solution. These studies are described in more detail in Chapter 2.1

Currently there is no truly effective prevention regimen or treatment for diabetes-related microcirculation impairment. In this chapter, a study designed to experimentally evaluate a novel therapy for the restoration and maintenance of impaired microcirculation in tissue and organs, which is significantly reduced due to diabetes based on the ability DRPs to provide blood with exceptionally low resistance to flow in the microcirculatory system which increases functional capillary density and markedly improve blood flow in microcirculatory disorders associated with diabetes.

4.2 METHODS

4.2.1 Animal Care Compliance

The surgical manipulations performed in this section of the study were approved by the Institutional Animal Care and Use Committee of the University of Pittsburgh (protocols #0408443, #0108461). All animal care and procedures conformed to the National Institutes of Health Guidelines for the Care and Use of Laboratory Animals.

4.2.2 Animals

Male Sprague-Dawley rats (250-300 g, SASCO; Charles River Laboratories, Wilmington, MA) were housed in solid bottom micro-isolator containers and fed rat chow and water *ad libitum* except during fasting periods, 2 hours prior to blood glucose measurements. The animals were allowed a 6-day acclimatization period after delivery before experimental procedures commenced. Animals were housed in plastic animal containers under constant conditions of temperature and light cycling (12 h light-12 h darkness). Bedding was changed daily in order to keep the animals clean and dry. The animals were randomly selected to either a diabetic group or control group. These two groups were further divided during acute hemodynamic experiments based on treatment (DRP or saline).

4.2.3 Development and care of a rodent model of diabetes.

The establishment of microcirculatory impairment caused by streptozotocin-induced diabetes in rats was evaluated by monitoring changes in microcirculatory blood flow through measurements of tissue perfusion using laser Doppler flowmetry.

Baseline hemodynamic parameters (systolic blood pressure and tissue perfusion) were measured non-invasively prior to diabetes induction and weekly thereafter. Baseline measurements of blood glucose concentration and weight were also attained.

Anesthesia was induced and maintained by inhalation of isoflurane (concentration 1.5-4%) in O_2. A thermistor probe (Yellow Springs Instruments) was inserted into the rectum and the animal placed on a heating pad in dorsal recumbency to maintain a body temperature of 37 °C.

Multiple sites were tested for their applicability in providing reliable and re-producible tissue perfusion measurements. The sites examined for the best tissue perfusion probe placement were the lip or buccal mucosa, the inner ear, the ear lobe, the ventral surface at the base of the tail, the ventral surface of the thigh of the hind-limb and the plantar surface of the front and hind paws. Tissue perfusion of the ventral surface of the thigh of the hind-limb and the plantar surface of the hind paw was measured with a non-invasive laser Doppler tissue perfusion probe (type DI; Transonic Systems, Ithaca, NY) that was affixed to the area with a piece of tape. Using a micromanipulator, a second tissue perfusion probe (N18, Transonic Systems) was clamped into position over the lip or buccal mucosa, the inner ear, the ear lobe, the ventral surface at the base of the tail, or the plantar surface of the front paw. The probes were mounted and positioned so that they applied minimal pressure to the surface, as to avoid occlusion of the local vessels and reduce perfusion. The probes' placements were chosen to minimize movement artifact and to avoid placement of the probes on a site containing large blood vessels. The perfusion probes

were subsequently connected to a BLF 21D tissue perfusion monitor (Transonic Systems). The flow monitor's output is proportional to absolute flow in the tissue being sampled. The tissue perfusion monitor's output was filtered with a 1.0 second time constant. Tissue perfusion readings were averaged over a several minute period of stable activity.

Systolic blood pressure was measured non-invasively by a piezoplethysmography system (Kent Scientific, Torrington, CT). Briefly, an inflatable occlusion cuff and a piezoelectric pulse sensor (distal placement) were placed on the animal's tail. The piezoelectric sensor was situated directly over the ventral tail artery. The occlusion cuff was inflated until the arterial pulse disappeared. The cuff was then slowly deflated until the pulse re-appeared. The systolic pressure corresponded to the occlusion cuff pressure at which the first appearance of the pulse was observed. The systolic pressure was taken as an average of three measurements. The pressure transducer was connected to a pressure channel of the laser Doppler flow meter (BLF 21D; Transonic Systems). The piezoelectric pulse sensor was coupled to a pre-amplifier connected to an analog input of the laser Doppler flow meter.

The signals containing the tissue perfusion and piezoplethysmography system data from the laser Doppler flow meter were acquired using a notebook PC computer connected via a serial connection. The data was continuously recorded (sample rate = 100 Hz) using WinDaq®/Pro software (DATAQ Instruments, Akron, OH) throughout the entire experiment. Average systolic blood pressure and the average tissue perfusion (minimum of 1 minute) were determined post hoc.

Diabetes was induced through an intraperitoneal injection of streptozotocin (STZ; 65 mg/kg, freshly dissolved in 0.1 M citrate buffer, pH 4.5) after a ~18 hour fasting period and confirmed by sustained blood glucose levels of 300 mg/dl (16.7 mM) or greater. The age and

weight-matched control group received the citrate buffer only. The injectant was sterilized via filter sterilization using a 0.22 μm syringe filter (Millipore).

Blood glucose levels were monitored twice weekly using a OneTouch® FastTake® glucometer (LifeScan, Milpitas, CA) from blood (10 μl) obtained by pricking the tip of the tail with a fine point lancet. Blood glucose measurements were timed so that they occurred several hours after the start of the 12 hour light cycle. Insulin (3-5 IU/day; Humulin® U; Eli Lilly, Indianapolis, IN) treatment was initiated ~4 weeks after STZ administration and continued throughout the study to reduce mortality and the potential of the animal's developing ketoacidosis.

Body weight was measured several times per week to ensure the health of the animal. Hemodynamic parameters (systolic blood pressure and tissue perfusion) were measured once weekly throughout the study period until the animals were taken into acute experiments.

4.2.4 Animal preparation and instrumentation for hemodynamic parameter measurement

Fifteen weeks after STZ administration, rats of both experimental and control groups were brought into acute experiments for testing the DRP effect on their hemodynamics (tissue perfusion and blood pressure).

Rats were catheterized in the right carotid artery for collection of arterial blood samples and for instantaneous measurement of arterial blood pressure and in the right jugular vein for intravenous infusion of the test solution (DRP or saline). Hemodynamic parameters including systolic, diastolic and mean arterial blood pressure, heart rate, spO_2 and skin tissue perfusion (plantar surface of hind paws) were monitored. Arterial blood samples were collected for the

measurements of PO_2, PCO_2, pH, HCO_3^-, aBE, hematocrit, total hemoglobin concentration, lactate, Ca^{++}, Na^+, and K^+.

Anesthesia was induced and maintained by inhalation of isoflurane (concentration 1.5-4%) in O_2. A thermistor probe (Yellow Springs Instruments) was inserted into the rectum and the animal placed on a heating pad in dorsal recumbency to maintain a body temperature of 37 °C and the ventral surface of the neck shaved. The carotid artery was cannulated with a 22 gauge IV catheter (Medex) as described in section 3.2.2.2. This catheter was used for arterial blood sampling and blood pressure measurement. A T-connector (Medex) filled with heparin lock (3.33 IU/ml of heparin in saline) was connected to the carotid artery catheter. A 3-way stopcock (Medex) also filled with heparin lock was then connected to the T-connector. One port of the stopcock was connected to a pressure transducer (Transpac, Abbott Laboratories, Abbott Park, IL) for arterial pressure measurement. The pressure transducer was connected to the pressure channel of the laser Doppler flow meter (BLF 21D; Transonic Systems). The other port of the T-connector was used for arterial blood sampling. Next, an incision approximately 1.5 cm long was made in the skin on the right ventrolateral aspect of the neck above the clavicle. The right external jugular vein was dissected free of surrounding fascia (caudal most landmark being where the vein courses underneath the pectoral muscle), ligated distally and cannulated with a 24 gauge IV catheter (Medex) for intravenous infusion of the test solutions. A 3-way stopcock (Medex) filled with heparin lock solution was connected to the IV catheter and then one port of the stopcock was connected through microbore extension tubing (Arrow International, Reading, PA) to a syringe filled with the test solutions on a syringe pump (Kent Scientific).

A pulse oximeter sensor (8600V, Nonin Medical, Plymouth, MN) was clipped onto a front paw and used to measure arterial blood oxygen saturation (SpO_2) and heart rate.

Non-invasive Laser Doppler tissue perfusion probes (type DI; Transonic Systems) were taped to the plantar surface of the hind paws to measure tissue perfusion. The perfusion probes were connected to the BLF 21D tissue perfusion monitor (Transonic Systems). The tissue perfusion monitor's analog output was filtered with a 1.0 second time constant.

The signals containing the tissue perfusion and blood pressure data from the laser Doppler flow meter and the pulse oximetry data were acquired using a DI-720 series acquisition system (DATAQ Instruments) connected to a notebook PC computer connected via a universal serial bus. The data was continuously recorded (sample rate = 80 Hz) using WinDaq®/Pro software (DATAQ Instruments) throughout the entire experiment. The systolic, diastolic, and mean arterial pressures and the average tissue perfusions (all based on a 500 sample average) were continuously monitored via the WinDaq Meter Add-on (DATAQ Instruments).

Arterial blood samples were collected after recording base hemodynamics (base sample) and the end of each acute experiment, 60 minutes post-infusion. DRPs were injected via the jugular vein at a final concentration of 1 μg/ml (0.22 nM).

Vascular resistance was calculated by dividing mean arterial pressure by mean tissue perfusion over the time period of interest. An increase in tissue perfusion and decrease in blood pressure indicate a reduction in vascular resistance and, thus, the ability of DRPs to improve microcirculatory flow.

4.2.5 Drag-reducing polymers

The synthetic drag-reducing polymer polyethylene oxide (MW – 4500 kD; PEO-4500; Dow Chemical) was employed in these studies at a final blood concentration of 1 μg/ml (0.22 nM). A description of the DRP preparation procedure was outlined in Chapter 3.2.2.1. A control

solution consisted of sterile nonpyrogenic isotonic saline (0.9%, Baxter). The diabetic and control (non-diabetic) animal groups were each further subdivided based on treatment: PEO-4500 or Control (saline) resulting in four total groups.

4.2.6 Statistical methods

A paired t-test was applied to determine the statistical significance of the difference between base and post injection parameters within each group. A student's un-paired t-test was applied to determine the statistical significance of the difference between diabetic and control groups. A $p < 0.05$ was considered to be statistically significant.

4.3 RESULTS AND DISCUSSION

The specific aim of this study was to demonstrate that the intravenous administration of DRP preparations in rats with streptozotocin-induced diabetes enhances impaired microcirculatory perfusion. This was accomplished through two phases; the first phase was to induce diabetes to begin the development of microcirculatory flow insufficiencies and other diabetic complications during which hemodynamic parameters (systolic blood pressure and tissue perfusion) were monitored non-invasively and the second phase was to evaluate in acute experiments the ability of DRP preparations to treat the microcirculatory hypoperfusion which developed due to diabetes in the first phase.

4.3.1 Streptozotocin-induced diabetic rat model

During the chronic development of diabetic complications, measurements of weight, blood glucose (BG), tissue perfusion (TP) and systolic blood pressure (SBP) were obtained before the initiation of diabetes and weekly thereafter. Animals were considered hyperglycemic if their blood glucose was above 300 mg/dl (16.7 mM). Diabetic animals exhibited a significant increase in blood glucose levels after diabetes induction as well as classic clinical symptoms associated with diabetes (i.e., polyuria, polydipsia and polyphagia). Diabetic animals also exhibited a decrease in weight during the study, another classic symptom of diabetes, while animals in the control group gained weight according to normal age-growth charts [132]. One of the biggest challenges in using diabetic animals in a chronic study is maintaining their health for the survival period needed to develop the complications. Some of the initial diabetic animals showed up to a 25-30% loss of weight from baseline and had to be sacrificed prematurely in order to minimize pain and distress. Therefore, daily administration of long acting insulin (3-5 IU/day, a dose to reduce ketone bodies but not normalize blood glucose) was started ~4 weeks after diabetes induction. Tissue blood perfusion was measured with a non-invasive laser-Doppler method which provided information on microcirculation near the surface (skin, mucosa). Initially we were planning to measure TP on the lip mucosa and a shaved area of the hind leg. However, the mask required to deliver the isoflurane anesthesia during the chronic studies obstructed access of the TP probe to the lip mucosa. Additionally, we stopped using the thigh of the hind leg as to avoid the transient hyperemia associated with shaving the area prior to performing measurements. Most importantly, due to a loss of subcutaneous adipose tissue in diabetic rats, we believed that the flow probe was affected by muscle perfusion which is much higher than the skin perfusion. Therefore, we examined several other sites for tissue perfusion measurements

including the inner ear, the ear lobe, the base of the tail, and surface of the front and hind paws. We found that measurements of perfusion on the plantar surface of hind paws seemed more informative since this area provides an easily accessible, hairless, flat surface which allowed us to take several measurements in different locations to obtain an average perfusion of the entire surface.

The STZ model of diabetes is a current and well-established animal model of diabetes. Alternatives for diabetes mellitus models are alloxan-induced diabetes, genetically-induced diabetes and pancreatectomy. Alloxan has been associated with a significantly higher mortality than STZ. It is also pointed out that STZ may induce a diabetic state that more closely resembles that observed in many humans in that human patients with diabetes exhibit hyperglycemia usually in the absence of ketone body formation. Alloxan-induced diabetes in rats is associated with an increase in free fatty acid levels and ketone bodies not seen in STZ diabetic animals. Chemical induction of diabetes mellitus with agents such as STZ and alloxan is advantageous over pancreatectomy because of the maintenance of pancreatic function in cells other than the β-cell. The surgical removal of the pancreas results in the removal of not only the β-cell and loss of insulin secretory function but also removal of both the α- and δ-cells and the loss of the counterregulatory hormones glucagons and somatostatin. In addition, there is a loss of the pancreatic enzymes necessary for proper digestion; therefore, the diet for pancreatectomized animals must be supplemented with these pancreatic enzymes [133].

The genetically diabetic BB/Worcester rat has been considered as an alternative but the expense and unpredictability with regard to diabetes onset made this model undesirable. For accuracy, it is not particularly feasible to acquire animals which may or may not become diabetic

during a large window of time. The literature demonstrates that the streptozotocin model is the most widely used, accepted, and characterized for this type of research.

4.3.2 Chronic hemodynamics in a streptozotocin-induced diabetic rat model

Based on the published information, we hypothesized that the development of diabetic microangiopathies would result in a significant decrease in tissue perfusion in the diabetic animals. **Table 4.1** shows the hemodynamic parameters of a subset of animals that were measured chronically under very light anesthesia prior and after diabetes induction. Measurements of SBP and TP did not show statistically significant changes from baseline in either group. However, mean values of tissue perfusion decreased by 19% in the diabetic group and by 9% in controls. In addition, **Table 4.1** shows the relative changes in SBP which increased in the control group by 6% and in the diabetic group by 20% ($p>0.05$ in both groups). Based on the blood pressure and TP data, microvascular resistance in these groups calculated as a ratio of blood pressure and TP, decreased in the Control group by 15% and in the diabetic group by 50% ($p < 0.05$). Causes for a decrease in TP and an increase in microvascular resistance might be different in the studied groups. The control animals gain weight and adipose tissue, which is much less vascularized. The diabetic rats do not gain and can even lose adipose tissue and thus a decrease in TP can be explained only by rarefaction of the perfused arterioles and capillaries. Blood glucose levels shown in **Table 4.1** significantly increased in diabetic rats and did not change in controls over an 8 week time period. Finally, **Table 4.1** shows that control rats gained about 17% body weight while diabetic rats have lost about 10% of their base weight in spite of insulin injections. Thus, these results suggest that we were able to develop severe diabetic conditions in rats with deterioration of microcirculation.

Table 4.1: Measurements of hemodynamic and physiological parameters in diabetic and normal (control) animals

	Diabetic		Control	
Parameter	Base	Final	Base	Final
TP (TPU)	35.8±3.0	29.1±3.3	40.7±3.3	36.9±6.4
SBP (mmHg)	101±4	121±5	108±4	115±3
BG (mg/dl)	114±4	533±33	100±14	97±4
Weight (grams)	359±32	326±29	355±46	417±17

Measurements of hemodynamic and physiological parameters in diabetic (n = 7) and normal (control; n= 4) animals. Base parameters were measured prior to induction of diabetes. Mean ± SEM

4.3.3 Effect of DRPs on vascular hemodynamics in streptozotocin-induced experimental diabetes

After at least 15 weeks post diabetes induction, animals were taken in acute experiments and, after collection of base hemodynamic data (blood pressure and tissue perfusion), injected with PEO-4500 (final blood concentration 1 μg/ml (0.22 nM), saline in control).

Table 4.2 shows the base hemodynamic data of control and diabetic rats collected in acute experiments. Note that the base TP is significantly lower in these animals than it was shown in **Table 4.1**. This may be potentially due to the depressive effects of long term, surgical plane anesthesia and invasive procedure on cardiovascular hemodynamics and respiratory parameters.

Table 4.2: Base hemodynamic data of control and diabetic rats collected in acute experiments.

Group	Tissue Perfusion (TPU)	Mean Arterial Pressure (mmHg)	Vascular Resistance (mmHg/TPU)	Heart rate (beats/min)
Control	14.2±6.0	90.2±6.8	7.7±3.9	322±28
Diabetic	9.4±4.6	92.0±8.6	11.9±6.2	287±29
p-value[*]	***0.014***	*0.567*	***0.011***	***0.010***

Mean ± SEM, $p < 0.05$ was considered to be statistically significant

Microvascular resistance and heart rate are statistically significantly lower in diabetic animals. Changes in microvascular resistance are consistent with the results of our chronic measurements of hemodynamics in normal and diabetic animals given in **Table 4.1**. Changes in heart rate are consistent with those reported in the literature [134].

Figure 4.1 (A) shows the results of tissue perfusion measurements made in Control rats before and after the injection of 1 μg/ml (0.22 nM) PEO-4500 solutions (saline in Control-Controls). The injection of saline in normal (non-diabetic) animals did not change tissue perfusion ($p>0.05$). However, the injection of PEO-4500 caused a statistically significant increase in TP by 40% ($p=0.014$). **Figure 4.1 (B)** shows the changes in TP after the injection of 1 μg/ml (0.22 nM) PEO-4500 in diabetic animals (saline in Diabetic-Controls). Again, the injection of saline in diabetic animals did not change tissue perfusion ($p>0.05$). However, the injection of PEO-4500 caused a statistically significant increase in TP by 20% ($p=0.027$).

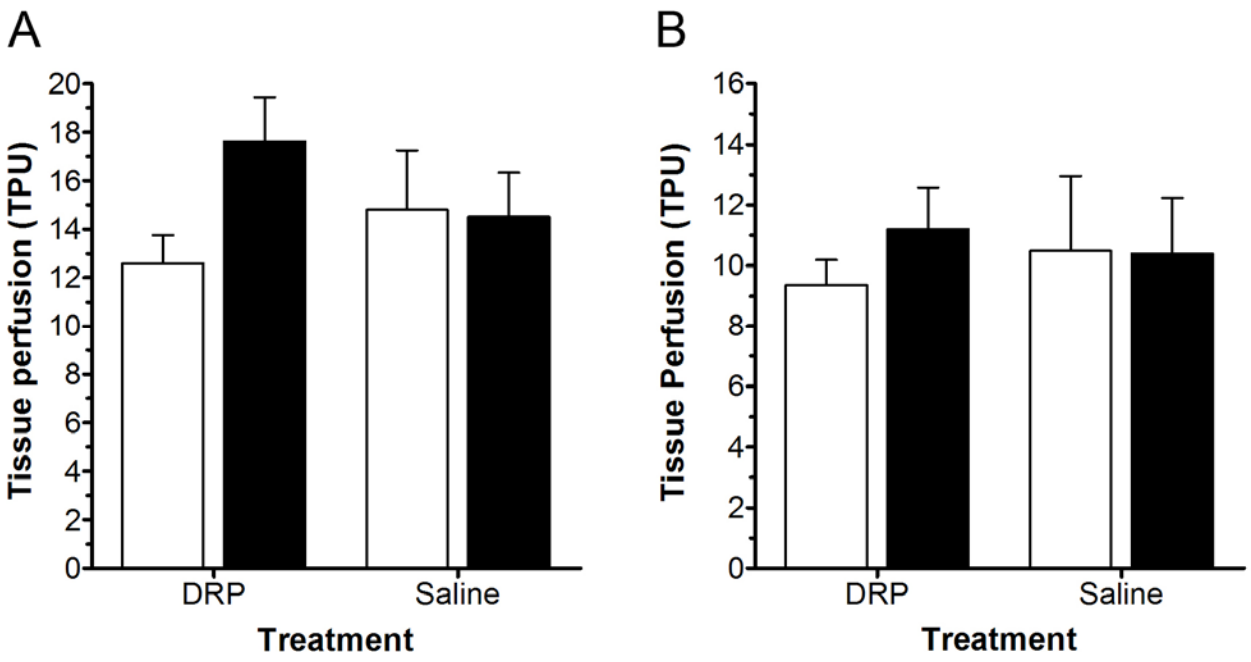

Figure 4.1: Effect of DRPs on the tissue perfusion in diabetic and non-diabetic (normal) rats

(A) Tissue perfusion in the hind-limb plantar surfaces of normal rats before (white bars) and after (black bars) the infusion of a DRP (PEO-4500) or saline. (B) Tissue perfusion in the hind-limb plantar surfaces of normal rats before (white bars) and after (black bars) the infusion of a DRP (PEO-4500) or saline.

Other hemodynamic parameters (MAP and heart rate) did not change statistically significantly after the injection of the DRPs (or saline in Control subgroups) in both Control (non-diabetic) and Diabetic groups.

Table 4.3 shows data obtained from blood samples collected in both Control (non-diabetic) and Diabetic groups. A statistically significant difference was found between base hematocrit values in Control and Diabetic groups. The higher hematocrit in diabetic animals could be related to a certain level of tissue hypoxia which can stimulate hematopoiesis. Other blood gas parameters were not statistically significantly different between Control and Diabetic groups in both the base and post-injection blood samples. A small but statistically significant difference between base and end blood gas parameters observed in both groups was related to the

acute experiment conditions (depressive effects of long term, surgical plane anesthesia and surgery on cardiovascular hemodynamics and respiratory parameters).

Table 4.3: Blood gases parameters of Control and Diabetic rats before and after PEO-4500 injection in acute experiments

	Pre-injection			Post-injection			
Parameter	Control	Diabetic	*p-value*	Control	Diabetic	*p-value*	*p-value*
Hematocrit (%)	46.4±2.2	48.8±2.5	0.020[a]	44.8±1.3	45.8±3.9	$p > 0.05$[a]	0.005[b], 0.000[c]
pH	7.41±0.06	7.37±0.06	$p > 0.05$[a]	7.38±0.05	7.33±0.09	$p > 0.05$[a]	0.004[b], 0.000[c]
pCO_2 (*mmHg*)	44.1±8.7	49.6±8.1	$p > 0.05$[a]	46.6±7.2	48.1±11.3	$p > 0.05$[a]	$p > 0.05$[b], $p > 0.05$[c]
ABE (*mmol/L*)	2.51±1.25	2.7±2.9	$p > 0.05$[a]	1.9±1.4	1.0±3.8	$p > 0.05$[a]	$p > 0.05$[b], 0.005[c]
K^+ (*mmol/L*)	4.7±0.5	4.8±0.7	$p > 0.05$[a]	4.8±0.4	5.2±0.6	$p > 0.05$[a]	$p > 0.05$[b], 0.013[c]
Na^+ (*mmol/L*)	136.9±2.1	137.1±4.1	$p > 0.05$[a]	137.6±2.2	138.0±4.5	$p > 0.05$[a]	$p > 0.05$[b], $p > 0.05$[c]
Ca^{++} (*mmol/L*)	1.35±0.07	1.33±0.14	$p > 0.05$[a]	1.33±0.09	1.33±0.14	$p > 0.05$[a]	$p > 0.05$[b], $p > 0.05$[c]

[a] Control vs. Diabetic, [b] Control pre vs. post and [c] Diabetic pre vs. post

This study demonstrates that a reproducible model of experimental diabetes in small animals (rats) with the ability to measure hemodynamic parameters using non-invasive methods was developed. Diabetic rats were found to have statistically significantly lower tissue perfusion than their non-diabetic matched control. We tested our polymers in both diabetic and control animals and have found that nanomolar concentrations of DRPs statistically significantly increased tissue perfusion in diabetic rats (as well as in normal animals) without affecting other hemodynamic parameters (blood pressure and heart rate). The stronger increase in tissue perfusion after the injection of DRPs in normal animals was probably related to the fact that diabetes mellitus causes significant changes in the vessel wall which reduces its response to shear stress.

The importance of this study is that we demonstrated the beneficial effects of our drag-reducing polymers on the microcirculation of diabetic animals which most likely was related to the ability of the DRPs to enhance blood flow structure and mechanical properties of red blood cells in microvessels. Therefore, DRPs may have a significant impact in the treatment of patients

suffering from microcirculatory related complications of diabetes. The future direction of this research should be focused on the treatment/prevention of those complications by chronically injecting DRPs over the course of diabetes development. This may includes studies on wound healing or diabetic neuropathy; conditions whose etiologies have been linked to poor microvascular perfusion.

5.0 STUDY OF POTENTIAL SIDE EFFECTS OF THE DRPS VIA ACUTE AND CHRONIC ANIMAL TESTS

5.1 INTRODUCTION

Previous *in-vivo* studies with DRPs have demonstrated that they represent great utility in many potential acute and chronic clinical applications. These were described in-depth in Chapter 2.1. However, before DRPs can be used clinically, any potential side effects and toxicity must be evaluated including deleterious effects on clotting and hemostasis. Therefore, in this chapter, experiments which were performed to evaluate the effects of acute and chronic DRP injections on several hematological, blood gas and blood coagulation parameters are described. This chapter also describes several studies which were designed and performed to determine the thresholds of DRP concentrations which could be safely used for intravenous infusions. In acute experiments, the hemodynamic response of normal animals to an intravenous infusion of high concentrations of several DRPs (PMNN, PEO and hyaluronic acid) was assessed. Tests also included bolus injections of several different concentrations of DRPs to determine if/which preparations of DRPs could be injected in relatively high concentrations in short time periods without an undesirable hemodynamic reaction.

5.2 METHODS

5.2.1 Animal Care Compliance

The surgical manipulations performed in this section of the study were approved by the Institutional Animal Care and Use Committee of the University of Pittsburgh (protocol #0408097 and #0510080). All animal care and procedures conformed to the National Institutes of Health Guidelines for the Care and Use of Laboratory Animals.

5.2.2 Animals

Male Sprague-Dawley rats (300-350 g, SASCO; Charles River Laboratories, Wilmington, MA) were housed in solid bottom micro-isolator containers and fed rat chow and water *ad libitum.* The animals were allowed a 6-day acclimatization period after delivery before experimental procedures commenced.

5.2.3 Acute DRP effect on hematological parameters

Any new blood additive must be evaluated for its potential effects on the blood coagulation system to exclude any deleterious effects on clotting and hemostasis. Accordingly, the potential acute effects of DRPs on several hematological parameters after IV administration to rats were evaluated in blood of these animals. These parameters included the measured parameters of a complete blood count with differential (CBC differential; hematocrit (Ht), hemoglobin (Hgb), mean corpuscular hemoglobin concentration (MCHC), mean corpuscular hemoglobin (MCH),

mean corpuscular volume (MCV), red blood cell count (RBC), white blood cell count (WBC), platelet count and differential white blood cell count ("differential")), prothrombin time (PT), activated partial thromboplastin time (aPTT), and fibrinogen and D-Dimer concentration. The effect of DRPs on clot formation time was also evaluated with blood collected from donor rats *in vitro*.

A surgical plane of anesthesia was induced and maintained with an IM injection of ketamine/xylazine (90/10 mg/kg; Phoenix Pharmaceutical) and heparin (60 IU heparin/kg body weight; Abbott Laboratories) was administered subcutaneously in eleven rats. IV catheters were placed in the right carotid artery for collection of arterial blood samples and for instantaneous measurement of arterial blood pressure and right jugular vein for IV infusion of the test solution (DRP or saline (control)) as described in Sections 3.2.2.2 and 4.2.4, respectively.

After the animal preparation was complete and after a stabilization period of 15 minutes, blood was drawn from the arterial catheter via a plastic syringe (Becton Dickinson (BD), Franklin Lakes, NJ) and transferred into glass blood collection tubes containing 3.2% sodium citrate (2.7 ml; BD) and 7.5% EDTA (2.7 ml; BD) to measure the CBC differential, PT, aPTT, and fibrinogen and D-Dimer concentration. Fifteen minutes post blood sampling, a predetermined volume (≤1.5 ml) of saline (Control; n = 5) or Poly(mannan) (PMNN; at the concentration of 100 μg/ml (16.7 nM); n = 6), as described in Section 3.2.2.1, was injected in the jugular vein over a 20 minute period through a microbore catheter (Arrow International) connected to a syringe on a syringe pump (PhD 2000; Harvard Apparatus, Holliston, MA). The infused volume (1-1.5 ml) was calculated based on animal weight, original DRP concentration (100 μg/ml (16.7 nM)) and the desired DRP dosage to be given to the animal (300 μg/kg or 5 μg DRP/ml blood (0.83 nM); a concentration that is known to be hemodynamically effective).

Blood volume was estimated as 6% of lean body weight. The animals of the Control group received the same weight-based volume of the control solution (NS). Thirty minutes following the end of the IV injection, post-injection blood samples were collected as described above. The animal was then sacrificed with an intracardiac (IC) bolus of supersaturated (2 mmol/kg) potassium chloride while under general surgical plane anesthesia. The blood collection tubes were sent to a veterinary diagnostic laboratory (Antech Diagnostics, Lake Success, NY) for hematological parameter measurement. Results are expressed as the mean ± standard deviation (SD). Hematological parameters in the DRP and Control groups were compared. Statistical significance of the difference in hematological parameters between groups and statistical significance of the difference in hematological parameters within each group before and after treatment was computed using a Student's un-paired t-test and a paired t-test, respectively. A $p < 0.05$ was considered to be statistically significant.

Additionally, the time for clot formation with and without DRPs was tested *in vitro*. Briefly, blood (un-heparinized) was collected via an IV catheter (Chapter 3.2.2.2) from three anesthetized rats and was transferred into glass tubes, with no anticoagulant, containing equal volumes of one of two DRPs (PMNN (10 μg/ml (1.7 nM) and PEO-4500 (10 μg/ml (1.7 nM))) solutions or saline (Control). Tubes were rocked on a laboratory rocker (Speci-Mix tube rocker, Barnstead Thermolyne, Dubuque, IA) until clot formation (a change in the consistency of the blood in the tube to a thick and fibrinous state). Results are expressed as the mean ± standard deviation. Clotting times between the DRP and Control tubes were compared. A one-way ANOVA with Tukey post hoc test was used to compute the statistical significance between the clotting times of DRP and Control tubes. A $p < 0.05$ was considered to be statistically significant.

5.2.4 Chronic DRP effect on arterial blood gas, blood serum chemistry and hematological parameters.

Blood additives must also be evaluated for their potential chronic effects on basic physiological function. Therefore, the potential chronic effects of DRPs on several physiological parameters, including arterial blood gas, blood serum chemistry and hematological parameters, after chronic IV administration (7 weeks) to rats were evaluated.

Healthy male SASCO Sprague-Dawley rats with pre-implanted jugular vein catheters were used in these studies (as approved by the Institutional Animal Care and Use Committee). The catheters (polyurethane tubing, 0.025" x 0.040") were placed by experienced technicians at Charles Rivers Laboratories several days prior to delivery. The catheter was routed under the skin and exited centrally between the scapulae and was tucked into a subcutaneous pocket when not in use. The catheter was filled with a lumen lock solution consisting of a 1:1 solution of 50% dextrose (Hospira, Lake Forest, IL) and heparin (1000 U/ml; Baxter) and was flushed twice weekly to maintain patency. The exterior end of the catheter was plugged when not in use.

After a 6 day acclimatization period, the animals (n=17) began to receive twice weekly injections of DRP solutions (PEO-4500, n=6; PMNN, n=6; and saline (Control), n=5) for a period of 7 weeks. The DRP solutions were prepared as described in Chapter 3.2.2.1. These animals were in a study that was being performed co-currently with this project so the end point chosen to evaluate chronic toxicity was based on the end point of the other project. This was done in order to minimize animal numbers. The animals were anesthetized for each injection procedure due to the time required for administration of the DRPs. Anesthesia was induced and maintained by inhalation of isoflurane (1.5-4%) in O_2. Animals were placed on a warming pad in ventral recumbency and the IV catheter was prepared for infusion. The catheter plug was

removed and the lumen lock solution was cleared from the catheter by connecting a 1 ml syringe with 23 gauge needle to the catheter and drawing back slowly until blood entered the syringe. A 23 gauge needle attached to a microbore catheter (Arrow International) and a syringe on a syringe pump (Kent Scientific) was then connected to the catheter and the DRP solutions (saline in control) were infused at a controlled rate over 3-5 minutes. The infused volume (1-2 ml) was calculated based on animal weight, original DRP concentration (PEO-4500 – 20 μg/ml (4.4 nM); PMNN – 40 μg/ml (6.7 nM)) and the desired DRP dosage to be given to the animal (PEO-4500 – 60 μg/kg or 1 μg DRP/ml blood (0.22 nM)); PMNN – 120 μg/kg or 2 μg DRP/ml blood (0.33 nM)). Blood volume was estimated as 6% of lean body weight. These concentrations were chosen because they are the typical doses applied to yield an effective hemodynamic response to DRPs. Control animals (n=5) were injected with an equal volume of the vehicle (saline). Upon completion of the infusion, the lumen lock solution was replaced. The catheter was plugged, disinfected with 70% ethanol alcohol and 5% povidone-iodine solution and tucked back into its subcutaneous pocket.

At the end of 7 weeks, the animals were anesthetized with isoflurane (1.5-4.0%) and blood samples were collected through an arterial catheter (Chapter 3.2.2.2) to measure blood gas parameters (pH, pCO_2, pO_2, $cHCO_3$, ABE, tHb, K^+, Na^+, Ca^{2+} and Lactate) using an ABL725 blood gas analyzer (Radiometer America, Westlake, OH), hematological parameters (CBC differential as previously described in Chapter 5.2.3) using a HESKA® CBC-Diff™ System (Heska, Loveland, CO) and several serum chemistries including blood urea nitrogen (BUN), glucose, alkaline phosphatase (ALP), total protein (T-Pro), alanine aminotransferase (ALT) and creatinine using a HESKA® Spotchem™ EZ System. These parameters were chosen as a measure of cardiovascular, respiratory, liver and renal function. The data was averaged amongst each

group, standard deviations calculated, and one-way ANOVA with Tukey post hoc test was used to compare each experimental group (animals injected with either PEO or PMNN) to the control group (animals injected with saline). A $p < 0.05$ was considered to be statistically significant.

5.2.5 *In-vivo* efficacy of hyaluronic acid and the hemodynamic effects of bolus infusions and infusions of extremely high concentrations of DRPs.

In this section of the chapter, some additional experiments which were performed to study the *in-vivo* efficacy of high molecular weight hyaluronic acid (Hyvisc®, Anika Therapeutics) on enhancing cardiovascular hemodynamics is discussed. Hyvisc® is a commercially available pharmaceutical grade hyaluronic acid preparation (MW=~2000 kD) that is currently used by veterinarians used to treat joint dysfunction in horses associated with equine osteoarthritis, *In-vitro* experiments revealed that Hyvisc® had good drag reducing properties and due to its commercial availability, it is a promising candidate for larger animal trials and future clinical use. Several other experiments were performed to investigate the hemodynamic effects of bolus injections of DRP solutions with relatively high concentrations (up to 100 μg/ml (50 nM)) and slow infusions of DRP solutions with extremely high concentrations (up to 3 mg/ml (1.5 μM) in the syringe). These injections resulted in blood concentrations up to 150 times the hemodynamically effective concentration.

5.2.5.1 Animal preparation for hemodynamic parameter measurement

Seven rats were prepared as described in Chapter 4.2.4 for the measurement of hemodynamic parameters (instantaneous arterial pressure (carotid artery) and tissue perfusion (left and right hind limb plantar surface)). In addition, the left carotid artery was exposed as

described in Chapter 3.2.2.2 and an ultrasonic perivascular flow probe (0.7VB; Transonic Systems) was placed around the vessel to monitor carotid artery blood flow. The probe was stabilized in position on the artery with a micromanipulator to minimize movement and ensure that the artery was centered within the probe window. The ultrasonic flow probe was connected to a T206 flow meter (Transonic Systems) whose signal was acquired and continuously recorded as described in Chapter 4.2.4. The maximum, minimum and mean flow rates were also monitored as described in that chapter. Data acquisition was performed at a minimum sample rate of 167 Hz.

5.2.5.2 Experiments to examine the hemodynamic efficiency of intravenous hyaluronic acid

Two experiments were performed to examine the effectiveness of a commercially available hyaluronic acid pharmaceutical on enhancing hemodynamics in a rat. In the first experiment, baseline hemodynamics were monitored and recorded for 20-30 minutes. Then, predetermined volumes of a hyaluronic acid solution (Hyvisc®; Anika Therapeutics) were intravenously infused via the jugular vein at concentrations of 50 (25 nM), 125 (62.5 nM), 250 (125 nM) and 250 μg/ml (125 nM) to yield final blood concentrations of 1 (0.5 nM), 6 (3 nM), 16 (8 nM) and 33 μg/ml (16.5 nM) of the DRP, respectively. Hemodynamic parameters were monitored and recorded for 30 minutes in between each increasing dose. After recording the final set of hemodynamic parameters, the animal was euthanized by an intracardiac bolus of supersaturated (2 mmol/kg) potassium chloride (Hospira).

In the second experiment, baseline hemodynamics were monitored and recorded for ~15 minutes and then, predetermined volumes of a hyaluronic acid solution were intravenously infused via the jugular vein at concentrations of 1.0 (0.5 μM) and 1.5 mg/ml (0.75 μM)to yield

final blood concentrations of 50 (25 nM) and 150 μg/ml (75 nM) of the DRP, respectively. Hemodynamic parameters were monitored and recorded for 30 minutes in between doses. After recording the final set of hemodynamic parameters, the animal was euthanized by an intracardiac bolus of supersaturated (2 mmol/kg) potassium chloride (Hospira).

5.2.5.3 Experiments to investigate the hemodynamic response to bolus infusions of PMNN and PEO-4500

As a measure of acute toxicity and in order to test the applicability of giving higher doses (PEO-4500 at ~100 μg/ml (22 nM) and PMNN at ~50 μg/ml (8.3 nM)) of DRPs in a short bolus infusion as it may be employed in the resuscitation during hemorrhagic shock, several experiments were performed in which DRPs were infused at concentrations ranging from 2 μg/ml (0.3 – 0.4 nM) to 100 μg/ml (22 nM) in a fixed volume (1 ml) over 10 seconds. In the case of a human patient with a normal blood volume of 5 liters, this would represent a bolus infusion of ~150 ml given in 10 seconds. Therefore, this procedure represents a radical simulation of a bolus infusion.

Two experiments were performed. In both experiments, baseline hemodynamic parameters were first monitored and recorded for ~10 minutes. In the first experiment, saline was injected as a control and then PEO-4500 was injected as a 1 ml bolus (rate of 6 ml/min) at concentrations of 2 (0.44 nM), 10 (2.2 nM), 50 (11.1 nM) and 100 μg/ml (22.2 nM) via the jugular vein which yielded final blood concentrations of ~0.06 (0.013 nM), 0.36 (0.08 nM), 1.90 (0.42 nM), and 4.90 μg/ml (1.09 nM) of the DRP, respectively. Hemodynamic parameters were monitored and recorded for 15 minutes in between each dose. The second experiment was carried out identically to the first except PMNN was injected at concentrations of 2 (0.33 nM),

10 (1.67 nM) and 50 μg/ml (8.33 nM) via the jugular vein which yielded final blood concentrations of ~0.06 (0.01 nM), 0.36 (0.06 nM) and 1.90 μg/ml (0.32 nM) of the DRP, respectively. After recording the final set of hemodynamic parameters, the animals were euthanized by an intracardiac bolus of supersaturated (2 mmol/kg) potassium chloride (Hospira).

5.2.5.4 Experiments to investigate an animal's response to infusions of hyaluronic acid and PMNN at extremely high concentrations.

An additional two experiments were performed to study the effects of a slow infusion of extremely high concentrations of PMNN and hyaluronic acid (Hyvisc®, Anika Therapeutics) on hemodynamic parameters and cardiovascular function.

In both experiments, baseline hemodynamic parameters were first monitored and recorded for ~30 minutes. In the first experiment, one ml of PMNN was infused via the jugular vein at a concentration of 1250 μg/ml (0.21 μM) at 0.05 ml/min resulting in a total blood concentration of ~60 μg/ml (1.0 nM) of the DRP. At the end of the infusion, an arterial blood sample was collected and then hemodynamic parameters were monitored and recorded for ~60 minutes. A final arterial blood sample was collected and the animal euthanized as previously described. The experimental conditions and procedures in the second experiment were identical to those of the first experiment except that one ml of hyaluronic acid was infused via the jugular vein at a concentration of 3000 μg/ml (1.0 μM) at 0.05 ml/min resulting in a total blood concentration of ~143 μg/ml (47.7 nM) of the DRP.

5.3 RESULTS AND DISCUSSION

DRPs may be utilized in many clinical applications for the treatment of various pathologies and conditions. These pathologies and conditions may be associated with coagulopathic conditions and increased risk of bleeding. Therefore, an investigation on the effects of DRPs on a variety of coagulation and hematological parameters was performed *in vitro* and *in vivo* after acute and chronic DRP administration to rats to exclude any deleterious effects of these long-chain molecules on clotting and hemostasis. Studies were also performed to investigate the effects of the intravenous infusion of high concentrations of DRP solutions. In acute experiments, the hemodynamic response of normal animals to an intravenous infusion of high concentrations of several DRPs (PMNN, PEO and hyaluronic acid) was assessed. Tests also included bolus injections of several different concentrations of DRPs to determine if preparations of DRPs could be injected in relatively high concentrations in short time periods without an undesirable hemodynamic reaction.

5.3.1 Effect of the acute injection of PEO-4500 solutions on hematological and blood coagulation parameters.

Experiments were performed in which arterial blood samples were collected before and 30 min after the intravenous injection of PEO-4500 (5 μg/ml (1.11 nM), saline in control) into anesthetized rats. Complete blood count (CBC) plus differential, prothrombin time (PT), partial thromboplastin time (PTT), fibrinogen and the fibrin degradation product D-Dimer were measured in these blood samples. Additionally, the time for clot formation with and without DRPs was tested *in vitro*.

Results of acute PEO injections in rats on hematological and blood coagulation parameters are given in **Table 5.1**. No change in PT (sec) was observed when comparing Control pre vs. post. However, a slight but statistically significant increase (3.8%, $p<0.05$) was observed in PT (sec) when comparing DRP pre vs. post. No statistically significant change was observed in PTT, D-Dimer MCV, MCH, MCHC, and platelet count when comparing pre vs. post samples of both PEO-4500 and Control animals suggesting that the drag-reducing polymer PEO-4500 did not alter these measured hematological and hemostatic parameters. Slight but statistical changes were observed in fibrinogen concentration, Ht, Hb, and WBC count. Since a similar difference was observed in Control Post and PEO-4500 Post samples, these changes did not signify any effect by the DRP but can be attributed to blood sampling (~25% of blood volume) during these *in-vivo* experiments.

The clotting times were 295 ± 66, 321 ± 85 and 279 ± 48 for the Control, PMNN and PEO samples, respectively. No statistical significance was found in these tests.

In general, no significant alteration was found in the major measured hematological and hemostatic parameters after PEO-4500 infusion demonstrating that PEO-4500 does not have any deleterious effects on clotting and hemostasis. It might be suggested that similar experiments be repeated in which smaller blood samples are drawn to reduce the effects of sampling.

Table 5.1: Results of acute PEO injections in rats on hematological and blood coagulation parameters

	Control		PEO		
Parameters	**Pre**	**Post**	**Pre**	**Post**	***p*-value**
Coagulation					
PT (sec)	15.5±0.5	15.7±0.4	15.6±0.8	16.2±1.0	$> 0.05^{a}$,$< \mathbf{0.05^{b}}$
PTT (sec)	19.4±3.2	19.4±2.0	18.5±2.1	18.2±2.1	$> 0.05^{a,b}$
Fibrinogen (mg/dl)	257±22	234±27	265±29	226±12	$\mathbf{< 0.05^{a,b}}$
D-Dimer (ng/ml)	< 250	< 250	< 250	< 250	*N/A*
Complete Blood Count					
Hb (g/dl)	14.4±0.6	13.3±0.5	14.8±0.7	13.8±1.4	$\mathbf{< 0.01^{a}}$,$\mathbf{< 0.05^{b}}$
Ht (%)	44±2	40±2	45±3	41±4	$\mathbf{< 0.001^{a,b}}$
WBC (10^3/µl)	4.1 ±1.1	2.8 ±1.2	5.5±1.7	2.8±1.2	$> 0.05^{a}$,$< \mathbf{0.05^{b}}$
RBC (10^6/µl)	7.8±0.3	7.0±0.4	8.0±0.5	7.4±0.6	$\mathbf{< 0.01^{a}}$,$\mathbf{< 0.001^{b}}$
MCV (fl)	60.0±1.9	59.4±2.6	58.3±3.4	58.0±3.5	$> 0.05^{a,b}$
MCH (pg)	18.5±0.6	19.0±0.6	18.5±0.6	18.5±1.1	$> 0.05^{a,b}$
MCHC (%)	30.9±1.2	32.0±2.0	31.7±1.2	31.9±0.5	$> 0.05^{a,b}$
Platelet Count (10^3/µl)	855±149	774±158	836±257	722±289	$> 0.05^{a,b}$
Differential					
Neutrophils (%)	18±7	28±8	23±7	40±15	$\mathbf{< 0.001^{a}}$,$\mathbf{< 0.01^{b}}$
Bands (%)	0	0	0	0	*N/A*
Lymphocytes (%)	79±7	69±8	75±7	57±15	$\mathbf{< 0.001^{a}}$,$\mathbf{< 0.005^{b}}$
Monocytes (%)	1±0	1±1	1±0	2±1	$> 0.05^{a,b}$
Eosinophils (%)	1±1	1±1	2±1	2±2	$> 0.05^{a,b}$
Basophils (%)	0	0	0	0	*N/A*

[a]Control pre vs. post [b]DRP pre vs. post

5.3.2 Effects of chronic infusions of DRPs on parameters of cardiovascular, respiratory, liver and renal function.

Experiments were performed in which blood gas, CBC differential, and blood serum chemistry parameters were measured in order to investigate the effects of chronic infusions of DRPs (2x/week over 7 weeks) on cardiovascular, respiratory, liver and renal function. Measurements of blood gas parameters (**Table 5.2**) showed relatively little difference between experimental and control animals. In these particular groups isoflurane anesthesia was administered via 100% O_2. The results of the measurement of CBC differential parameters showed no difference between control and experimental groups (**Table 5.3**). Blood serum chemistry measurements also demonstrated that no difference exists between control and experimental groups (**Table 5.4**). The abnormally high blood glucose levels seen in these results are likely due to the animal's response to the stress of being handled, anesthesia and blood collection.

Table 5.2: Blood gas parameters measured in rats injected twice weekly with DRPs (PEO and PMNN, saline in control) for 7 weeks

Parameter	**Control**	**PEO**	**PMNN**	***p*-value**
pH	7.403±0.036	7.389±0.044	7.422±0.042	>0.05[a,b]
pCO_2 *(mmHg)*	46.8±5.5	45.7±7.1	44.4±6.4	>0.05[a,b]
pO_2 *(mmHg)*	105.3±24.3	94.2±6.6	80.9±16.0	>0.05[a,b]
$cHCO_3$ *(mmol/L)*	28.4±1.1	26.8±1.8	28.2±1.2	>0.05[a,b]
ABE *(mmol/L)*	3.4±0.6	1.8±1.1	3.7±0.2	>0.05[a,b]
tHb *(%)*	14.7±0.4	14.6±0.7	14.9±0.3	>0.05[a,b]
K^+ *(mmol/L)*	4.5±0.5	4.8±0.5	4.6±0.4	>0.05[a,b]
Na^+ *(mmol/L)*	136±2	136±1	136±1	>0.05[a,b]
Ca^{2+} *(mmol/L)*	1.39±0.02	1.40±0.04	1.38±0.02	>0.05[a,b]
Lactate *(mmol/L)*	0.9±0.2	0.7±0.2	1.4±0.3	>0.05[a,b]

[a]Control vs. PEO, [b]Control vs. PMNN

Table 5.3: CBC differential results measured in rats injected twice weekly with DRPs (PEO and PMNN, saline in control) for 7 weeks

Parameters	Control	PEO	PMNN	*p*-value
Complete Blood Count				
Hemoglobin *(g/dl)*	14.0±0.4	14.1±0.7	14.2±0.5	>0.05[a,b]
Hematocrit *(%)*	41.3±1.4	41.0±2.0	42.3±1.1	>0.05[a,b]
WBC *(10^3/ul)*	8.1±2.6	6.9±1.7	8.6±5.0	>0.05[a,b]
RBC *(10^6/ul)*	8.1±0.3	8.1±0.4	8.4±0.2	>0.05[a,b]
MCV *(fl)*	50.8±1.9	50.7±2.1	50.6±0.5	>0.05[a,b]
MCH *(pg)*	17.2±0.7	17.4±0.8	17.0±0.2	>0.05[a,b]
MCHC *(g/dl)*	34.0±0.7	34.4±0.4	33.6±0.6	>0.05[a,b]
MPV *(fl)*	6.4±0.4	6.2±0.1	6.1±0.2	>0.05[a,b]
Platelet Count *(10^3/ul)*	731±96	678±114	741±103	>0.05[a,b]
RDW *(%)*	14.1±0.3	14.4±1.6	15.2±1.2	>0.05[a,b]
Differential				
Lymphocytes *(10^3/ul)*	6.0±2.1	5.3±1.4	5.2±1.8	>0.05[a,b]
(%)	74.1±10.5	77.0±6.4	66.0±16.0	>0.05[a,b]
Monocytes *(10^3/ul)*	0.5±0.1	0.3±0.2	1.0±0.6	>0.05[a,b]
(%)	7.1±1.1	4.1±2.7	7.8±2.0	>0.05[a,b]
Granulocytes *(10^3/ul)*	1.9±1.1	1.5±0.7	3.0±3.0	>0.05[a,b]
(%)	23.1±7.8	20.7±5.1	30.1±13.0	>0.05[a,b]

[a]Control vs. PEO, [b]Control vs. PMNN

Table 5.4: Blood serum chemistry results measured in rats injected twice weekly with DRPs (PEO and PMNN, saline in control) for 7 weeks

Parameters	Control	PEO	PMNN	*p*-value
BUN *(mg/dl)*	19±5	18±3	20±3	>0.05[a,b]
Glucose *(mg/dl)*	300±52	306±32	270±35	>0.05[a,b]
ALP *(IU/l)*	240±42	284±46	263±72	>0.05[a,b]
T-Pro *(g/dl)*	4.9±0.3	5.3±0.5	5.1±0.3	>0.05[a,b]
ALT *(IU/l)*	16±3	16±5	15±3	>0.05[a,b]
Creatinine *(mg/dl)*	0.5±0.1	0.5±0.1	0.6±0.1	>0.05[a,b]

[a]Control vs. PEO, [b]Control vs. PMNN

These experiments demonstrated that long-term (7 week) intravenous injections of DRPs (PEO and PMNN) at concentrations found to be hemodynamically effective (1-2 μg/ml (0.17 – 0.44 nM)) for the reduction of vascular resistance have no effect on the blood gas, CBC differential, and blood serum chemistry parameters measured in this study and suggests no effect on the cardiovascular, respiratory, liver and renal function.

5.3.3 Hemodynamic efficiency of the intravenous infusion of the pharmaceutical grade hyaluronic acid solution

Two experiments were performed to evaluate the *in vivo* hemodynamic efficiency of a pharmaceutical grade hyaluronic acid preparation (Hyvisc®, Anika Therapeutics). In these experiments, healthy male Sprague-Dawley rats were anesthetized and instrumented in order to monitor arterial blood pressure (right carotid artery), heart rate, carotid flow rate (left carotid artery), and skin tissue perfusion (plantar surface of both hind paws – relative changes compared to baseline).

In the first experiment, the hyaluronic acid solution was intravenously infused via the jugular vein at concentrations of 50 (16.7 nM), 125 (41.7 nM), 250 (83.3 nM) and 250 μg/ml (83.3 nM) to yield final blood concentrations of 1 (0.33 nM), 6 (2.0 nM), 16 (5.33 nM) and 33 μg/ml (11.0 nM) of the DRP, respectively. **Figure 5.1** shows a portion of the record of the measured hemodynamic parameters (tissue perfusion (left and right plantar surface of hind paw), average arterial blood pressure and average carotid flow rate) taken before infusion and 20 minutes after infusion of the hyaluronic acid DRP. In this particular case, at the highest polymer dose (33 μg/ml (11.0 nM)), there was an increase in tissue perfusion in the left and right plantar

hind paw, of up to 37 and 51% respectively and an increase in carotid flow rate by 33%. The percent change in each hemodynamic parameter at each polymer dose is shown in **Table 5.5**. No change was observed in blood pressure and heart rate. The calculated vascular resistance for tissue perfusion measurements (MAP/tissue perfusion) of the left and right plantar surface of the hind paw and for carotid flow measurements (MAP/average carotid flow rate) before the infusion and 20 minutes after each polymer dose is shown in **Figure 5.2**.

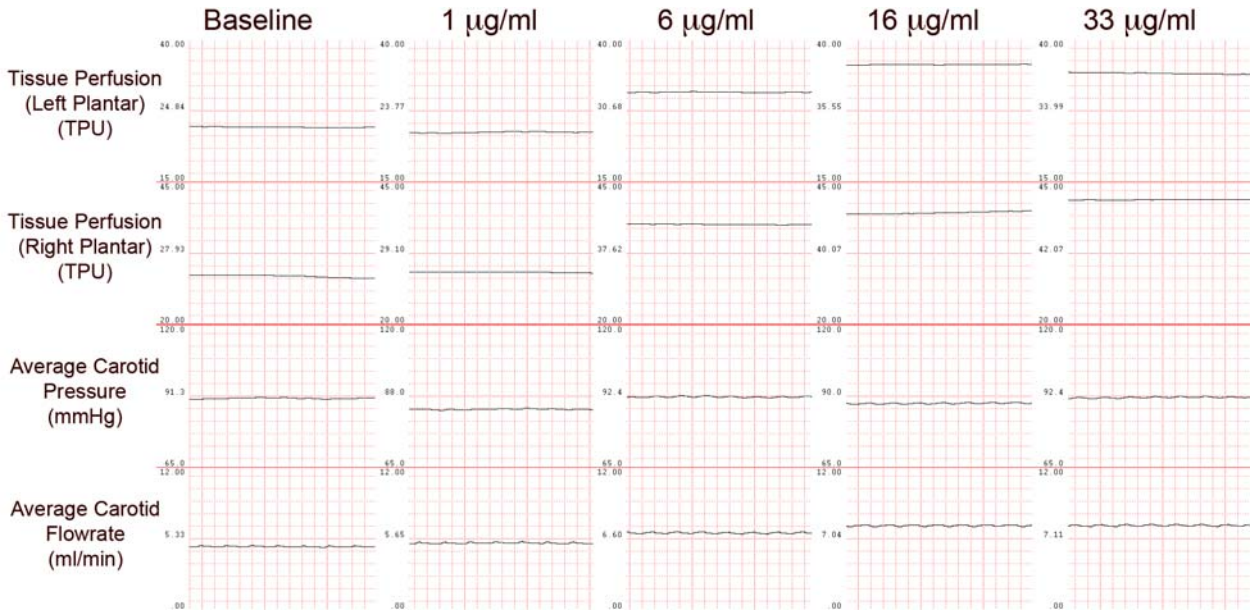

Figure 5.1: Portion of a hemodynamic recording of the infusion of a hyaluronic acid DRP at concentrations up to 33 μg/ml (11 nM).

A portion of a record of the hemodynamic parameters (tissue perfusion (left and right plantar surface of hind paw), average arterial blood pressure and average carotid flow rate) shown before infusion and 20 minutes after infusion of the hyaluronic acid DRP Hyvisc® at a final blood concentration of 1 (0.33 nM), 6 (2.0 nM), 16 (5.33 nM) and 33 μg/ml (11.0 nM).

Table 5.5: Percent change in hemodynamic parameters from baseline measurements 20 minutes after infusion of the hyaluronic acid DRP, Hyvisc®

	Blood Concentration of Hyaluronic Acid (μg/ml)			
Parameters	**1**	**6**	**16**	**33**
Tissue Perfusion (LP, TPU)	no effect	24 %	43 %	37 %
Tissue Perfusion (RP, TPU)	4 %	35 %	44 %	51 %
Average Carotid Flow Rate (ml min^{-1})	6 %	24 %	32 %	33 %

The percent change in hemodynamic parameters (tissue perfusion (left and right plantar (LP and RP, respectively) surface of hind paw) and average carotid flow rate) from baseline measurements 20 minutes after infusion of the hyaluronic acid DRP, Hyvisc®, at final blood concentrations of 1 (0.33 nM), 6 (2.0 nM), 16 (5.3 nM) and 33 μg/ml (11.0 nM). No change was observed in average carotid blood pressure.

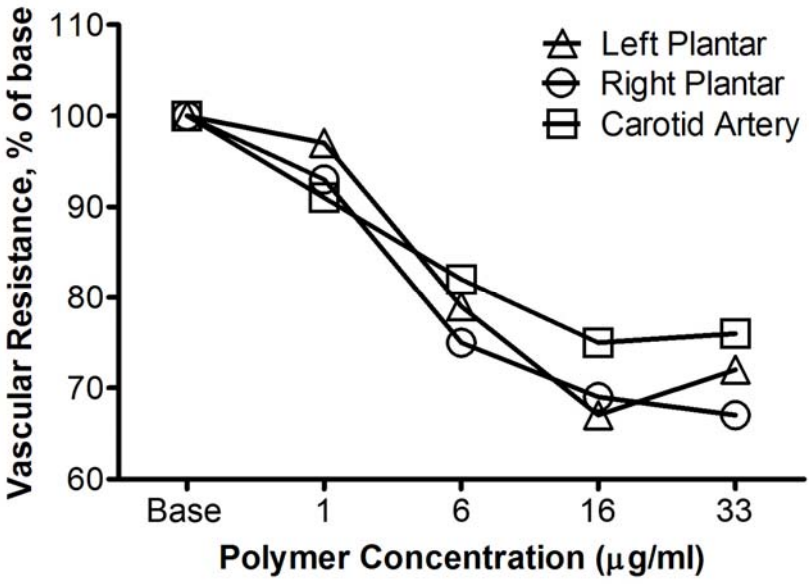

Figure 5.2: Calculated vascular resistance for hemodynamic measurements during baseline and 20 minutes after the infusion of the hyaluronic acid DRP, Hyvisc® at 4 final concentrations

Vascular resistance was calculated for tissue perfusion measurements (MAP/tissue perfusion) of the left and right plantar surface of the hind paw and for carotid flow measurements (MAP/average carotid flow rate) during baseline and 20 minutes after each polymer dose.

In another study, hyaluronic acid was injected at concentrations up to 1500 μg/ml (0.5 μM) to yield a final blood concentration of 150 μg/ml (50 nM). **Figure 5.3** shows a portion of a record of hemodynamic parameters (tissue perfusion (left and right hind paw), mean arterial blood pressure, and average carotid flow rate) taken before the infusion and 15 and 10 minutes after the infusion of the hyaluronic acid DRP at a final blood concentration of 50 (16.7 nM) and 150 μg/ml (50 nM), respectively. An increase in tissue perfusion in the left and right plantar hind paw, an increase in carotid flow rate and a slight increase in mean arterial pressure were observed. However, after increasing the DRP concentration in blood to 150 μg/ml (50 nM), the tissue perfusion and carotid flow rate slightly decreased but were still significantly higher than before DRP infusion. The percent change in each hemodynamic parameter at each the polymer dose is shown in **Table 5.6**. A potential reason for this decrease might be an increase in blood viscosity due to this high polymer concentration (relative to the usual concentration given to observe beneficial hemodynamic effect of DRPs, ~1 μg/ml (0.17 – 0.33 nM)). The animal tolerated the higher concentration infusion very well, and no adverse effects (i.e., hematuria) were found from infusing the hyaluronic acid DRP at these higher concentrations.

In these experiments, Hyvisc® (Anika Therapeutics), a commercially available pharmaceutical grade hyaluronic acid preparation, demonstrated a hemodynamic effect (decrease in vascular resistance) similar to other commonly used DRPs (PEO and PMNN).

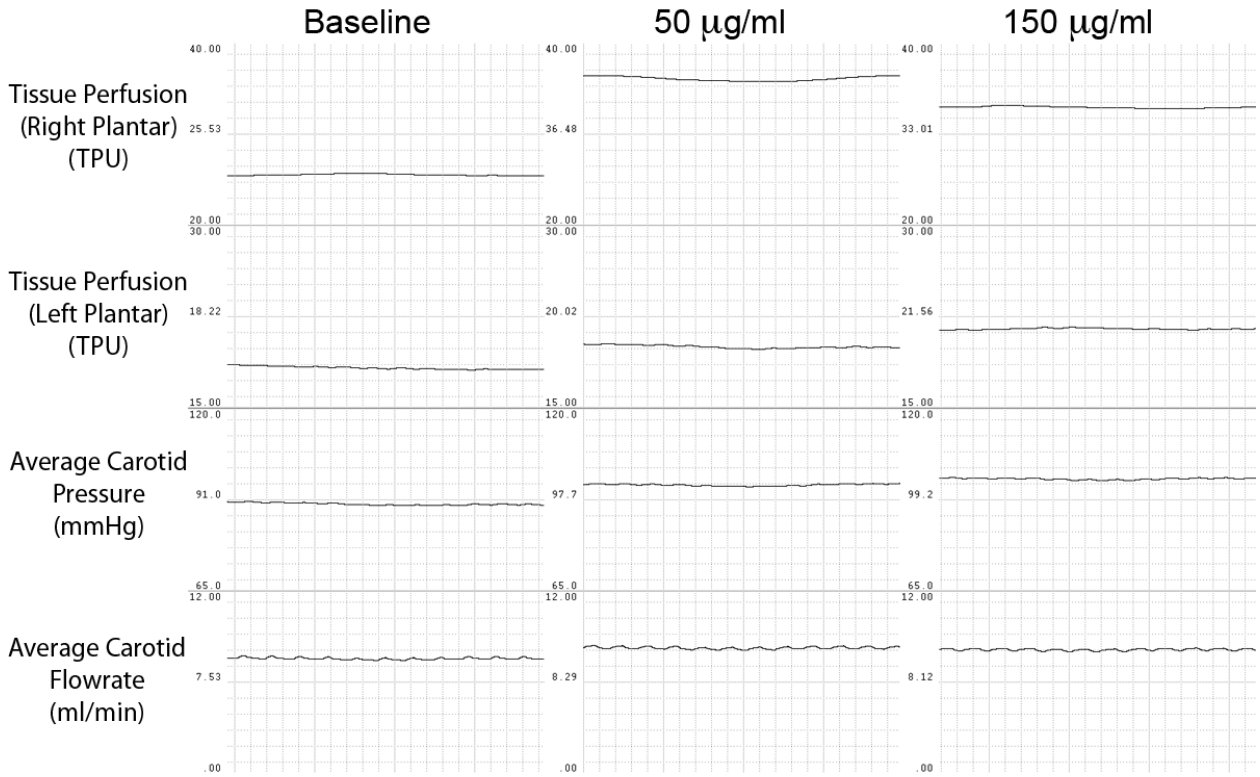

Figure 5.3: Portions of a record of the hemodynamic parameters taken before infusion and 30 minutes after infusion of the hyaluronic acid DRP Hyvisc®

Shown above is a portion of a record of the hemodynamic parameters (tissue perfusion (left and right plantar surface of hind paw), average arterial blood pressure and average carotid flow rate) taken before infusion and 30 minutes after infusion of the hyaluronic acid DRP Hyvisc® at a final blood concentration of 50 (16.7 nM) and 150 µg/ml (50 nM).

Table 5.6: Percent change in hemodynamic parameters from baseline measurements 30 minutes after infusion of the hyaluronic acid DRP, Hyvisc®

	Blood Concentration of Hyaluronic Acid (µg/ml)	
Parameters	**50**	**150**
Tissue Perfusion (L; TPU)	43 %	29 %
Tissue Perfusion (R; TPU)	10 %	18 %
Average Carotid Flow Rate (ml/min)	10 %	8 %
Average Carotid Pressure (mmHg)	7 %	9 %

The percent change in hemodynamic parameters (tissue perfusion (left and right plantar surface of hind paw) and average carotid flow rate) from baseline measurements 30 minutes after infusion of the hyaluronic acid DRP, Hyvisc®, at final blood concentrations of 50 (16.7 nM) and 150 µg/ml (50 nM).

5.3.4 Outcomes of bolus infusions of PMNN and PEO-4500

As a measure of acute toxicity and in order to test the applicability of giving higher doses (~100 μg/ml (up to ~22 nM)) of DRPs in a short bolus infusion as one might see in the resuscitation during hemorrhagic shock, two experiments were performed in which PEO-4500 and PMNN were infused at concentrations ranging from 2 (0.44 nM) to 100 μg/ml (22.2 nM) and 2 (0.33 nM) to 50 μg/ml (8.33 nM), respectively, in a fixed volume (1 ml) over 10 seconds. In the case of a human patient with a normal blood volume of 5 liters, this would represent a bolus infusion of ~150 ml given in 10 seconds. Therefore, this procedure represents a radical simulation of a bolus infusion.

In general, the animals tolerated the bolus infusions at tested DRP concentrations well and no adverse reactions were observed. A slight increase in mean arterial pressure was observed after the DRP injection but quickly returned to pre-injection values.

The results of these experiments suggest that PMNN and PEO-4500 can be delivered in small volumes at relatively higher concentrations without adverse effects. This may prove to be relevant in the treatment of hemorrhagic shock where small volume resuscitation is important.

A limitation in the significance of this test is the gradual increase in the blood DRP concentration versus a primary bolus of 50 (1.1 – 8.3 nM) or 100 μg/ml (22.2 nM). By gradually increasing the DRP concentration, the vascular system may adapt to the DRP intravascular effect therefore masking any potential side effects that would occur by a single bolus infusion of 100 μg/ml (22.2 nM). Future studies may focus on investigating the side effects of giving a series of short bolus infusion of gradually increasing concentration versus a single short bolus infusions of

higher DRP concentration. This would provide insight into dosing protocols for conditions where DRPs need to be infused via a bolus injection.

5.3.5 Outcomes of the infusions of extremely high concentrations of PMNN and a pharmaceutical grade hyaluronic acid solution.

Two experiments were performed to investigate the hemodynamic effect of a slow infusion of extremely high concentrations, up to 150 times the hemodynamically effective concentration, of PMNN and hyaluronic acid (Hyvisc®; Anika Therapeutics). PMNN was infused at a concentration of 1250 μg/ml (0.42 μM) over 20 min resulting in a total blood concentration of ~60 μg/ml (20 nM) of the DRP. A slight deterioration of the measured hemodynamic parameters (a slight increase in arterial blood pressure, and decrease in tissue perfusion and carotid artery flow rate) was observed during the infusion and might be explained by a local increase in blood viscosity due to poorer mixing of the DRP solution in the venous system. Blood samples obtained immediately following the infusion of PMNN and immediately prior to the end of the experiment showed little to no difference in blood gas values and blood hematocrit. However, a high plasma free hemoglobin concentration (hemolysis), ~300 mg/dl, was detected in the final blood sample (60 minutes post infusion). This may have lead to vasoconstriction related to a free hemoglobin effect on endothelial nitric oxide (reduction of the NO concentration) which may further explain the slight decrease in tissue perfusion and carotid artery flow rate that were observed. This phenomenon was previously discussed in the literature where in earlier animal studies using much higher doses of DRPs (both synthetic and natural) than those which are needed to produce beneficial hemodynamic effects, hematuria and hemolysis occurred through unknown mechanisms [6, 32]. Interestingly enough, the infusion of the hyaluronic acid DRP

solution at the same flow rate and at a much higher concentration in the syringe (3000 μg/ml (1 μM), asymptotic viscosity ~40 cP at 22°C) did not cause any hemolysis, although the final DRP concentration in the animal's blood was ~150 μg/ml (50 nM). The test results with Hyvisc® show that this DRP may be a strong candidate for larger animal trials and future clinical use.

5.4 SUMMARY

In this chapter, an investigation on the effects of DRPs on a variety of coagulation, hematologic, blood gas and serum chemistry parameters was performed *in vitro* and *in vivo* after acute and chronic DRP administration, at hemodynamically effective concentrations, to rats to exclude any deleterious effects of these long-chain molecules on hemostasis, hematology and organ function. Acute injections of DRPs (PEO-4500) showed no significant effects on clotting and hemostasis. Likewise, long-term (7 week) intravenous injections of DRPs (PEO-4500 and PMNN) produced no noticeable effect on the studied hematologic, blood gas and serum chemistry parameters suggesting that chronic injections of DRPs do not alter cardiovascular, respiratory, liver and renal function.

In another set of experiments, a new DRP Hyvisc® (Anika Therapeutics), a commercially available pharmaceutical grade hyaluronic acid preparation, demonstrated a hemodynamic effect (decrease in vascular resistance) similar to other previously used DRPs (PEO and PMNN). These results are significant for the future clinical translation of DRPs. Potential "off-label" use of pharmaceutical grade hyaluronic acid preparations could dramatically lessen the time required to move these studies from the laboratory bench to use in patients.

Pilot studies were also performed to investigate the potential problems related to the intravenous infusion of high concentrations of DRP solutions. In acute experiments, the hemodynamic response of normal animals to an intravenous infusion of high concentrations of several DRPs (PMNN, PEO-4500 and hyaluronic acid) was assessed. Tests also included bolus injections of several different concentrations of DRPs (PMMN and PEO-4500) to determine if these preparations could be injected in relatively high concentrations in short time periods without an undesirable hemodynamic reaction. Tests with bolus injections of solutions with relatively high concentrations of DRPs and slow infusions of solutions with extremely high DRP concentrations, up to 150 times the hemodynamically effective concentration, showed that the hyaluronic acid can be safely delivered into the vascular system in small volumes and at high infusion rate. However, PMNN, which was shown to be safe and effective when injected at relatively low concentrations, was found to produce hemolysis in blood after a slow injection at extremely high concentration which can be related to the fact that there are still some impurities in this homemade preparation. Delivery of small volumes at relatively high concentrations is relevant in the treatment of hemorrhagic shock in situations where small volume resuscitation is important.

6.0 EFFECTS OF DRPS ON BIODEGRADATION AND TISSUE DEVELOPMENT IN SYNTHETIC SCAFFOLDS

6.1 INTRODUCTION

Over the last decade tissue engineering has intensively explored the development of biological, synthetic or biosynthetic hybrid substitutes of almost every mammalian tissue. One of the challenges of these new regenerative therapies is the restoration and maintenance of blood flow to provide nutrients to and remove waste products from these engineered tissues and biomaterials. Angiogenesis, the growth of blood vessels from those pre-existing, is a critical component of this process, especially in the biointegration and biocompatibility of biomaterials and healing of wounds. It was previously shown that a sustained hemodynamic wall shear stress stimulates neovascularization and repair of damaged tissue *in vivo* [77]. Blood-soluble drag reducing polymers (DRPs) were recently shown to restructure the distribution of red blood cells (RBCs) in *in vitro* models of microvessels with diameters below 300 μm and significantly increase wall shear stress [11]. Previously demonstrated beneficial hemodynamic effects of DRPs are related in part to this ability to decrease the cell-free plasma layer in microvessels leading to facilitation of gas transport and, at the same time, to an increase in the near-wall blood viscosity which would load vessel walls with higher shear stresses. This latter effect might

promote angiogenesis and vasculogenesis via mechanotransduction mechanisms that translate these mechanical forces into biological responses of endothelial cells.

The original focus of the study presented in this chapter was to investigate the hypothesis that the chronic intravascular injection of DRPs, which are able to increase microcirculatory blood flow and wall shear stresses in microvessels, would facilitate increased blood vessel formation and thus improved tissue infiltration in a biodegradable synthetic scaffold implanted subcutaneously in rat. Later we reconsider the aim of this study mostly concentrating on the collagen tissue formation and structure and amount of foreign bogy giant cells (FBGC) presented in biodegraded scaffolds. Experiments were carried out with porous polymeric scaffolds which were implanted subcutaneously in rats. The animals were injected prior to and twice weekly for 7 weeks post scaffold implantation with DRP solutions (saline as Control). Histological and digital analysis techniques were used for assessment of tissue infiltration and growth and collagen deposition as well as blood vessel growth inside the scaffold matrix following scaffold explant.

6.2 METHODS

6.2.1 Fabrication of PLLA scaffolds

Porous poly(L-lactide) (PLLA) scaffold implants were prepared by the combination of solvent casting and thermally induced phase separation (TIPS) by Dr. Ravikumar Thangappan in the laboratory of Professor Alan J. Russell (McGowan Institute of Regenerative Medicine, University of Pittsburgh, Pittsburgh, PA). Medical grade PLLA (RESOMER® L 210; Boehringer Ingelheim Pharma GmbH & Co KG, Ingelheim, Germany) was used in the

fabrication of the scaffolds. The PLLA used had an inherent viscosity of 3.3-4.3 dl/g (0.1% in chloroform, 25 °C) and a residual monomer of less than 0.1%. To obtain ~100 cm^2 of the scaffold sheet, 1.0 g of amorphous PLLA was dissolved in 10 ml of anhydrous 1,4-Dioxane (99.8%, Sigma Aldrich, St. Louis, MO) and mixed by a magnetic stirrer for 2 hours. After the polymer was thoroughly mixed and homogenized, it was poured into a pre-cooled (-20º C) aluminum pan (10 cm x 10 cm) to form a 1-mm thick PLLA sheet. The aluminum pan with PLLA sheet was immediately placed into a freezer (–20° C). After 24 hours, the PLLA sheet was lyophilized for three days to completely remove the solvent. The polymer sheet was sliced into ~1 cm^2 size pieces using a surgical blade to make the scaffold implants and subsequently cold gas sterilized (38 °C) by exposure to ethylene oxide (EtO). The EtO sterilization process included a 4.5-hour cycle with exposure to EtO gas and a subsequent 36-hour aeration cycle for the complete removal of the EtO gas. The scaffolds were stored in their sterilization pouch until implantation.

6.2.2 Examination of PLLA scaffolds by SEM

PLLA scaffold pieces (n = 4) were examined before and after EtO sterilization using a scanning electron microscope (SEM) (JEOL JSM6330F, Tokyo, Japan) at 2.5 kV at 25x, 50x, 150x, 1000x, and 2500x magnification to examine gross morphology, to ensure uniformity and to measure scaffold porosity. For SEM examination, scaffolds, randomly chosen before and after sterilization, were cut into smaller sections by a surgical blade, mounted on an aluminum stub covered with a carbon adhesive, critical point dried and then sputter-coated with gold particles.

The images were collected at 1000x and 2500x from various regions of the scaffold. Using the public domain NIH Image program (Version 1.38x; developed at the U.S. National

Institutes of Health and available on the Internet at http://rsb.info.nih.gov/nih-image/) on a personal computer, pores were differentiated from the PLLA scaffold structure using image thresholding. The thresholded image was subsequently used to calculate porosity (%). An average porosity was calculated for the scaffolds before and after sterilization and statistical analysis was executed using a pair wise comparison (paired t-test). A $p < 0.05$ was considered to be statistically significant.

6.2.3 Animal Care Compliance

The surgical procedures and animal treatments performed in this study were approved by the Institutional Animal Care and Use Committee of the University of Pittsburgh (protocol #0511167). All animal care and procedures conformed to the National Institutes of Health Guidelines for the Care and Use of Laboratory Animals.

6.2.4 Animals

Male Sprague-Dawley rats (350-400 g, SASCO; Charles River Laboratories, Wilmington, MA) were housed in solid bottom micro-isolator containers and fed rat chow and water *ad libitum*. The animals were allowed a 6-day acclimatization period after delivery before experimental procedures commenced.

6.2.5 Drag-reducing polymers

Two drag-reducing polymers were employed in these studies: a synthetic DRP (polyethylene oxide with MW of 4500 kD, PEO-4500; Dow Chemical) and a natural aloe-based DRP obtained in our laboratory (Poly(mannan), PMNN; MW=~4000-6000 kD). Descriptions of these DRP preparation were outlined in Chapter 3.2.2.1. A control solution consisted of sterile nonpyrogenic isotonic saline (0.9%, Baxter). Three groups (5 animals/group) were included in this study: PEO, PMNN and Control.

6.2.6 Chronic intravenous infusion of DRP solutions in animals

The animals received intravenous (IV) injections of DRPs two times per week, on Monday and Thursday, via the dorsal penile vein beginning on the day prior to scaffold implantation. The animals were anesthetized for the injection procedure due to the time required for administration of the DRPs and to minimize pain and distress on the animals. Anesthesia was induced and maintained by inhalation of isoflurane (1.5-4%) in O_2 to sustain a surgical plane of anesthesia evidenced by the absence of pedal reflex. Animals were placed on a warming pad in dorsal recumbency and the penis was extruded from its sheath to visualize the dorsal penile vein. The injection site was disinfected with 70% ethanol alcohol and then a 5% povidone-iodine solution. The DRP solutions were infused using a 27 gauge needle, attached to a microbore catheter (Arrow International, Reading, PA) and a syringe on a syringe pump (PhD 2000; Harvard Apparatus, Holliston, MA), that was inserted into the penile vein at a controlled rate of infusion over 3-5 minutes. The infused volume (~1 ml) was calculated based on animal weight, original DRP concentration (50 μg/ml (1.1 – 8.3 nM)) and the desired DRP dosage to be given to the

animal (120 μg/kg or 2 μg DRP/ml blood (0.33 – 0.44 nM)). Blood volume was estimated as 6% of lean body weight. The animals of the Control group received the same number of intravenous injections and the same weight-based volume of the control solution. Sterile gauze was held over the injection site until bleeding ceased.

Due to their very high MW and long-chain structure of molecules, the DRPs can be only delivered into blood through IV administration. Although the DRP solutions were injected at concentrations as low as 50 μg/ml (1.1 – 8.3 nM), the ~ 1 ml solution was injected slowly (over 3-5 min) to provide better mixing of the DRP molecules with the blood, to eliminate the risk of potential hemolysis due to rapid injecting the polymers as a bolus infusion as previously reported [6], and to reduce the risk of overwhelming the capacity of the small veins during the injection.

6.2.7 Surgical procedures and animal care during 7-week scaffold implantation study

6.2.7.1 Scaffold implant procedure.

The scaffolds were implanted on the day following the first DRP infusion. Anesthesia was induced and maintained by inhalation of isoflurane in O_2. The isoflurane concentration (1.5-4%) was adjusted to maintain a surgical plane of anesthesia evidenced by the absence of pedal reflex. Animals were placed on a warming pad in ventral recumbency and the surgical site prepared. A portion of the dorsal surface, from the base of the skull to the midline of the dorsum, was shaved and disinfected with 70% ethanol alcohol and then a 5% povidone-iodine solution. Aseptic technique was followed by using sterile instruments, drapes and techniques. A 1.5-cm incision was made at the dorsum midline, orthogonal to the sagittal plane, down to the level of the panniculus carnosus, 1 cm caudal to the scapulae. A subcutaneous pocket was created caudal to the incision with blunt scissors, and a saline-moistened and sterile 1 cm^2 PLLA scaffold was

positioned in the pocket ~2-cm from the incision in order to avoid possible effects from healing. The incision was closed using several sterile 9-mm stainless-steel wound clips (MikRon Precision, Gardena, CA) which were removed by post-operative day (POD) 7.

6.2.7.2 Post-operative care.

All animals received a single subcutaneous (SQ) post-surgical prophylactic dose of gentamicin (5 mg/kg, APP Pharmaceuticals, Schaumburg, IL). The dorsal surface was cleansed with sterile saline and the animal was then removed from anesthesia and allowed to recover fully before returning to normal housing with free access to food and water for the remainder of the study duration.

Post surgical analgesia was provided by acetaminophen (PCCA, Houston, TX) administered via the animals' drinking water at a dose of 3.7 mg acetaminophen/ml drinking water during the 7 days prior to surgery and 5.4 mg acetaminophen/ml drinking water post-operatively up to POD 3. This dosage calculation is based on the normal water consumption of a rat which is 8-11 ml/100 gm body weight/day and that a daily oral dose of acetaminophen adequate to provide post surgical analgesia is 300 mg/kg [135]. The addition of the acetaminophen to the drinking water during 7 pre-operative days was necessary to allow adaptation of the animals to the altered taste of the water and avoid "neophobia". The concentration of acetaminophen was increased after surgery based on the assumption of reduced water consumption during the post surgical period.

6.2.7.3 Scaffold explant procedure.

At 7-weeks post-operative, the animals were anesthetized using isoflurane to obtain a surgical plane of anesthesia. The animal was placed in dorsal recumbency and was euthanized by an

intracardiac bolus of supersaturated (2 mmol/kg) potassium chloride (Hospira). Following euthanasia, the implant site of the PLLA scaffold was identified. The implant, along with adjacent native tissue, was surgically excised, photographed, and fixed in 10% neutral buffered formalin (Surgipath Medical Industries, Richmond, IL) for 24 hours at 25°C.

6.2.8 Histological Analysis

After fixation of the samples, the implants were prepared for histological analysis using routine processes. Briefly, the implants were dehydrated using a graded ethanol-xylene series, bisected in cross-section through the center and embedded in paraffin with the cut side down to provide cross section of the scaffold center. Two 5-μm thick sections, 100 μm apart, were prepared with a microtome and mounted on a microscope slide. By bisecting the scaffold, two samples per scaffold center were created. The sections were then deparaffinized and hydrated by a xylene-ethanol series and subsequently stained with Masson's trichrome which labeled collagen tissue blue and inflammatory cells of the granulomatous tissue a red to purple hue. The percentage of the area of the scaffold consisting of collagen and foreign body giant cells, collagen fiber orientation, and remaining scaffold material were quantified in the Masson's trichrome-stained cross-sections. Physical parameters (height, width, perimeter and area) of the implants were also evaluated.

Brightfield microscopy was performed on a Leica DM IRB inverted phase-contrast/fluorescence microscope (Leica Microsystems, Bannockburn, IL) equipped with a 4x objective (HI PLAN 4x/NA 0.10; Leica Microsystems). The cross section was panned in both the x- and y-axis and six to eight overlapping images (2560 x 1920 pixels; 8.90 mm^2) were obtained with a 12 bit 2588 x 1960 pixel CCD camera (DFC 480; Leica Microsystems) and PC-based

imaging management software (IM50; Leica Microsystems). The captured images were subsequently joined together (Canon Utilities PhotoStich; Canon USA, Lake Success, NY) to produce a composite image that consisted of the entire scaffold cross section. Digital analysis to quantify collagen and granulomatous tissue content, collagen alignment and the remaining PLLA implant area and measurements of the scaffold cross section physical parameters was performed on personal and Macintosh computers using the public domain NIH Image program and Adobe Photoshop 7.0 (Adobe Systems, San Jose, CA). A total of 30 images (2 images/scaffold) were analyzed.

6.2.8.1 Quantification of the number of blood vessels

Brightfield images of the tissue cross sections were captured with a 10x objective (N PLAN 10x/NA 0.25; Leica Microsystems) on the same inverted phase-contrast/fluorescence microscope system used to create composite images of the scaffold sections. The images were analyzed post hoc using NIH Image. Blood vessels were identified and counted in each field in a single-blinded manner. Blood vessels were identified by a luminal structure bordered with endothelial cell pattern containing RBCs within the intra luminal space. A total of 13 non-overlapping fields (1.43 mm^2) were examined in one of the two cross sections prepared from each scaffold. The cross section was chosen randomly. The number of vessels was counted and the tissue area of each image was quantified. Vessels were categorized in three sizes: 0-25 μm, 25-50 μm and greater than 50 μm. A blood vessel density was then calculated for each scaffold. Results are expressed as the mean ± standard deviation.

6.2.8.2 Quantification of granulomatous and collagen tissue

The quantification of the granulomatous and collagen tissue content of the scaffold cross sections was performed using a threshold HSI filter (Hue-Saturation-Intensity; Fovea Pro 1.0; Reindeer Graphics, Ashville, NC) in Adobe Photoshop 7.0. The Threshold HSI plug-in allowed for easy discrimination of the different tissue types by converting the color space to a graphical representation of the Hue-Saturation-Intensity space. Hue and Saturation were presented on a circle where the angle corresponded to the hue and the radius to the saturation while the darkness of the point (gray level) represented the number of pixels with that particular value. The user then highlighted the area on the circle corresponding to particular region of interest. To begin the analysis, the pixel dimensions of the 32-bit true color composite images produced from the Masson's trichrome-stained cross sections were decreased to reduce the image size from ~ 8 million to ~2 million pixels to make image analysis more manageable. The area in the image representing the scaffold was then selected in order to exclude the tissue area outside (i.e., the fibrous collagen capsule) from the analysis. The total number of pixels of the implant area was then computed from this selection and recorded. The Threshold HSI plug-in was then used to highlight the regions in the implant area corresponding to granulomatous and collagen tissue, respectively. The filter output was 2-bit images in which either the granulomatous or collagen tissue appeared black and all other tissues white. The total number of thresholded (black) pixels in the implant area was then computed and recorded. For each cross section, the area corresponding to granulomatous and collagen tissue was added to yield the total stained tissue area. The area in the scaffold cross sections consisting of granulomatous or collagen tissue as a percentage of the total stained tissue area was then calculated. Individual data points that were greater than two standard deviations from the mean value of the remaining data were discarded.

6.2.8.3 Collagen alignment analysis

The quantification of the alignment of the collagen tissue in the scaffold cross sections was performed using NIH Image using modifications to the methods previously described by Noorlander et al. [136]. The 32-bit true color composite images produced from the Masson's trichrome-stained cross sections were first converted into three separate 8-bit grayscale images containing the Red (R), Blue (B) and Green (G) color components of the original image using RGB Split. The red color component image was digitally subtracted from the blue color component image resulting in an 8-bit grayscale image which highlighted the collagen, represented by gray levels, against a black background. By subtracting color components, the probability of error in the analysis associated with potential variability in the levels of staining between tissue specimens is reduced. The grayscale image was then thresholded using the automatic threshold function in NIH Image to produce a 2-bit image in which pixels that met the threshold criteria (i.e., collagen fibers) were set to 0 (black) and all other pixels (i.e., background) were set to 255 (white). A flowchart illustrating the steps in the process to isolate collagen tissue in a scaffold cross section is shown in **Figure 6.1**. Automatic thresholding in NIH Image is based on the iterative technique developed by Ridler and Calvard [137]. Briefly, the image histogram was first divided into two parts based on an initial threshold which was chosen as half the maximum dynamic range. Then, the sample means of the gray values associated with the foreground pixels and those associated with the background pixels were computed and a new threshold was chosen as the average of these two sample means. This step was repeated until the new threshold value was the same as the threshold value in the previous iteration. The use of the automatic threshold function eliminates the potential bias introduced by a human observer. The

area in the image pertaining to the implant area (i.e., scaffold) was then selected to exclude area outside (i.e., the fibrous capsule) from further analysis.

An analysis was then performed on the thresholded (black) pixels with an area greater than 50 pixels^2 in which best fitting ovals were calculated for each black object. The area (pixels^2), length (number of pixels) of the major and minor axis, angle and circularity of each best-fit oval were then determined. Angle was defined as the angle (0-180°) between the major axis and a line parallel to the x-axis of the image. Circularity was defined as $4*\pi*(\text{area}/\text{perimeter}^2)$. A value of 1.0 indicated a perfect circle. As the value approached 0.0, it indicated an increasingly elongated polygon. Ovals with a circularity above 0.75 were eliminated from the analysis to reduce the probability of introducing error in the analysis. The results of the NIH Image calculations were copied into a spreadsheet (Excel XP; Microsoft Corp) and sorted based on major axis length. The coincidence of the angles of the 50 longest major axes was determined using the frequency function in Excel. This function produced an angle histogram with bins 10° wide starting from 0°. A collagen orientation index was then calculated by dividing the max value of the angle histogram (the angle that occurred most often) by the arithmetic mean of the angle frequency (the average of all angles). This produced a collagen orientation index ranging from a value of 1 (least organized) where the maximum value of the angle histogram was equal to the mean angle frequency to a value of 19 (most organized; equal to the total number of 10° angle bins) where all angles were in the same angle bin. Since the desired range was 0 to 1 for the collagen orientation index, the result above was divided by the total number of bins, 19, to product an index with a range of 1/19 to 1, which was considered close enough to a range of 0 to 1 to be easily interpreted. Individual data points that were greater than two standard deviations from the mean of the remaining data were discarded.

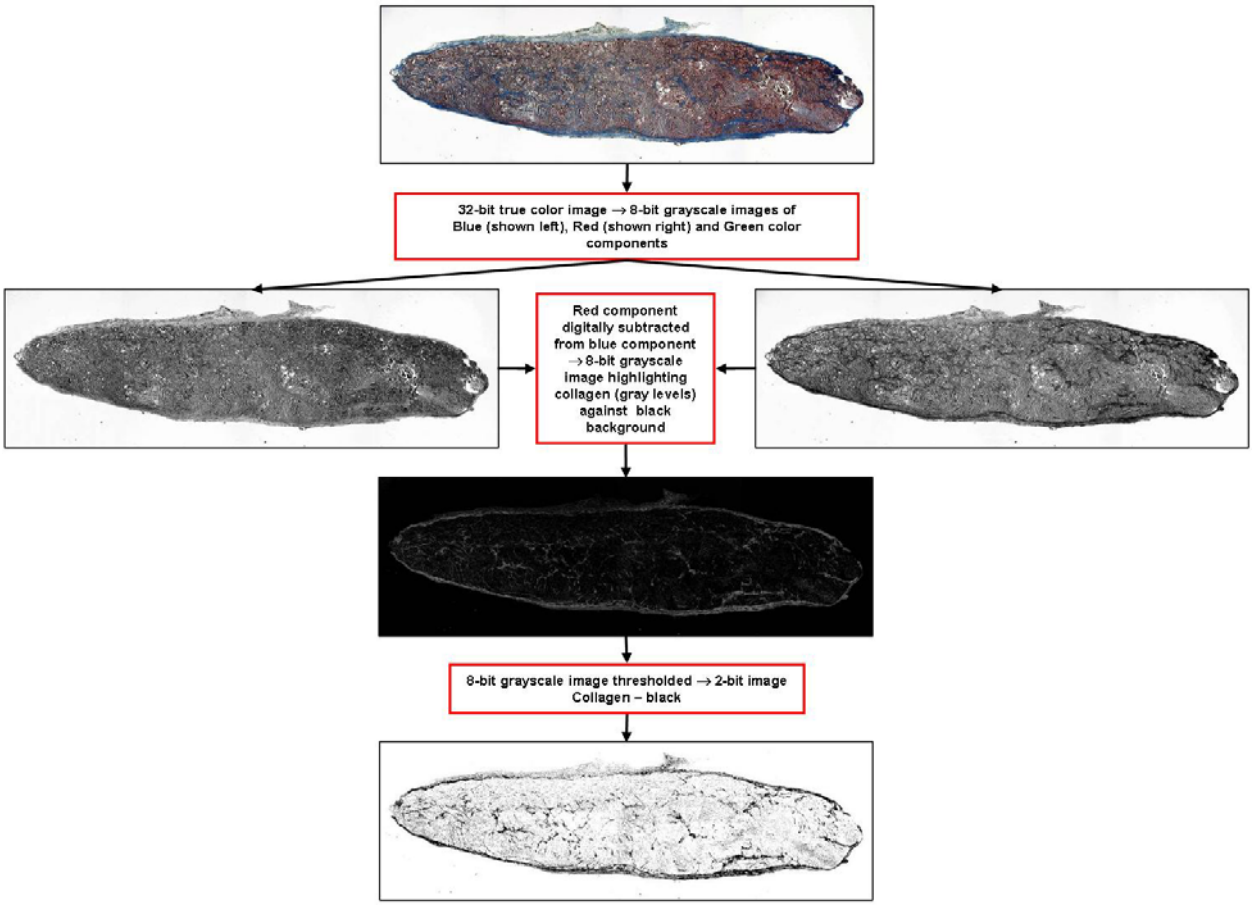

Figure 6.1: Flowchart illustrating the digital image analysis used to isolate collagen tissue in a scaffold cross section

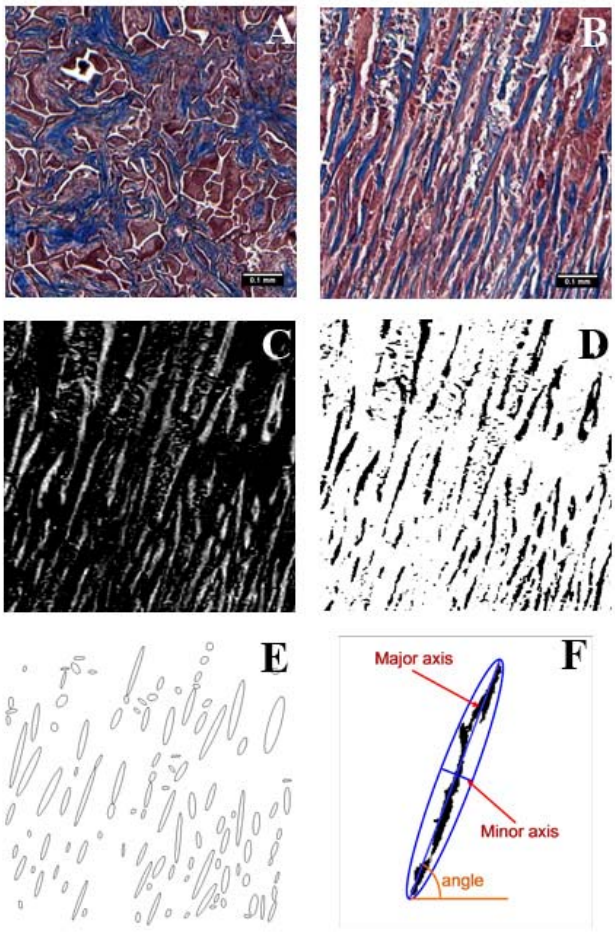

Figure 6.2: Demonstration of the techniques performed to quantify the orientation of collage fibers in the scaffold cross sections

(A,B) Brightfield images of PLLA scaffolds stained with Masson's trichrome from the Control group (A) which demonstrates disorganized collagen and the PEO group (B) which demonstrates organized collagen. (C) 8-bit grayscale image showing isolated collagen structures of the image B. (D) 2-bit image obtained after thresholding on the collagen fibers (black). (E, F) Best fit ovals were placed around collagen structures. A major axis length and its angle from a line parallel to the x-axis were calculated which were used to determine an orientation index.

6.2.8.4 Quantification of the remaining scaffold material

The birefringence of the PLLA polymer was used to quantify the amount of remaining PLLA material in the Masson's trichrome-stained scaffold cross sections via polarized light microscopy.

Scaffold cross sections were placed between two crossed polarization filters and images were captured on a Nikon TE2000 inverted phase-fluorescence microscope (Nikon Instruments, Melville, NY) equipped with a 10x plan fluorite objective (Plan Fluor DL 10x/NA 0.30 w/phase ring PhL; Nikon Instruments) and a 12 bit 1600 x 1200 pixel CCD camera (Spot; Diagnostic Instruments, Sterling Heights, MI) coupled to a Macintosh computer (Power PC; Apple Computer, Cupertino, CA). Two 10x images (0.95 mm^2) were captured from each scaffold cross section. A corresponding brightfield image was also captured of the same area to allow for comparison.

The polarized light images were then analyzed with NIH Image on a personal computer. The 32-bit true color composite images were first converted into 8-bit grayscale images. The grayscale image was then manually thresholded to produce a 2-bit image in which pixels that met the threshold criteria (i.e., remaining PLLA particles) were set to 0 (black) and all other pixels (i.e., background and tissues) were set to 255 (white). The total area of each 10x image (0.95 mm^2) that was comprised of black pixels was then computed. The results obtained from the two images captured from each scaffold cross section were averaged. Individual data points that were greater than two standard deviations from the mean value of the remaining data were discarded.

6.2.8.5 Statistical analysis

Results are expressed as the mean ± standard error for each group unless previously noted. Each cross sectional image was considered to be an independent sample from the group. In each group, a total of five animals were each implanted with a single scaffold. During histological processing, two cross-sections were cut from a single scaffold. Therefore, the mean and standard error calculations of the measured parameters were based on 10 samples/group unless otherwise noted. Since there were three treatment groups in this study, a one-way ANOVA with Tukey post-hoc test was used to compare the mean value of the parameter of interest in the experimental groups (i.e., PEO-4500 and PMNN injected animals) to that of the Control group. A $p < 0.05$ was considered to be statistically significant.

6.3 RESULTS AND DISCUSSION

6.3.1 SEM analysis of PLLA scaffolds before implantation

Scanning electron micrographs were collected at 25x, 50x, 150x, 1000x and 2500x to assess the general morphology of PLLA scaffold samples **(Figure 6.3)**. Examination of four samples, each from different preparations, demonstrated consistency in the fabrication technique. The scaffold morphology closely resembled that previously described in the literature [138]. Using these images, we also confirmed that the EtO sterilization process did not affect the scaffold morphology.

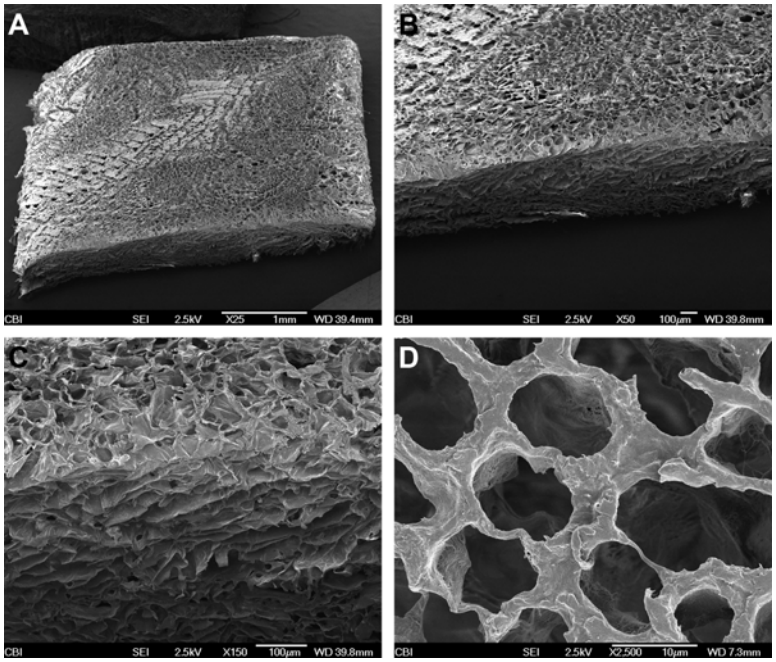

Figure 6.3: SEM micrographs of a PLLA scaffold

SEM images show a piece of a PLLA scaffold taken at (A) 25x, (B) 50x, (C) 150x and (D) 2500x

Micrographs taken at 1000x and 2500x magnification underwent further examination to estimate the porosity of the PLLA scaffolds for comparison before and after EtO sterilization. NIH Image was able to distinguish the pores from the scaffold structure and porosity was estimated from these images. The scaffold porosity, as calculated in 1000x magnification images, was 49 ± 7% before sterilization (n = 4) and 52 ± 2% after sterilization (n = 4) **(Figure 6.4)**. No statistical difference was observed. The porosities were 47 ± 15 vs. 57 ± 2 when estimated in the 2500x images taken before (n = 3) and after (n = 4) sterilization, respectively ($p > 0.05$). The slight differences can be attributed to the region chosen for the SEM analysis. Since the scaffold structure thickness is not completely uniform, there may be regions where more scaffold structure is present and the image analysis technique resulted in a lower porosity. However, comparison by gross examination revealed that the porosities tend to be fairly uniform

over the entire scaffold structure and also pre- and post-sterilization. It is also noteworthy to mention that the pore size ranged from ~10-50 μm.

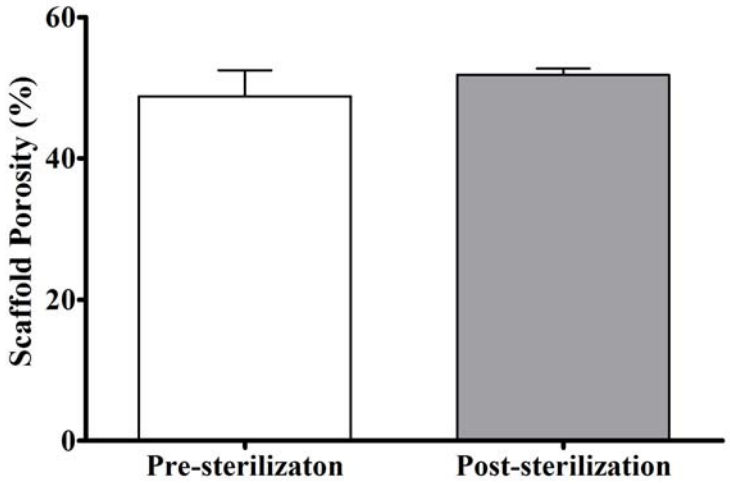

Figure 6.4: Scaffold porosity calculated before and after cold-gas EtO sterilization

Scaffold porosity was calculated from SEM images (1000x magnification) taken before and after cold-gas EtO sterilization of the PLLA scaffolds. Porosity did not change (49±7% vs. 52±2%, Pre vs. Post, respectively, $p > 0.05$, n = 4) demonstrating that the implants retained their porous structure after the EtO cold-gas sterilization procedure; Mean ± SEM.

6.3.2 Outcomes of Scaffold Implantation and Bi-weekly DRP injections

The subcutaneous implantation of the PLLA scaffolds into the animals was without adverse events. No complications were seen from the twice-weekly intravenous infusions of PEO-4500 and PMNN (saline in control animals). All animals (n=5 for each group – Control, PEO-4500 and PMNN) survived to the study endpoint (7 weeks) at which time the animals were anesthetized, euthanized and the scaffolds explanted for histological examination. The scaffolds

were dissected free from the subcutaneous tissue without any issues. The constructs were encapsulated by thin, vascularized tissue.

6.3.3 Histologic Findings for the Subcutaneously Implanted PLLA scaffolds

Histologic examination was first performed by a blinded expert (Professor Harry C. Blair, MD, Departments of Pathology and Cell Biology and Physiology, University of Pittsburgh). At 7 weeks post implant, chronic inflammation or a typical foreign body reaction to the PLLA implant characterized by the presence of foreign body giant cells (FBGCs) and the components of granulation tissue: macrophages, fibroblasts and capillaries [139, 140], to the PLLA implant was observed. In addition, macrophages and FBGCs were present at the tissue-PLLA interface. A similar fibrous capsule that ranged in thickness from 50 to 400 μm surrounded scaffolds of all groups.

Upon further examination, a major difference was apparent between the PLLA scaffolds of DRP-treated and saline-treated groups. In all but one (both cross-sections) of the scaffolds of the Control group (saline-treated), the PLLA implant was comprised of mainly randomly oriented collagenous tissue and granulomatous inflammation with a large number of apparent macrophages and FBGCs. Scaffolds explanted from both PEO and PMNN-treated animals showed significantly less granulomatous inflammation. The collagenous tissue in the scaffolds of the DRP-treated animals also appeared to be greater in concentration and significantly more organized. The collagen tissue fiber bundles were not only similarly oriented to each other but were preferentially aligned parallel to the transverse plane or the short axis of the scaffold. In other words, the collagen fiber bundles ran perpendicular to the muscle and skin layers between

which the scaffold was implanted. No apparent difference in vascularization was noticeable during the initial histological assessment and further microscopic analysis had to be performed.

Figure 6.5 shows the histologic appearance of the PLLA implants of each treatment group (Control (saline), PEO-4500 and PMNN) 7 weeks after surgery.

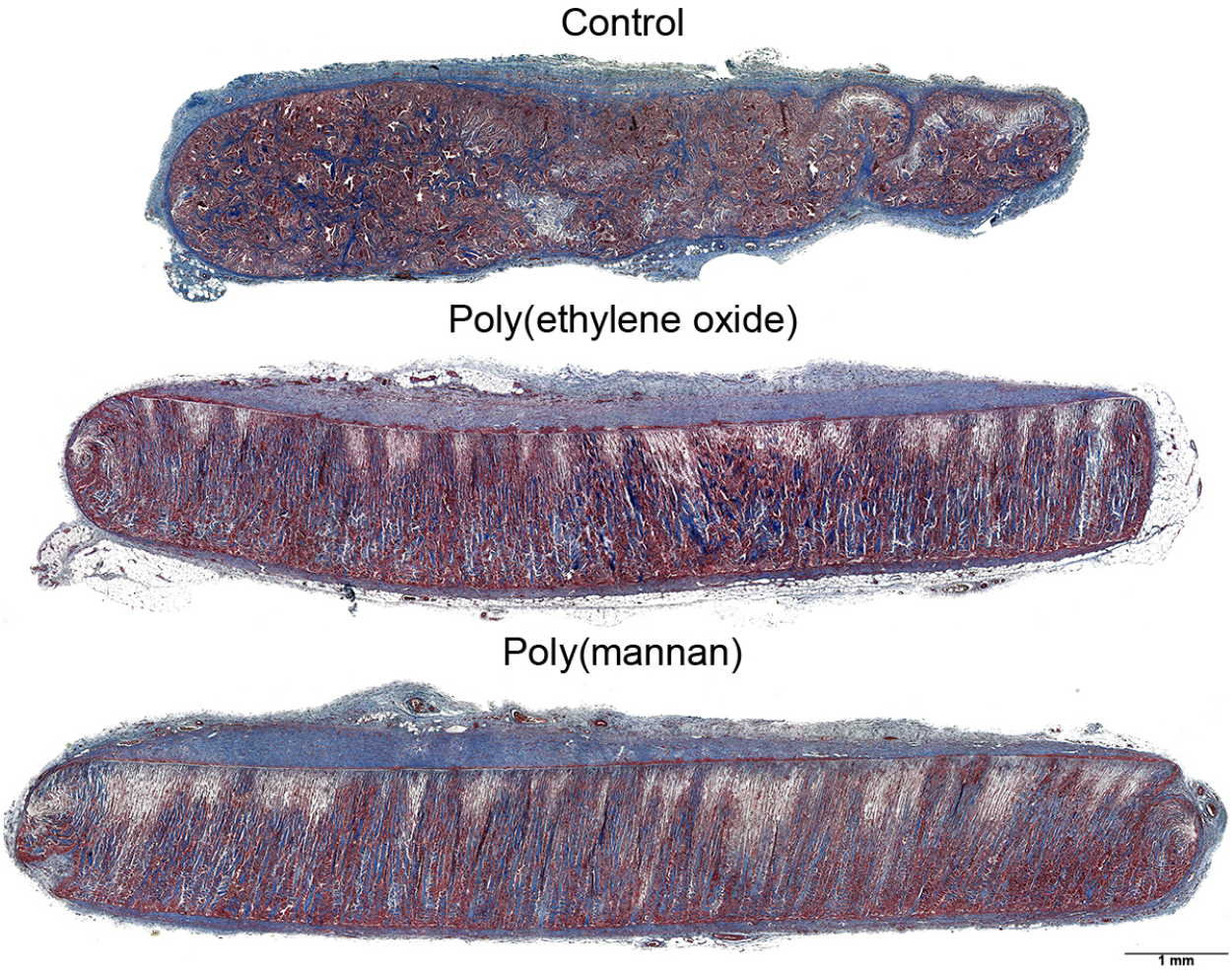

Figure 6.5: Sample cross sections of PLLA scaffolds explanted from animals infused with DRPs (saline in control)

Photomicrographs show composite images Samples of Masson's trichrome-stained PLLA scaffold cross sections explanted from animals infused with either saline (Control; top), poly(ethylene oxide) (MW = 4500 kDa; middle) or poly(mannan) (bottom).

6.3.4 Results of the quantification of inflammatory and collagenous tissue content and analysis of collagen organization

The initial histological examination of the Masson's trichrome-stained scaffold sections revealed a clearly discernable difference between scaffolds of Control and DRP groups. This prompted a histomorphometric analysis to quantify the area in the scaffolds that was comprised of inflammatory cells and collagen tissue. Each tissue element was easily discriminated using the Threshold HSI filter (Fovea Pro 1.0; Reindeer Graphics), which operated as a subroutine in Photoshop 7.0 (Adobe Systems). **Figure 6.7 (A)** shows photomicrographs of sample fields (0.77 mm^2) of Masson's trichrome-stained scaffold cross-sections before (left panels) and after the separation of collagen (middle panels) and FBGCs (right panels) by digital subtraction of Threshold HSI selected groups. This demonstrates the effectiveness of the selection algorithm in discriminating tissue elements. Additionally, a meaningful quantitative interpretation of the tissue was achieved with scaffold sections prepared with a simple, inexpensive and routine histology stain. In each row, the same field is represented as either a 24-bit RGB image or a digitally separated element.

The quantitative digital analysis showed that the IV administration of PEO-4500 and PMNN had a profound effect on the percentage of the total stained tissue area of the explanted scaffolds that was inflammatory cells (FBGCs) or collagenous tissue (**Figure 6.7 (B)**). The quantitative analysis confirmed the findings of the initial histologic examination in which scaffolds explanted from both PEO and PMNN-treated animals showed significantly less granulomatous inflammation and increased amounts of collagenous tissue. The reduction in the percentage of FBGCs per stained tissue area was the greatest and statistically significant (p =

0.0012 vs. Control) in scaffolds explanted from animals treated with PEO-4500 (by 30%) and slightly less so in scaffolds explanted from animals treated with PMNN (by 11%). The observed reduction in FBGC content in the scaffolds of the DRP-treated animals was balanced with increased amounts of collagenous tissue. Therefore, since the scaffolds of the animals treated with PEO-4500 showed the largest reduction in inflammatory tissue, they also demonstrated the biggest increase in the percentage of collagen per stained tissue area (by 30%, $p = 0.0012$ vs. Control). A modest increase (10%) in collagen tissue occurred in scaffolds explanted from animals treated with PMNN.

The FBGC area to collagen area was inversely proportional suggesting that the areas not filled with FBGCs contained active fibroblasts that secreted collagen. This implies that the reduction in the inflammatory response is extremely significant for the integration of other cell types in the scaffolds. The percentage of the two tissue types were nearly equal (~50%) in the scaffolds of the Control group whereas the scaffolds of the PEO-4500 group contained roughly 65% collagen and only 35% FBGCs. The secreted substances of activated macrophages, such as reactive oxygen and nitrogen intermediates, acidic hydrolases and cytokines are capable of being cytotoxic [141]. One particular study by Lam et al. [142] found that cell damage and necrosis were caused by the phagocytosis of PLLA particles by peritoneal macrophages. Hence, it is reasonable that the higher degree of inflammatory tissue in the scaffolds of the Control group created an unfavorable environment for the proliferation of other cell types such as fibroblasts. These results are extremely significant for patients with orthopedic implants. The phagocytosis of wear debris from orthopedic implant materials by macrophages have been implicated in the pathogenesis of osteolysis and aseptic loosening [143]. The major cause of joint replacement

failure and the most important clinical problem associated with total hip and knee replacement is the pathologic bone resorption around the prosthetic implant itself [143, 144].

Fascinatingly enough, the observed serendipitous phenomenon may be explained in part by the same mechanisms that lead to our hypothesis regarding the ability of DRPs to promote angiogenesis via the regulation of hemodynamic forces. During a response to a foreign body, blood circulating monocytes, a type of leukocyte, move radially from the central blood stream to the vessel wall; a process known as margination. Margination is necessary for the monocytes to begin to make contact and roll along the vessel wall. RBCs have been shown to be one of the most influential contributing factor to leukocyte margination [145, 146]. More importantly, it was demonstrated that leukocyte margination is dependent on RBC aggregation (RCA); RCA enhanced leukocyte margination and in its' absence, margination does not occur [147, 148]. Interestingly, once animals which have blood that does not normally demonstrate the RBC aggregation phenomenon (e.g., ovine, bovine), present with pathological conditions such as infection or an inflammatory reaction caused by surgery and implantation of heart-assist devices, RBCs start to aggregate (as shown in **Figure 6.6**), thus promoting leukocyte margination and further aggravation of animal conditions.

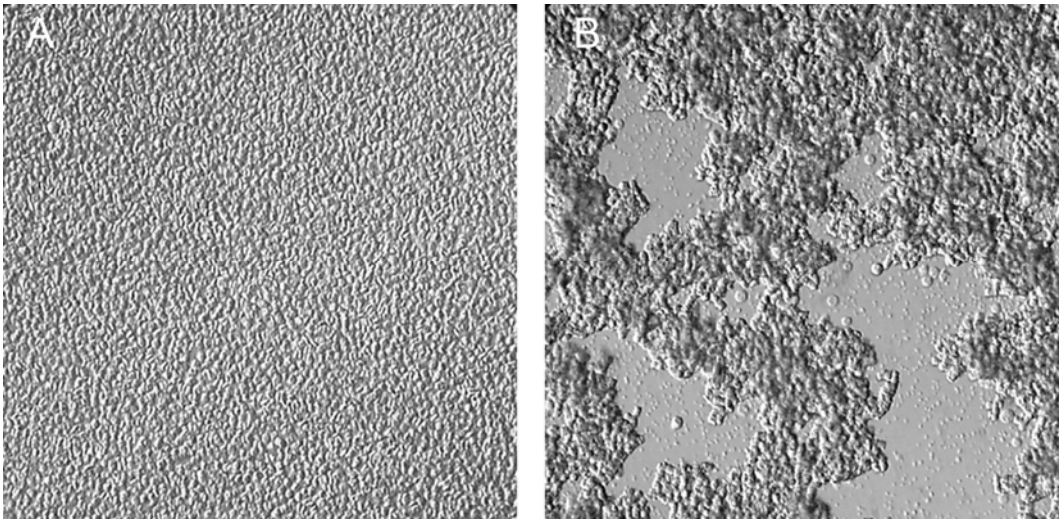

Figure 6.6: Blood from a normal healthy bovine and from a bovine calf implanted with ventricular-assist device (VAD)

Photomicrographs of bovine blood: (A) Blood from a normal healthy bovine does not demonstrate aggregation. (B) Blood from a bovine calf implanted with a VAD demonstrates aggregation due to the inflammatory reaction caused by surgery and implantation of heart-assist devices. This would thus promote leukocyte margination and further aggravate animal conditions (photos by Kameneva MV, with permission).

Therefore, margination may be manipulated, either increased or reduced, through the regulation of RCA mediators. As the monocytes roll along the surface, signals from cells at the foreign body implant site cause endothelial cells to become activated and express adhesion molecules. Receptors on the monocytes' surface allow the cells to then bind to the endothelium and become immobilized. At this point, through diapedesis, or extravasation, the cells migrate from the intravascular space through the endothelium toward the implant [140, 149]. Our results showed that the number of inflammatory cells, macrophage and FBGCs, in the scaffold implants of animals infused with DRP solutions was reduced compared to those of Controls. In terms of hemodynamic influence, the DRPs' abilities to redistribute RBCs toward the microvessel wall and to remarkably enhance microvascular perfusion would produce considerable effects on the wall shear stresses imposed on the endothelium. If the shear rates were to be increased above that which would be endurable by adhesive bonds of leukocytes to the endothelium, the end result

would be fewer cells available for diapedesis. In an *in vitro* study, Theilmeier et al. [150] showed that the threshold for adherence of human monocytoid THP-1 cells to resting human umbilical vein endothelial cells was around 300 s^{-1}. Activation of the endothelial cells by phorbol myristate acetate only increased this threshold to 400 s^{-1}. Therefore, it is plausible that the high concentration of RBCs near the vessel wall and/or an increase in blood perfusion due to the presence of DRPs would have a significant enough effect to hinder or prevent the rolling and adhesion of leukocytes. This hypothetical mechanism of reduction of leukocyte margination and rolling in small vessels due to the presence of DRPs in blood was proposed by Dr. Kameneva several years ago but yet to be proven experimentally. Furthermore, since, RBC aggregates are easily break down due to an increase in shear rates, even a minor increase in blood flow would result in disaggregation of RBC rouleaux and reduction of leukocyte margination. Additionally, the redistribution and relocation of RBCs from the core flow toward the near-wall space in microvessels would hinder margination, rolling and adhesion by: effectively limiting the space near the endothelial cell wall for leukocytes, causing RBC-leukocyte collisions and reducing the hematocrit in the central core flow which would reduce the propensity for RBCs to aggregate. Furthermore, this effect may be of great utility in preventing leukocyte margination in those pathologies where RCA is increased due to reduced blood flow such as inflammation, hypovolemic and septic shock and ischemia [151]. It may also imply potential beneficial effects of DRPs in disorders and diseases associated with hematological and hemorheological disturbances such as elevated levels of fibrinogen, polycythemia and changes in RBC deformability and surface charge [151].

The slight differences we observed in the FBGC and collagen content of scaffolds of the animals injected with either PEO-4500 or PMNN may be explained by differences in the

circulating half-life of the polymers *in-vivo.* Future studies may involve more frequent infusions of PMNN to determine what regimen is necessary to achieve the desired level of inflammatory mediation.

These results also support the proposed explanation on the similarity of blood vessel densities between DRP-treated and saline-treated groups that suggested that the increased number of inflammatory cells in the Control group elevated angiogenic molecule production to increase the number of blood vessels. The stimulus from the inflammatory response may have been greater than the stimulus from the DRP intravascular effect. This is discussed in more detail in Section 6.3.6.

The initial histological examination also found that collagen tissue in the scaffolds of animals injected with DRPs was also better organized. Therefore, quantitative digital analysis was completed to look at the congruency in the alignment of collagen fiber bundle elements. In a study by Noorlander et al. [136], changes in the orientation of collagen fibers in the dermis of pig skin were determined after mechanical stretching by placing best fit ovals around collagen structures and calculating the mean length of the major axes of the 10 largest ovals. This value was considered to be the collagen alignment index. However, this computation only accounts for stretching of the collagen fibers and fails to take into account the overall orientation. Additionally, the image analysis software may also interpret adjacent collagen fibers as one element generating enlarged best-fit ovals, introducing a potential erroneous computation. In our analysis, we not only took into account the lengths of the major axes of the best-fit ovals but also their angles, as determined from the x-axis. This offers further interpretation on the similarity of the orientation of the collagen bundles to each other. The collagen alignment index was computed from the coincidence of the angles of the 50 longest ovals. The collagen orientation

index ranged from a value of close to 0 (least organized) to a maximum value of 1 (most organized). Collagen was statistically significantly more aligned (p<0.0001) in the scaffolds explanted from animals injected with PEO-4500 (by 113%, n=9) and PMNN (by 110%, n=9) than those of the Control animals (n=10) (**Figure 6.7 (C)**).

Collagen fiber orientation dictates the flexibility and tensile mechanical strength of soft tissues [152]. Soft tissues with preferential fiber alignment are anisotropic and have extraordinary mechanical properties in the direction of the fibers. In the scaffolds of the DRP-treated animals, the preferred direction of the collagen fibers is typically orthogonal to the skin and muscle layers; this is the short axis of the scaffold. Therefore, the largest surface area of scaffold is in contact with the skin and muscle layers and provides the most probable means for cells to infiltrate the pores. The most possible reason for the observed collagen architecture is the migration of fibroblasts along the pores from one surface to the other. However, in the Control group, its higher degree of inflammatory tissue had likely eroded the PLLA scaffold at a faster rate leaving less bearing on the path of collagen formation. Additionally, since more of the pores were filled with FBGCs, fibroblasts would have likely had a more tortuous path to follow. It is also possible that since the DRPs might provide better perfusion of the ensuing fibrotic capsule surrounding the implant, the fibroblasts and other cellular components would follow the direction of shortest distance from supply.

Future studies may be performed to analyze the types of collagen present in the scaffolds as well as the thickness of the collagen fibers. By determining the types of collagen and the fibers thicknesses in the scaffold, the progression of the healing process and the foreign body reaction could be determined. For instance, type III collagen would be indicative of that produced by young fibroblasts in granulation tissue; the tissue that makes up the majority of the

scaffold cross sections while Type I collagen is the toughest of all collagen types and is end product of scar formation. Additionally, thin fibers are seen at earlier stages than thick fibers with close packing.

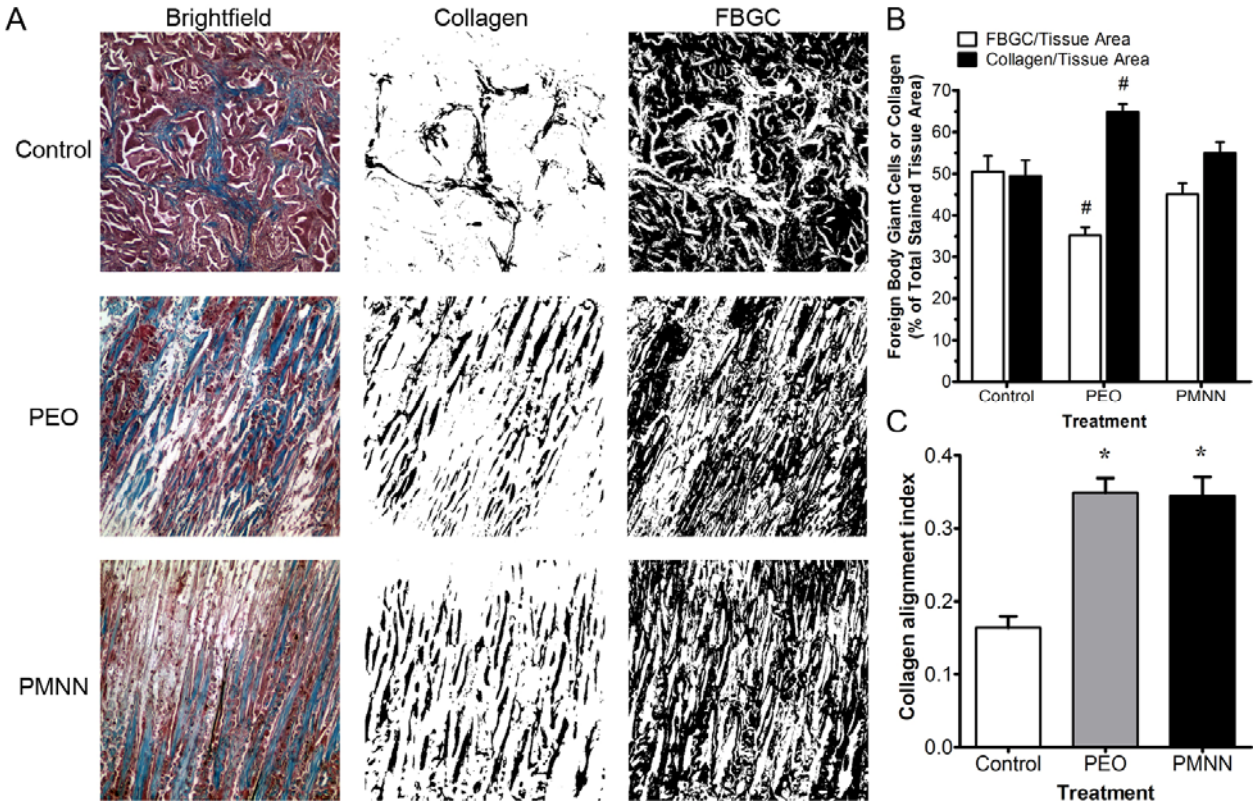

Figure 6.7: Effect of the DRPs PEO-4500 and PMNN on macrophage infiltration and granulomatous response in subcutaneously implanted PLLA scaffolds

(A) Photomicrographs show sample fields (0.77 mm^2) which demonstrate the separation of collagen and FBGCs by digital subtraction of threshold HSI selected groups indicating the efficacy of the selection algorithm. Rows show the same field either as a 24-bit RGB image or a digitally separated element. (B) Graph shows the effect of the infusion of PEO-4500 and PMNN (both at a blood concentration 2 μg/ml (0.3 – 0.4 nM), saline in Control) on the percentage of the total stained tissue area in photomicrographs (examples shown in Figure 6.5) of Masson's trichrome stained scaffold cross sections that is FBGCs (white bars) or collagen (black bars); $^{\#}p$=0.0012 vs. Control, individual data points > 2 SD from the mean of the remaining data were discarded, Control – n = 8, PEO – n = 10, PMNN – n = 9, Mean ± SE. (C) Effect of the infusion PEO-4500 and PMNN (both at a blood concentration 2 μg/ml (0.3 – 0.4 nM), saline in Control) on the alignment of collagen tissue in a subcutaneously implanted PLLA scaffold. A collagen orientation index was calculated in Masson's trichrome stained scaffold cross section photomicrographs (examples shown in Figure 6.5) to express the degree of organization of the collagen tissue within the scaffold. A value close to 0 indicates the least amount of organization and a value close to 1 denotes the most amount of organization; $^{*}p$<0.0001 vs. Control, individual data points > 2 SD from the mean of the remaining data was discarded, Control – n = 10, PEO – n = 9, PMNN – n = 9, Mean ± SE.

6.3.5 Results of PLLA degradation quantification

The scaffold cross-sections were also observed with polarized light microscopy to quantify the residual PLLA polymer and to determine the effect of reducing the inflammatory response on its degradation. Photomicrographs in **Figure 6.8 (A)** show brightfield (left panels) and polarized light (right panels) sample fields (0.26 mm^2) of the Masson's trichrome stained sections. In the brightfield images, the PLLA appears as a clear non-stained element but in the polarized light images, the birefringence of the PLLA was very distinct and appeared as bright areas against the dark background of the surrounding tissue. This property made the quantification of the remaining PLLA implant with digital image analysis very straightforward because the bright areas could be easily discriminated from the dark background.

The un-degraded scaffold material was quantified in two (10x – 0.95 mm^2) polarized light photomicrographs per scaffold cross section. The PLLA was significantly more ($p < 0.0001$ vs. both DRP groups), and almost entirely, degraded in the scaffolds of the Control group. The cross-sectional area of remaining PLLA in the scaffolds of PEO-4500 and PMNN injected animals was $24.16x10^3 \pm 3.08x10^3$ μm^2 and $18.22x10^3 \pm 3.10x10^3$ μm^2 out of a total field area of $95.04x10^4$ μm^2, respectively, versus $0.70x10^3 \pm 0.31$ $x10^3$ μm^2 in Control (**Figure 6.8 (B)**). This corresponds to 2.54 ± 1.02 % and 1.92 ± 1.03 % of the total field area (PEO-4500 and PMNN, respectively), versus 0.07 ± 0.09 % in Control.

Macrophages and their multinucleated variants, foreign body giant cells, are known to secrete acidic hydrolases as part of the inflammatory response to phagocytize foreign body particles [143]. At a biomaterial interface, macrophages and FBGCs may lower the pH

significantly from that of physiological (7.4). In fact, the phagolysosomal vacuoles inside macrophages have been described as having a pH as low as 3. Since the degradation of PLLA has been recognized to occur by acid hydrolysis [153, 154], it can be concluded that the degradation of the PLLA scaffolds in all scaffold groups in this study was by the infiltrating FBGCs. This conclusion is well supported by the results of the FBGC area quantification where the extent of FBGC infiltration seems to correspond to the degree of degradation of the PLLA scaffold. Thus, the Control group which demonstrated the highest level of FBGC infiltration showed almost complete degradation of the PLLA and the PEO-4500 group which had the lowest level of FBGC infiltration had the lowest degree of PLLA degradation of the three groups. The strongest correlation is found when comparing the difference in the percentage of FBGC content between PEO-4500 and PMNN (~30%) to the difference in the percentage of remaining PLLA of these two groups (~25%). However, the same is not true when comparing these differences between the two DRP groups to the Control group. The percentage of FBGC area in the scaffolds of the Control group was only ~12% higher than that of the scaffolds of the PMNN, which contained the highest level of FBGC infiltration of the two DRP-treated groups. It remains unclear whether such a small difference in FBGC infiltration would cause such a dramatic degradation of the PLLA. This may be explained by the possibility that the quantification of the FBGC area in the Control group does not represent the maximum amount of inflammatory tissue that had infiltrated the tissue. What may be seen is the waning of the foreign body response in these scaffolds due to almost complete degradation of the PLLA.

These results may also explain the difference in collagen alignment between the scaffolds of DRP-treated animals and those of the Controls. It is clear that the higher degree of scaffold degradation in the Control group would lead to very little control of the collagen fiber orientation as the porous structure would have been less defined.

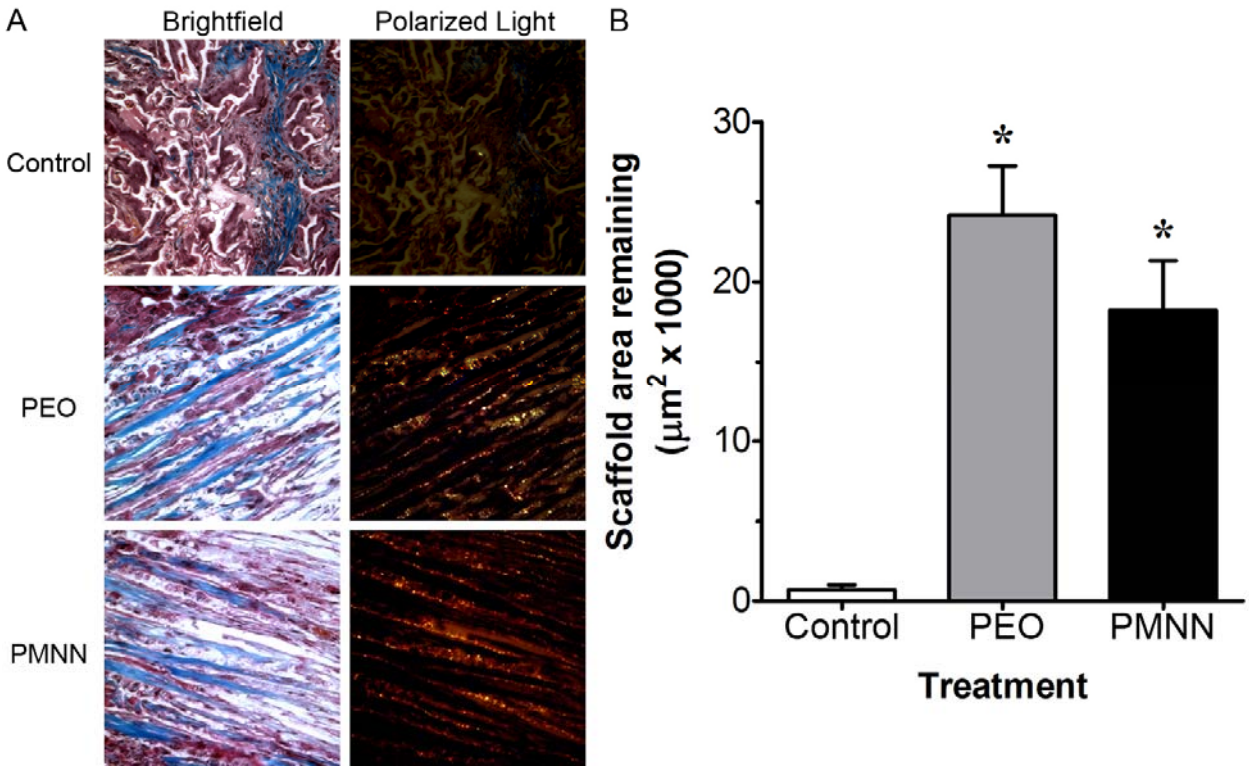

Figure 6.8: Reduced degradation of implanted PLLA scaffolds in animals infused with the DRPs PEO-4500 and PMNN

(A) Photomicrographs show sample fields (0.26 mm^2) (brightfield (left panels) and polarized light (right panels)) of the cross sections of PLLA scaffolds stained with Masson's trichrome that were explanted from animals infused with either saline (Control) (top left panel), PEO-4500 (middle left panel) or PMNN (bottom left panel) used to quantify the percentage of the remaining PLLA implant. The remaining PLLA implant demonstrated birefringence and is shown as the bright areas in the polarized light photomicrographs (right panels). (B) Graph shows that the effect of the infusion of PEO-4500 and PMNN on the reduction in the FBGC infiltration reduces the degradation of the PLLA implant. Remaining scaffold material was quantified from two (10x – 0.95 mm^2) polarized light photomicrographs per scaffold cross section. The remaining PLLA in the scaffolds of PEO and PMNN injected animals was 2.54±1.02% and 1.92±1.03% of the total field area, respectively, versus 0.07±0.09% in Control; $^{*}p<0.0001$ vs. Control, individual data points > 2 SD from the mean of the remaining data was discarded, Control – n = 8, PEO – n = 10, PMNN – n = 10, Mean ± SE.

6.3.6 Results of blood vessel density quantification

Using Masson's trichrome stained scaffold sections, the blood vessel density was determined within the scaffold and within the encapsulation tissue. The vessels were categorized by size (0-25 μm, 26-50 μm and greater than 50 μm) and identified by locating structures that met the selected criteria (luminal structure bordered with endothelial cell pattern containing RBCs within the intraluminal space). The results are summarized in **Table 6.1**. Little to no difference ($p > 0.05$) was observed when comparing the blood vessel densities of the DRP-treated animals to those treated with saline (Control).

Endothelial cells are known to be sensitive to intravascular mechanical stimuli such as the shear stress caused by blood flow [155]. *In vivo* observations have shown that high flow rates, which generate high intravascular shear stresses on endothelial cells, are important for capillary growth [156-159]. Increased capillarity has been shown to occur by intussusceptive angiogenesis through the administration of prazosin, an α-sympathetic blocker capable of vasorelaxation, to increase blood flow and thus elevate shear stress [160, 161]. We had hypothesized based on our *in vitro* microchannel findings that, the relocation and redistribution of RBCs closer to the endothelial cells of the vessel wall (vessels less than 300 μm) due to presence of DRPs in blood would increase the near-wall hematocrit, would lead to elevated shear stresses which would promote vascular remodeling. At first glance, the results of the blood vessel density quantification in the present study may suggest that this hypothesis was disproved. However, a possible considerable limitation to testing this hypothesis was the model chosen. Biomaterial implants can invoke a substantial foreign body response. It is well known that the inflammatory cells related to wound healing, in this case macrophages and FBGCs, secrete the

necessary cytokines and growth factors that lead to effective angiogenesis [143] to provide the metabolically active fibroblasts and macrophages the necessary supply of oxygen and nutrients. For example, macrophages are capable of secreting angiogenic molecules such as basic fibroblast growth factor, tumor necrosis factor α and vascular endothelial growth factor [162]. The preliminary histological assessment of the scaffolds suggested that the number of inflammatory cells was greater in the Control group. In this case, it is possible that the inflammatory mediated angiogenic response lead to increased numbers of blood vessels which were required to nourish a significantly elevated number of cells over which was necessary in the scaffolds of DRP-treated animals. The relocation of RBCs to the near-wall space would also improve gas exchange to the tissue in the scaffolds implanted in the DRP-treated animals. This would reduce the requirements of the inflammatory cells to signal neovascularization. Thus, it is uncertain whether the DRP effect on the endothelium would be great enough to overcome the strong angiogenic signaling generated by the inflammatory cells. It is therefore suggested that further investigation of this shear stress hypothesis be carried out in a different model such as the rabbit with an implanted ear chamber where changes in vascularity could be monitored.

Table 6.1: Blood vessel density measured in PLLA scaffolds and encapsulation tissue

		Blood vessel diameter (μm)		
Treatment	Tissue area	**0-25**	**25-50**	**> 50**
Control	**Scaffold**	4.7±2.1	0.5±0.4	0
	Encapsulation	26.3±13.4	3.9±3.2	0.6±0.8
PEO	**Scaffold**	4.1±2.1	0.3±0.2	0
	Encapsulation	20.0±14.2	1.1±1.1	0
PMNN	**Scaffold**	3.6±2.3	0.3±0.2	0
	Encapsulation	27.5±10.8	3.0±2.3	1.8±3.1

Blood vessel density per mm^2 of scaffold and encapsulation tissue as measured in Masson's trichrome stained sections. Mean ± SD, n=5 for each Group.

The methods used here for identifying blood vessels was limited as it only allows for a rough interpretation of the blood vessel density accounting for only vessels containing RBCs. Therefore, those vessels, functioning or non-functioning, in which RBCs were not contained within the intraluminal space were not counted. Additionally, other intracellular spaces resembling a luminal structure containing RBCs that may have been dislocated from their respective vessels during histological processing may have been falsely counted. More specific techniques for the quantification of blood density are recommended for future studies. The techniques commonly employed entail the immunolabeling of vascular endothelial cells with antibodies for either CD31 or von Willebrand Factor. CD31 (PECAM-1: platelet endothelial adhesion molecule) and von Willebrand Factor (vWF; Factor VIII Related Antigen) are expressed and synthesized by endothelial cells for various functions and are typically used as cell markers for studying angiogenesis/neovascularization. A pilot study to label blood vessels in a small number of scaffold sections using immunohistochemical techniques for the detection of vWF was unsuccessfully performed in this work. In that study, the immunoperixodase method of signal detection was used. This method can be complicated by the presence of endogenous peroxidase in the cells and tissues. The scaffold sections were filled with macrophages and FBGCs, cells which produce reactive oxygen intermediates such as hydrogen peroxide and which are rich in peroxidase activity. The histological outcome was nonspecific staining of the tissue sections. Therefore, it may be suggested that an alternative enzyme label, such as calf intestinal alkaline phosphatase or a different immunolabeling technique that utilizes a fluorescent secondary be used for future investigations of the blood vessel density in these sections.

6.4 SUMMARY

The experiments performed in this chapter followed up the discovery of the DRP effect observed in *in vitro* microchannel studies which showed the axial relocation of RBCs toward the channel wall; an effect which when applied to blood flow in microvessels *in vivo* would increase the near-wall hematocrit leading to elevated vessel wall shear stresses. We first hypothesized that the chronic intravascular injection of DRPs would facilitate increased blood vessel formation and thus improved tissue cell infiltration in a biodegradable synthetic scaffold implanted subcutaneously in rat. To study the DRP effects *in vivo*, experiments were carried out in which animals, implanted with subcutaneous porous PLLA scaffolds, were infused with DRPs (2x/week for 7 weeks) post implant. Assessment of tissue infiltration and growth and collagen deposition inside the scaffold matrix as well as blood vessel growth were made. At 7 weeks post implant, using histological and digital analysis techniques, what was found were significant differences between the PLLA scaffolds of DRP-treated groups and those of saline-treated group. This analysis concluded that scaffolds of the DRP treated groups had significantly less granulomatous inflammation and the collagenous tissue was not only greater in concentration but also significantly more organized. Vascularization was comparable in all groups. Therefore, the mechanism of the observed differences in tissues of Control and DRP-treated animals was not directly related to the new vessel formation inside the scaffold tissue (at least as observed at the 7 week time point). Actually, this may be owed to the differences in the inflammatory response due to changes in blood microcirculation rheological behavior in DRP-treated animals in general. Additionally, the inflammatory and foreign body responses to the scaffolds of the saline-treated animals led to rapid and almost complete degradation of the PLLA implant.

Our study has uncovered a beneficial effect of drag reducing polymers with extraordinary impact factor. These results are potentially of great utility as treatment of early post-operative response to implanted or transplanted materials, organ fibrosis, and diseases producing granulomatous inflammation. Due to the potential impact of this work on the development of novel anti-inflammatory and anti-rejection therapies, a filing with the US Patent and Trademark Office for a provisional patent has been granted and the patent is now pending [163].

7.0 CONCLUSIONS

The goal of this dissertation was to investigate potential mechanisms of the enhanced hemodynamics conferred to the cardiovascular system via the addition of minute concentrations of drag reducing polymers and several potential biomedical applications of these effects. The specific aims of the study were as following: to determine whether the DRP additives affected red blood cell deformability, to demonstrate that the intravenous infusion of DRP preparations would enhance the impaired microcirculation in rats with streptozotocin-induced diabetes, and to study the ability of DRPs to improve cell proliferation and tissue in-growth and facilitate angiogenesis in synthetic scaffolds.

Two techniques were successfully implemented in order to study the DRP effect on the mechanical properties of red blood cells, i.e., their deformability. Using a filtration technique, the filterability of normal RBCs in dilute cell suspensions was found to be statistically significantly enhanced after the addition of DRPs. The effectiveness of this technique was shown by determining the filterability of RBCs treated with glutaraldehyde which significantly reduces RBC deformability. The addition of DRPs to glutaraldehyde-treated RBCs was found to cause a statistically significant increase in RBC filterability, restoring the filterability index value to that of normal RBCs. A rheological technique was also successfully employed to demonstrate that measurements of viscoelasticity of animal blood using a Vilastic-3 viscoelastometer (Vilastic Scientific), would provide a sensitive standard method of evaluation of changes in RBC

deformability. Using this technique, the viscoelasticity of whole blood from diabetic animals was found to be significantly higher than that of normal animals. An increase in viscosity and elasticity signifies a reduction in RBC deformability. The addition of DRPs to the diabetic blood samples resulted in a slight decrease in the viscosity suggesting that the deformability was increased. The addition of D-glucose to animal blood, *in vitro*, resulted in a hyperosmolar condition, which unlike the effects observed in human blood, led to RBC shrinkage and a reduction in their deformability. This phenomenon did not allow us to observe the effects of glycosylation on the cell membranes and hemoglobin.

A reproducible model of experimental diabetes in small animals (rats) with the ability to measure hemodynamic parameters (blood pressure, heart rate and tissue perfusion) using non-invasive methods was developed. Diabetic rats were found to have statistically significantly lower tissue perfusion than their non-diabetic matched control. Intravenous nanomolar concentrations of DRPs statistically significantly increased tissue perfusion in diabetic rats (as well as in normal animals) without affecting other hemodynamic parameters (blood pressure and heart rate). This study demonstrated the beneficial effects of drag-reducing polymers on the microcirculation of diabetic animals which most likely was related to the ability of the DRPs to enhance blood flow structure and mechanical properties of red blood cells in microvessels.

Acute and chronic (7 week) injections of DRPs produced no noticeable effects on clotting and hemostasis and on hematologic, blood gas and serum chemistry parameters suggesting that DRPs do not alter hematology and cardiovascular, respiratory, liver and renal function. In another set of experiments, a commercially available pharmaceutical grade hyaluronic acid preparation, Hyvisc® (Anika Therapeutics) proven in our laboratory to be a DRP, demonstrated a decrease in vascular resistance similar to other previously used DRPs (PEO and PMNN). Pilot

studies with bolus injections of solutions with relatively high concentrations of DRPs and slow infusions of solutions with extremely high DRP concentrations, up to 150 times the hemodynamically effective concentration, showed that hyaluronic acid can be safely delivered into the vascular system in small volumes and at a high infusion rate. However, PMNN, which was shown to be safe and effective when injected at relatively low concentrations, was found to produce hemolysis in blood after a slow injection at extremely high concentrations which can be related to the fact that there are still some impurities in this homemade preparation.

Finally, experiments performed to study the new potential applications of DRPs in tissue engineering concluded that chronic injections of DRPs significantly reduced the foreign body response in animals subcutaneously implanted with a porous synthetic scaffold. Scaffolds of the DRP-treated groups had significantly less granulomatous inflammation. Moreover, the collagenous tissue was not only greater in concentration but also significantly more organized in the animals treated with DRPs. Vascularization was comparable in all groups. Additionally, the inflammatory and foreign body responses to the scaffolds of the saline-treated animals led to rapid and almost complete degradation of the scaffold implant while the DRP-treated rats had statistically significantly slower rate of the scaffold degradation. DRPs may provide treatment of the early post-operative response to implanted or transplanted materials, organ fibrosis, and diseases producing granulomatous inflammation.

This dissertation provided a potential new mechanism behind the intravascular effect of DRPs as well as a foundation for several new medical applications of these blood soluble long-chain viscoelastic polymers.

APPENDIX A

ERROR PROPAGATION

Many physical quantities can be easily calculated from other directly measurable parameters. However, all of these measurements have error associated with them. Therefore, physical quantities which are calculated from these measurements will have an error due to the contributions of the individual errors from the measured quantities. Propagation of error is the effect of variables' errors on the uncertainty of a function that is based on those variables. An error analysis can be performed by assuming λ is a computed quantity that can be calculated from α, β, and γ, which are either directly measurable or previous calculated quantities. If each has an unknown certainty, σ, then propagation of error can be easily calculated by Equation 6 [164].

$$\sigma_\lambda^2 = \left(\frac{d\lambda}{d\alpha}\right)^2_{\beta,\gamma} \sigma_\alpha^2 + \left(\frac{d\lambda}{d\beta}\right)^2_{\alpha,\gamma} \sigma_\beta^2 + \left(\frac{d\lambda}{d\gamma}\right)^2_{\alpha,\beta} \sigma_\gamma^2 \qquad (6)$$

The differentials in Equation 6 represent the effect of a change in α, β and γ on λ. Equation 6 may be used to derive equations for the propagation of error associated with addition, subtraction, multiplication and division of the measured parameters in the computation of λ.

In the case of addition, λ can be computed using Equation 7.

$$\lambda = \alpha + \beta + \gamma \tag{7}$$

Using Equation 7, the differentials of Equation 6 become

$$\frac{d\lambda}{d\alpha} = \frac{d\lambda}{d\beta} = \frac{d\lambda}{d\gamma} = 1 \tag{8}$$

The basic equation for the calculation of propagation of error can be simplified to Equation 9 by substituting the results of Equation 8 into Equation 6.

$$\sigma_\lambda^2 = \sigma_\alpha^2 + \sigma_\beta^2 + \sigma_\gamma^2 \tag{9}$$

If the calculation would involve subtraction, the result would be the same since the partial derivatives are squared. Therefore, Equation 9 tells us that the total error of a calculated quantity is the sum of all the errors of the measured quantities when addition or subtraction is performed.

In the case of multiplication, λ can be computed using Equation 10.

$$\lambda = \alpha\beta\gamma \tag{10}$$

Using Equation 10, the differentials of Equation 6 become

$$\frac{d\lambda}{d\alpha} = \beta\gamma; \frac{d\lambda}{d\beta} = \alpha\gamma; \frac{d\lambda}{d\gamma} = \alpha\beta \tag{11}$$

The basic equation for the calculation of propagation of error can be simplified to Equation 12 by substituting the results of Equation 11 into Equation 6.

$$\sigma_\lambda^2 = (\beta\gamma)^2 \sigma_\alpha^2 + (\alpha\gamma)^2 \sigma_\beta^2 + (\alpha\beta)^2 \sigma_\gamma^2 \tag{12}$$

Equation 12 can be further simplified by dividing through by $\lambda^2 = \alpha^2\beta^2\gamma^2$ to yield

$$\%\sigma_\lambda^2 = \%\sigma_\alpha^2 + \%\sigma_\beta^2 + \%\sigma_\gamma^2 \tag{13}$$

where the percentage of errors are computed as

$$\%\sigma_i = \frac{\sigma_i}{i} \times 100\% \tag{14}$$

If the calculation would involve division, the result would be the same since the partial derivatives are squared. Therefore, Equation 13 tells us that the total error of a calculated quantity is the sum of all the percentage of errors of the measured quantities when multiplication or division is performed.

In the case of multiplication with quantities raised to a power, λ can be computed using Equation 15.

$$\lambda = \alpha^a \beta^b \gamma^c \tag{15}$$

Using Equation 15, the differentials of Equation 6 become

$$\frac{d\lambda}{d\alpha} = a\alpha^{a-1}\beta^b\gamma^c ; \frac{d\lambda}{d\beta} = b\beta^{b-1}\alpha^a\gamma^c ; \frac{d\lambda}{d\gamma} = c\gamma^{c-1}\alpha^a\beta^b \tag{16}$$

The basic equation for the calculation of propagation of error can be simplified to Equation 19 by substituting the results of Equation 16 into Equation 6.

$$\sigma_\lambda^2 = \left(a\alpha^{a-1}\beta^b\gamma^c\right)^2\sigma_\alpha^2 + \left(b\beta^{b-1}\alpha^a\gamma^c\right)^2\sigma_\beta^2 + \left(c\gamma^{c-1}\alpha^a\beta^b\right)^2\sigma_\gamma^2 \tag{19}$$

Equation 19 can be further simplified by dividing through by $\lambda^2 = \alpha^{2a}\beta^{2b}\gamma^{2c}$ to yield

$$\%\sigma_\lambda^2 = a^2\%\sigma_\alpha^2 + b^2\%\sigma_\beta^2 + c^2\%\sigma_\gamma^2 \tag{20}$$

If the calculation would involve division, the result would be the same since the partial derivatives are squared. Therefore, Equation 20 tells us that the total error of a calculated quantity is the sum of all the percentage of errors of the measured quantities, each multiplied by the square of their respective power, when multiplication or division is performed.

A.1 PROPAGATION OF ERROR CALCULATIONS FOR VASCULAR RESISTANCE

Peripheral vascular resistance (PVR) represents a physical quantity that is calculated in this dissertation from directly measured quantities and can be calculated using Equation 21.

$$PVR = \frac{MAP}{TP} \tag{21}$$

where, MAP is the measured mean arterial pressure in mmHg and TP is the measured tissue perfusion in TPU. The propagation of error in the calculated quantity (i.e., PVR) can be assessed after determining the uncertainty in the directly measured parameters (i.e., MAP and TP).

The uncertainty in the measurement of MAP, σ_{MAP}, and TP, σ_{TP}, can be defined by the accuracy of the scales by which these parameters are read. Pressure readings were made with a disposable strain gauge manometer which was calibrated using a standard clinical plethysmography gauge that had a scale that was accurate to ±1.0 mmHg. Since the pressure transducers were re-zeroed and re-calibrated immediately prior to data acquisition in each experiment, drift was not included in the error. Tissue perfusion measurements were made using a laser Doppler flow meter whose scale was readable to ±0.1 TPU.

Therefore,

$$\sigma_{MAP} = 1.0 \text{ mmHg and } \sigma_{TP} = 0.1 \text{ TPU} \tag{22}$$

If vascular resistance is calculated using typical values of MAP = 90 mmHg and TP = 18 TPU as measured during hemodynamic experiments, then the percentage of errors, calculated by substituting the values from Equation 22 in to Equation 14, are

$$\%\sigma_{MAP} = \frac{1}{90} \times 100\% = 1.1\% \text{ and } \%\sigma_{TP} = \frac{0.1}{18} \times 100\% = 0.6\% \tag{23}$$

Substitution of the values of Equation 23 into Equation 13 and taking the square root produces

$$\%\sigma_{PVR} = 1.3\% \quad (24)$$

Using the errors in the measured quantities, the expected total error in the calculation of the peripheral vascular resistance is 1.3%.

Similarly, the propagation of error in calculations of vascular resistance can be determined for the case where carotid blood flow, Q, was measured with an ultrasonic perivascular flow probe. The accuracy of the flow probe used in those studies is $\%\sigma_Q = \pm 3\%$ [165]. Therefore, by substituting $\%\sigma_Q$ and $\%\sigma_{MAP}$ into Equation 13 and taking the square root produces

$$\%\sigma_{VR} = 3.2\% \quad (25)$$

Using the errors in the measured quantities, the expected total error in the calculation of the vascular resistance is 3.2%.

APPENDIX B

EFFECT OF PEO AND PMNN ON MACROPHAGE ADHESION

Chapter 6.0 presented *in vivo* experiments performed to investigate new potential applications of DRPs in tissue engineering based on findings which demonstrated their ability to regulate the axial distribution of flowing RBCs in *in vitro* models of microvessels with diameters below 300 μm. This effect leads to a significant increase in wall shear stress via an increase in the near-wall viscosity. These studies concluded that chronic injections of DRPs significantly reduced the foreign body response in animals subcutaneously implanted with a porous synthetic scaffold. The results and a potential mechanism are described in detail in section 6.3. This appendix describes a pilot study which was performed to examine the effect of DRPs on macrophage adhesion *in vitro*.

B.1 TISSUE CULTURE CELL LINES

RAW 264.7 murine macrophage cell line, obtained from American Type Culture Collection (ATCC – TIB71, Manassas, VA) were grown to ~80-90% confluency and routinely passaged in Dulbecco's Modified Eagles Medium (BioWhittaker® DMEM; Lonza, Walkersville, MD) with

4.5 g/L glucose and L-glutamine supplemented with 10% heat-inactivated Fetal Bovine Serum (FBS; Hyclone, Logan, UT) and 100 U/ml penicillin and 100 μg/ml streptomycin (0.01% P/S). Cell passage was performed by: twice washing with Dulbecco's Phosphate Buffered Saline (DPBS; Mediatech, Manassas, VA), treating with Trypsin/EDTA (Gibco®; Invitrogen, Grand Island, NY) for 5 min, scraping and resuspending into fresh growth medium, centrifuging at 300 x g (Sorvall, model number, city, state) for 10 min, washing with fresh medium and re-seeding cells onto fresh culture plates (Corning, Lowell, MA). Cells were incubated at 37 °C in humidified air with 5% CO_2. Sterile tissue-culture techniques in a laminar flow hood were followed for all cell manipulations and experimental procedures. The passage number of the cell line subcultures used did not exceed fifteen beyond that as received from ATCC.

B.2 MACROPHAGE ADHESION ASSAY

B.2.1 Methods

RAW cells were grown on two 60 mm culture plates (Corning) to ~80% confluency. Cells were washed once with DPBS (Mediatech) and harvested by treatment with Trypsin/EDTA (Invitrogen) for 5 min and scraping into fresh medium. The cell suspension was pelleted by centrifugation at 300 x g for 10 min (Sorvall Biofuge Primo™ R; Thermo Fisher Scientific, Waltham, MA), the supernatant was discarded and the cells thoroughly resuspended in 5 ml of media. The cell suspension was then divided into three aliquots, centrifuged at 300 x g for 10 min (Microfuge® 18 Microcentrifuge; Beckman Coulter, Fullerton, CA), the supernatants removed, and the cells resuspended in 1.7 ml of one of the following three media: normal growth

medium (Control), normal growth medium + 5 μg/ml (1.1 nM) PEO-4500, or normal growth medium + 5 μg/ml (0.8 nM) PMNN. One hundred microliters of suspended cells from each of the three media was then added to 400 μl of the corresponding media pre-filled in wells of 24-well plates (Corning). The plates were then incubated for 0, 60 and 120 min at 37 °C in humidified air with 5% CO_2. Each condition was repeated in triplicate wells of cells. After the incubation period, the medium was removed and the wells washed once with DPBS (Mediatech) with agitation to remove the non-adherent cells. The adherent cells were fixed by incubation with 3% formalin at room temperature for 15 minutes after which the formalin was removed and DPBS (Mediatech) with 2 mM EDTA (Sigma Aldrich) was added for storage (at 4 °C) until the number of attached cells could be quantified. Phase contrast images of the 24-well plates were captured with a 4x plan fluorite objective (Plan Fluor DL 4x/NA 0.30 w/phase ring PhL; Nikon Instruments) on the same Nikon TE2000 inverted phase-fluorescence microscope system described in section 6.2.8.4. Digital analysis to quantify the number of adherent cells/well was performed on a personal computer with the NIH Image program. The results are expressed as the mean number of adherent cells/well ± S.D. for each condition. A two-way ANOVA with Bonferroni post hoc test was used to compare the average number of adherent cells per well of each experimental condition to that of the control of the corresponding time point. A $p < 0.05$ was considered to be statistically significant.

B.2.2 Results and Discussion

The average number of adherent macrophages after incubation for 0, 60 and 120 minutes in growth medium containing either of the two DRPs was compared to that in growth medium alone (Control) (**Figure 7.1**).

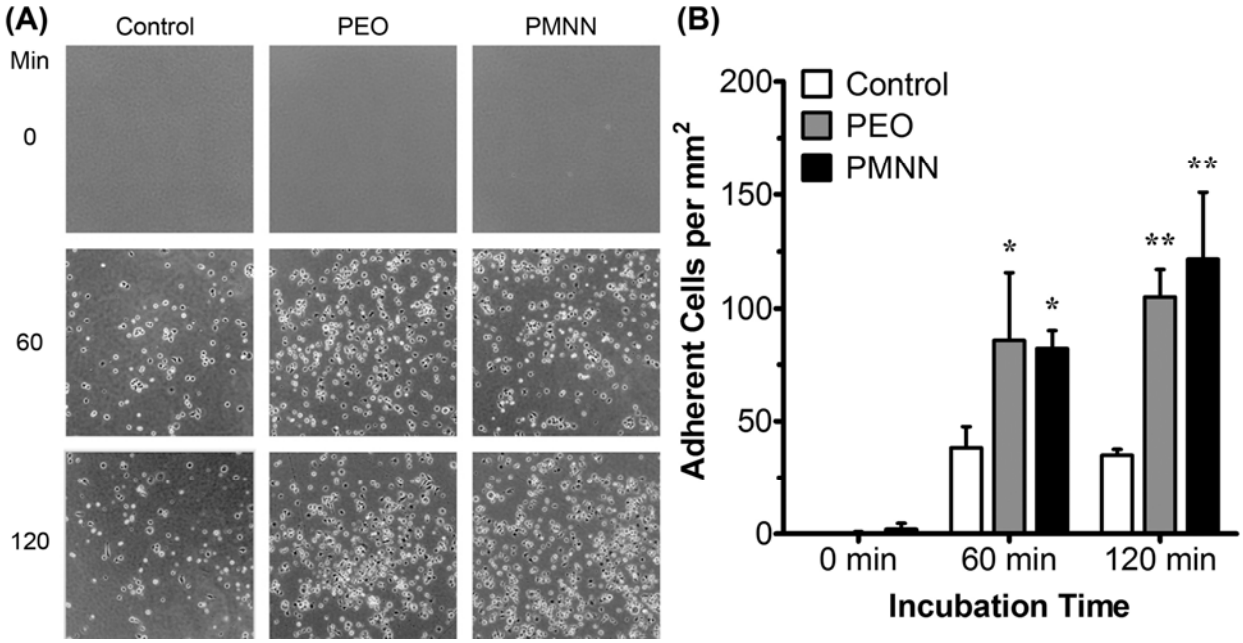

Figure 7.1: DRP effect on RAW 264.7 macrophage cell adhesion

(A) Photomicrographs The average number of adherent macrophages after incubation for 0, 60 and 120 minutes in growth medium containing either of the two DRPs was compared to that in growth medium alone (Control). Results represent mean number of adherent cells per mm^2 ± SD in three wells for each condition. Statistics were performed using a two-way ANOVA with Bonferroni post hoc test to compare each experimental condition to the control of the same time point.*$p < 0.01$, **$p < 0.001$.

These experiments demonstrated that macrophage cell adhesion was statistically significantly increased when DRPs (PEO-4500 and PMNN) were present in their growth medium during an incubation period up to 120 minutes. After an incubation time of 60 minutes, the number of adherent cells/mm^2 was 121% and 110% greater in wells with growth medium

containing PEO-4500 (5 μg/ml (1.1 nM)) and PMNN (5 μg/ml (0.8 nM)), respectively, than those wells with normal growth medium (Control). After incubation for 120 minutes, the number of adherent cells/mm^2 in wells with growth medium containing PEO-4500 (5 μg/ml (1.1 nM)) and PMNN (5 μg/ml (0.8 nM)) was 200% and 249%, respectively, greater than the wells filled with normal growth medium (Control).

The increase in the adhesion of macrophages in the presence of DRPs may help to explain the results which were outlined in Chapter 6.0 In those studies, we found that chronic injections of DRPs significantly reduced the foreign body response in animals subcutaneously implanted with a porous synthetic scaffold. The results of those studies and a potential hemodynamic mechanism were described in detail in section 6.3. The hemodynamic mechanism was based on the DRP effect that was observed in *in vitro* microchannel studies which showed the axial relocation of RBCs toward the channel wall; an effect which when applied to blood flow in microvessels *in vivo* would increase the near-wall hematocrit leading to elevated vessel wall shear stresses. These elevated vessel wall shear stresses might effectively overcome the adhesive bonds of leukocytes to the endothelium, reducing the number of cells available for diapedesis. In the pilot study performed here (1 experiment), it is suggested that the DRPs influence, in this case increase, the adhesion of the macrophages. This would in turn reduce the motility of the macrophages during extravasation and essentially reduce the number of macrophages that could reach the foreign body.

These experiments were limited in that we performed only a small pilot study with 1 experiment. It is suggested that these experiments be repeated several more times. Additionally, to further evaluate the influential role of DRPs on macrophage behavior, experiments should be performed to evaluate the DRP effect on macrophage differentiation and migration *in vitro.*

BIBLIOGRAPHY

1. Greene, H.L., R.F. Nokes, and D.C. Thomas, *Biomedical implications of drag reducing agents.* Biorheology, 1971. **7**(4): p. 221-223.

2. Polimeni, P.I., J. al-Sadir, and A.F. Cutilletta, *Rhamnogalactogacturonan (RGGu): a drug increasing cardiac output in rats, perhaps by a novel mechanism.* Physiologist, 1977. **20**: p. 75.

3. Polimeni, P.I., J. Al-Sadir, and A.F. Cutilletta, *Polysaccharide for enhancement of cardiac output*. 1979, The University of Chicago: United States.

4. Polimeni, P.I., B.T. Ottenbreit, and P.B. Coleman, *Enhancement of aortic blood flow with a linear anionic macropolymer of extraordinary molecular length.* Journal of Molecular & Cellular Cardiology, 1985. **17**(7): p. 721-724.

5. Kameneva, M.V. and A.S. Parfenov, *Resistance-reducing polymers and some hydrodynamic problems in atherosclerosis.* Doklady Akademii Nauk SSSR, 1986. **288**: p. 575-577.

6. Coleman, P.B., B.T. Ottenbreit, and P.I. Polimeni, *Effects of a drag-reducing polyelectrolyte of microscopic linear dimension (Separan AP-273) on rat hemodynamics.* Circulation Research, 1987. **61**: p. 787-796.

7. Polimeni, P.I. and B.T. Ottenbreit, *Hemodynamic effect of Polyox WSR N-60K, a drag reducing macropolymer of microscopic length.* Can. Fed. Biol. Soc., 1987. **30**: p. 31.

8. Polimeni, P.I., et al., *Drag-reducing polymers: a novel category of drugs potentially useful in cardiovascular disease?* Journal of Applied Cardiology, 1988. **3**(1): p. 57-66.

9. Polimeni, P.I. and B.T. Ottenbreit, *Hemodynamic effects of a poly(ethylene oxide) drag-reducing polymer, Polyox WSR N-60k, in the open-chest rat.* Journal of Cardiovascular Pharmacology, 1989. **14**(3): p. 374-80.

10. Grigorian, S.S. and M.V. Kameneva, *Resistance-reducing polymers in the blood circulation*, in *Contemporary Problems of Biomechanics*, G.G. Chernyi and S.A. Regirer, Editors. 1990, Mir Publishers, CRC Press: Moscow, USSR, Boca Raton. p. 99-110.

11. Kameneva, M.V., et al., *Blood soluble drag-reducing polymers prevent lethality from hemorrhagic shock in acute animal experiments.* Biorheology, 2004. **41**(1): p. 53-64.

12. Macias, C.A., et al., *Survival in a rat model of lethal hemorrhagic shock is prolonged following resuscitation with a small volume of a solution containing a drag-reducing polymer derived from aloe vera.* Shock, 2004. **22**(2): p. 151-6.

13. McCloskey, C.A., et al., *Tissue hypoxia activates JNK in the liver during hemorrhagic shock.* Shock, 2004. **22**(4): p. 380-6.

14. Grigorian, S.S., et al., *Possibility of increasing the resistance of live organisms to hypobaric hypoxia.* Doklady Akademii Nauk SSSR, 1985. **283**: p. 339-340.

15. Kameneva, M.V., et al., *Drag-reducing polymers prevent lethality and improve blood chemistry parameters in animals exposed to acute hypobaric hypoxia.* ASAIO Journal, 2002. **48**(2): p. 153.

16. Pacella, J.J., M.V. Kameneva, and F.S. Villanueva. *The effect of drag reducing polymers on myocardial perfusion during coronary stenosis*. In *American Heart Association Fellows Day*. 2002.

17. Golub, A.S., et al., *Influence of polyethylene oxide on the capillary blood flow in diabetic rats.* Proceedings of the Soviet National Academy of Sciences, Soviet Physics - Doklady, 1987(32): p. 620-621.

18. Mostardi, R.A., et al., *Suppression of atherosclerosis in rabbits using drag reducing polymers.* Biorheology, 1978. **15**(1): p. 1-14.

19. Greene, H.L., R.A. Mostardi, and R.F. Nokes, *Effect of drag reducing polymers on initiation of atherosclerosis.* Polymer Engineering Science, 1980. **20**: p. 499-504.

20. Faraqui, F.I., M.D. Otten, and P.I. Polimeni, *Protection against atherogenesis with the polymer drag-reducing agent Separan Ap-30.* Circulation, 1987. **75**(3): p. 627-35.

21. Sawchuk, A.P., J.L. Unthank, and M.C. Dalsing, *Drag reducing polymers may decrease atheroschlerosis by increasing shear in areas normally exposed to low shear stress.* Journal of Vascular Surgery, 1999. **30**: p. 761-764.

22. Kameneva, M.V., M.S. Polyakova, and E.V. Fedoseeva, *Effect of drag-reducing polymers on the structure of the stagnant zones and eddies in models of constricted and branching blood vessels.* Fluid Dynamics (USSR), 1990. **25**(6): p. 956-959.

23. Toms, B.A. *Some observation on the flow of linear polymer solutions through straight tubes at large Reynolds numbers*. In *Proc. 1st Intl. Congr. on Rheology*. 1949. Amsterdam.

24. Keller, A., G. Kiss, and M.R. Mackley, *Polymer drag reduction in Taylor vortices.* Nature, 1975. **257**(5524): p. 304-305.

25. Driels, M.R. and S. Ayyash, *Drag reduction in laminar flow.* Nature, 1976. **259**(5542): p. 389-390.

26. Hoyt, J.W., *The effect of additives on fluid friction.* Transactions ASME, J Basic Eng, 1972. **94**: p. 258-285.

27. Shenoy, A.V., *A review on drag reduction with special reference to micellar systems.* Colloid & Polymer Science, 1984. **262**: p. 319-337.

28. Kulicke, W.M., M. Kötter, and H. Gräger, *Drag reduction phenomenon with special emphasis on homogeneous polymer solution*, in *Advances in Polymer Science*. 1989, Springer-Verlag. p. 1-68.

29. Singh, R.P., et al., *Application of drag-reducing polymers in agriculture.* Current Science, 1995. **68**: p. 631-641.

30. Savins, J.G., *Drag-reducing additives improve drilling fluid hydraulics.* Oil & Gas Journal, 1995. **93**: p. 79-80.

31. Gannushkina, I.V., et al., *The possibility that after circulatory ischemia of the brain the blood circulation can be restored by introducing special polymers into the blood.* Soviet Physics - Doklady, 1981. **26**(4): p. 376.

32. Grigorian, S.S., M.V. Kameneva, and A.A. Shakhnazarov, *Effect of high molecular weight compounds dissolved in blood on hemodynamics.* Soviet Physics - Doklady, 1976. **21**(12): p. 702-703.

33. Hutchison, K.J., J.D. Campbell, and E. Karpinski, *Decreased poststenotic flow disturbance during drag reduction by polyacrylamide infusion without increased aortic blood flow.* Microvasc Res, 1989. **38**(1): p. 102-9.

34. Mostardi, R.A., et al., *The effect of drag reducing agents on stenotic flow disturbances in dogs.* Biorheology, 1976. **13**(2): p. 137-41.

35. Unthank, J.L., et al., *Improvement of flow through arterial stenoses by drag reducing agents.* Journal of Surgical Research, 1992. **53**(6): p. 625-630.

36. Greene, H.L., et al. *Potential biomedical applications of drag reducing agents*. In *Proc. Int. Conf. Drag Reduction*. 1974. Cambridge.

37. Pacella, J.J., et al., *A novel hydrodynamic approach to the treatment of coronary artery disease.* European Heart Journal, 2006. **27**(19): p. 2362-2369.

38. Sakai, T., et al., *I.V. infusion of a drag-reducing polymer extracted from aloe vera prolonged survival time in a rat model of acute myocardial ischaemia.* British Journal of Anaesthesia, 2007. **98**(1): p. 23-8.

39. Nokes, R.F., H.L. Greene, and L.C. Thomas. *Ventricular myograph tracing during polyacrylamide perfusion*. In *24th ACEMB*. 1971. Las Vegas, NV.

40. Marhefka, J.N., et al., *Poly(N-vinylformamide)-A drag-reducing polymer for biomedical applications.* Biomacromolecules, 2006. **7**(5): p. 1597-603.

41. Secomb, T.W., *Red blood cell mechanics and capillary blood rheology.* Cell Biophysics, 1991. **18**(3): p. 231-51.

42. Goldsmith, H.L., G.R. Cokelet, and P. Gaehtgens, *Robin Fåhraeus: evolution of his concepts in cardiovascular physiology.* American Journal of Physiology, 1989. **257**(3 Pt 2): p. H1005-15.

43. Mayer, G.A., *Relation of the viscosity of plasma and whole blood.* American Journal of Clinical Pathology, 1966. **45**(3): p. 273-6.

44. Rand, P.W., N. Barker, and E. Lacombe, *Effects of plasma viscosity and aggregation on whole-blood viscosity.* American Journal of Physiology, 1970. **218**(3): p. 681-8.

45. Chien, S., et al., *Effects of hematocrit and plasma proteins on human blood rheology at low shear rates.* Journal of Applied Physiology, 1966. **21**(1): p. 81-7.

46. Begg, T.B. and J.B. Hearns, *Components in blood viscosity. The relative contribution of haematocrit, plasma fibrinogen and other proteins.* Clinical Science, 1966. **31**(1): p. 87-93.

47. Brooks, D.E., J.W. Goodwin, and G.V. Seaman, *Interactions among erythrocytes under shear.* Journal of Applied Physiology, 1970. **28**(2): p. 172-7.

48. Barbee, J.H., *The effect of temperature on the relative viscosity of human blood.* Biorheology, 1973. **10**(1): p. 1-5.

49. Fåhraeus, R., *Suspension stability of blood.* Physiological Reviews, 1929. **9**: p. 241.

50. Dintenfass, L., *Considerations of the internal viscosity of red cell and its effects on the viscosity of whole blood.* Angiology, 1962. **13**: p. 333.

51. Chien, S., et al., *Shear-dependent deformation of erythrocytes in rheology of human blood.* American Journal of Physiology, 1970. **219**(1): p. 136-42.

52. Chien, S., et al., *Blood viscosity: influence of erythrocyte deformation.* Science, 1967. **157**: p. 827.

53. Thurston, G.B., *Viscoelasticity of human blood.* Biophysical Journal, 1972. **12**(9): p. 1205-17.

54. Skovborg, F., et al., *Blood viscosity in diabetic patients.* Lancet, 1966. **1**: p. 129.

55. Barnes, A.J., et al., *Is hyperviscosity a treatable component of diabetic microcirculatory disease?* Lancet, 1977. **ii**: p. 789-791.

56. Schmid-Schonbein, H. and E. Volger, *Red-cell aggregation and red-cell deformability in diabetes.* Diabetes, 1976. **25**(2 SUPPL): p. 897-902.

57. Juhan, I., et al., *Abnormalities of erythrocyte deformability and platelet aggregation in insulin-dependent diabetics corrected by insulin in vivo and in vitro.* Lancet, 1982. **1**(8271): p. 535-7.

58. McMillan, D.E., N.G. Utterback, and J. La Puma, *Reduced erythrocyte deformability in diabetes.* Diabetes, 1978. **27**(9): p. 895-901.

59. Lowe, G., D.O., *Clinical Blood Rheology*, ed. G.D.O. Lowe. Vol. 1. 1988, Boca Raton, Florida: CRC Press.

60. Meiselman, H.J., *Measures of blood rheology and erythrocyte mechanics*, in *Erythrocyte Mechanics and Blood Flow*, G.R. Cokelet, H.J. Meiselman, and D.E. Brooks, Editors. 1985, Alan R. Liss: New York. p. 75.

61. Merrill, E.W., *Rheology of blood.* Physiological Reviews, 1969. **49**(4): p. 863-88.

62. Thurston, G.B., *Rheological parameters for the viscosity viscoelasticity and thixotropy of blood.* Biorheology, 1979. **16**(3): p. 149-62.

63. Thurston, G.B., *Plasma release-cell layering theory for blood flow.* Biorheology, 1989. **26**(2): p. 199-214.

64. Thurston, G.B., *Viscoelastic properties of blood and blood analogs*, in *Advances in Hemodynamics and Hemorheology*, T.C. Howe, Editor. 1996, JAI Press. p. 1-30.

65. Vilastic Scientific Inc. *FAQ: Blood Viscoelasticity*. [cited 2006]; Available from: www.vilastic.com.

66. Reid, H.L., et al., *A simple method for measuring erythrocyte deformability.* Journal of Clinical Pathology, 1976. **29**(9): p. 855-8.

67. Heath, B.P., et al., *Deformability of isolated red blood cell membranes.* Biochimica et Biophysica Acta, 1982. **691**: p. 211.

68. Centers for Disease Control and Prevention, *National diabetes fact sheet: general information and national estimates on diabetes in the United States, 2005*. 2005, U.S. Department of Health and Human Services, Centers for Disease Control and Prevention: Atlanta, GA.

69. Akbari, C.M. and F.W. LoGerfo, *Diabetes and peripheral vascular disease.* Journal of Vascular Surgery, 1999. **30**(2): p. 373-384.

70. Tooke, J.E., *Microvasculature in diabetes.* Cardiovascular Research, 1996. **32**(4): p. 764-71.

71. White, W.B., L.M. Prisant, and J.T. Wright, Jr., *Management of patients with hypertension and diabetes mellitus: advances in the evidence for intensive treatment.* American Journal of Medicine, 2000. **108**(3): p. 238-45.

72. Lee, Y.H., et al., *Microcirculatory changes following reperfusion insult in diabetic rat skeletal muscles.* Microsurgery, 2000. **20**(2): p. 77-84.

73. MacDonald, M.J., *Conventional and human insulin: complications of insulin therapy in children.* Primary Care; Clinics in Office Practice, 1983. **10**(4): p. 691-706.

74. Teuscher, A. and K. Reinli, *Severe hypoglycaemia in Diabetes Control and Complications Trial.* Lancet, 1994. **343**(8905): p. 1097-8.

75. Fujiwara, T., et al., *Troglitazone, a new antidiabetic agent possessing radical scavenging ability, improved decreased skin blood flow in diabetic rats.* Life Sciences, 1998. **63**(22): p. 2039-47.

76. Stadelmann, W.K., A.G. Digenis, and G.R. Tobin, *Impediments to wound healing.* American Journal of Surgery, 1998. **176**(2A Suppl): p. 39S-47S.

77. Ichioka, S., et al., *Effects of shear stress on wound-healing angiogenesis in the rabbit ear chamber.* Journal of Surgical Research, 1997. **72**(1): p. 29-35.

78. Myers, M.B. and G. Cherry, *Blood supply of healing wounds: functional and angiographic.* Archives of Surgery, 1971. **102**(1): p. 49-52.

79. Chen, K.D., et al., *Mechanotransduction in response to shear stress. Roles of receptor tyrosine kinases, integrins, and Shc.* Journal of Biological Chemistry, 1999. **274**(26): p. 18393-400.

80. Davies, P.F., *Flow-mediated endothelial mechanotransduction.* Physiological Reviews, 1995. **75**(3): p. 519-60.

81. Karau, K.L., G.S. Krenz, and C.A. Dawson, *Branching exponent heterogeneity and wall shear stress distribution in vascular trees.* American Journal of Physiology - Heart & Circulatory Physiology, 2001. **280**(3): p. H1256-63.

82. Skalak, T.C. and R.J. Price, *The role of mechanical stresses in microvascular remodeling.* Microcirculation, 1996. **3**(2): p. 143-65.

83. Van Gieson, E.J., et al., *Enhanced smooth muscle cell coverage of microvessels exposed to increased hemodynamic stresses in vivo.* Circulation Research, 2003. **92**(8): p. 929-36.

84. Wu, Z.J., et al. *Modification of flow behavior of red blood cells by blood soluble drag-reducing polymers*. In *International Congress on Biological and Medical Engineering*. 2002. Singapore.

85. Kameneva, M.V., et al., *Artificial blood fluids and microflow drag reducing factors for enhanced blood circulation.*, USPTO, Editor. 2002: USA. p. 1-26.

86. University of California San Diego Institutional Animal Care and Use Committee. *IACUC Policy 5.0.3, Guidelines for Blood Collection*. 11/17/04 [cited 2004]; Available from: http://iacuc.ucsd.edu/policies/Policy5.03.pdf

87. Baskurt, O.K., R.A. Farley, and H.J. Meiselman, *Erythrocyte aggregation tendency and cellular properties in horse, human, and rat: a comparative study.* American Journal of Physiology, 1997. **273**(6 Pt 2): p. H2604-12.

88. Shasha, S.M., et al., *Red cell filterability in cigarette smokers and its relations to cardiac hypertrophy.* Atherosclerosis, 1993. **98**(1): p. 91-8.

89. Yoshida, H., et al., *Participation of serum albumin and LDL-cholesterol in impaired blood cell-filterability affected by white blood cells in patients with cerebral thrombosis.* Scandinavian Journal of Clinical & Laboratory Investigation, 1992. **52**(7): p. 641-6.

90. Belch, J.J., et al., *Increased prostacyclin metabolites and decreased red cell deformability in patients with systemic sclerosis and Raynaud's syndrome.* Prostaglandins Leukotrienes & Medicine, 1985. **18**(3): p. 401-2.

91. Sowemimo-Coker, S.O. and P. Turner, *The effect of pentoxifylline on filterability of normal red blood cells and their adhesiveness to cultured endothelial cells.* European Journal of Clinical Pharmacology, 1985. **29**(1): p. 55-9.

92. Kovacs, I.B. and J. O'Grady, *Prostacyclin increases filterability of normal and rigidified human red blood cells in vitro.* Agents & Actions, 1984. **14**(2): p. 306-10.

93. Sabo, A., M. Stanulovic, and V. Jakovljevic, *Phytomenadione improves red cell deformability in laboratory animals.* International Journal of Clinical Pharmacology, Therapy, & Toxicology, 1992. **30**(12): p. 587-90.

94. Leyrat-Maurin, A., et al. *Flow Of A Red Blood Cell Through A Filter Pore*. In *Engineering in Medicine and Biology Society, 1992. Vol.14. Proceedings of the Annual International Conference of the IEEE*. 1992.

95. Mirossay, L., et al., *Comparison of two methods in erythrocyte microrheology determination using glutaraldehyde-treated cells.* Clinical Hemorheology & Microcirculation, 1997. **17**(3): p. 187-92.

96. Ogura, E., P.J. Abatti, and T. Moriizumi, *Measurement of Human Red Blood Cell Deformability Using a Single Micropore on a Thin Si_3N_4 Film.* IEEE Transactions on Biomedical Engineering, 1991. **38**(8).

97. Marascalco, P., Ritchie, SP, Snyder, TA, Kameneva, MV, *Development of Standard Tests to Examine Viscoelastic Properties of Blood of Experimental Animals for Pediatric Mechanical Support Device Evaluation.* ASAIO, 2006. **52**(5): p. 567-574.

98. Nash, G.B. and H.J. Meiselman, *Alteration of red cell membrane viscoelasticity by heat treatment: effect on cell deformability and suspension viscosity.* Biorheology, 1985. **22**(1): p. 73-84.

99. Popel, A.S., et al., *Capacity for red blood cell aggregation is higher in athletic mammalian species than in sedentary species.* Journal of Applied Physiology, 1994. **77**(4): p. 1790-4.

100. Windberger, U., et al., *Whole blood viscosity, plasma viscosity and erythrocyte aggregation in nine mammalian species: reference values and comparison of data.* Experimental Physiology, 2003. **88**(3): p. 431-40.

101. Cokelet, G.R. and H.J. Meiselman, *Rheological comparison of hemoglobin solutions and erythrocyte suspensions.* Science, 1968. **162**(850): p. 275-7.

102. Dintenfass, L., *Internal viscosity of the red cell and a blood viscosity equation.* Nature, 1968. **219**(157): p. 956-8.

103. Chien, S., et al., *Comparative hemorheology--hematological implications of species differences in blood viscosity.* Biorheology, 1971. **8**(1): p. 35-57.

104. Cokelet, G.R., *Rheology and hemodynamics.* Annual Review of Physiology, 1980. **42**: p. 311-24.

105. Rogausch, H., *Modifications of the erythrocyte deformability alter the effect of temperature on the relative viscosity of human blood.* Biorheology, 1982. **19**(1/2): p. 237-44.

106. Whittington, R.B. and J. Harkness, *Whole-blood viscosity, as determined by plasma viscosity, haematocrit, and shear.* Biorheology, 1982. **19**(1/2): p. 175-84.

107. Linderkamp, O., et al., *Contributions of red cells and plasma to blood viscosity in preterm and full-term infants and adults.* Pediatrics, 1984. **74**(1): p. 45-51.

108. Eckmann, D.M., et al., *Hematocrit, volume expander, temperature, and shear rate effects on blood viscosity.[see comment].* Anesthesia & Analgesia, 2000. **91**(3): p. 539-45.

109. Thurston, G.B., *Frequency and shear rate dependence of viscoelasticity of human blood.* Biorheology, 1973. **10**(3): p. 375-81.

110. Copley, A.L., et al., *Microscopic observations of viscoelasticity of human blood in steady and oscillatory shear.* Biorheology, 1975. **12**(5): p. 257-63.

111. Thurston, G.B., *The viscosity and viscoelasticity of blood in small diameter tubes.* Microvascular Research, 1976. **11**(2): p. 133-46.

112. Thurston, G.B., *Effects of hematocrit on blood viscoelasticity and in establishing normal values.* Biorheology, 1978. **15**(3-4): p. 239-49.

113. Nash, G.B., C.S. Johnson, and H.J. Meiselman, *Influence of oxygen tension on the viscoelastic behavior of red blood cells in sickle cell disease.* Blood, 1986. **67**(1): p. 110-8.

114. More, R.B. and G.B. Thurston, *Intrinsic viscoelasticity of blood cell suspensions: effects of erythrocyte deformability.* Biorheology, 1987. **24**(3): p. 297-309.

115. Hell, K.M., et al., *Importance of blood viscoelasticity in arteriosclerosis.* Angiology, 1989. **40**(6): p. 539-46.

116. Chmiel, H., I. Anadere, and E. Walitza, *The determination of blood viscoelasticity in clinical hemorheology.* Biorheology, 1990. **27**(6): p. 883-94.

117. Thurston, G.B., *The elastic yield stress of human blood.* Biomedical Sciences Instrumentation, 1993. **29**: p. 87-93.

118. Windberger, U., et al., *The viscoelasticity of blood and plasma in pig, horse, dog, ox, and sheep.* Journal of Experimental Animal Science, 1994. **36**(2-3): p. 89-95.

119. Thurston, G.B., N.M. Henderson, and M. Jeng, *Effects of erythrocytapheresis transfusion on the viscoelasticity of sickle cell blood.* Clinical Hemorheology & Microcirculation, 2004. **30**(2): p. 83-97.

120. Long, J.A., et al., *Viscoelasticity of pediatric blood and its implications for the testing of a pulsatile pediatric blood pump.* ASAIO Journal, 2005. **51**(5): p. 563-6.

121. Brookshier, K.K. and J.M. Tarbell, *Effect of hematocrit on wall shear rate in oscillatory flow: do the elastic properties of blood play a role?* Biorheology, 1991. **28**(6): p. 569-87.

122. Diamantopoulos, E.J., et al., *Impaired erythrocyte deformability precedes vascular changes in experimental diabetes mellitus.* Hormone & Metabolic Research, 2004. **36**(3): p. 142-7.

123. Gillings, D.B., *Pentoxifylline and intermittent claudication: review of clinical trials and cost-effectiveness analyses.* Journal of Cardiovascular Pharmacology, 1995. **25 Suppl 2**: p. S44-50.

124. Leonhardt, H. and H.G. Grigoleit, *Effects of pentoxifylline on red blood cell deformability and blood viscosity under hyperosmolar conditions.* Naunyn-Schmiedeberg's Archives of Pharmacology, 1977. **299**(2): p. 197-200.

125. Aviado, D.M. and J.M. Porter, *Pentoxifylline: a new drug for the treatment of intermittent claudication. Mechanism of action, pharmacokinetics, clinical efficacy and adverse effects.* Pharmacotherapy, 1984. **4**(6): p. 297-307.

126. Buhler, I., R. Walter, and W.H. Reinhart, *Influence of D- and L-glucose on erythrocytes and blood viscosity.* European Journal of Clinical Investigation, 2001. **31**(1): p. 79-85.

127. Chien, S., *Red cell deformability and its relevance to blood flow.* Annual Review of Physiology, 1987. **49**: p. 177-92.

128. Jung, C., *Carrier-mediated glucose transport across human red cell membranes*, in *The Red Blood Cell*, D.M.N. Surgenor, Editor. 1975, Academic Press: New York. p. 705-751.

129. Arai, T., et al., *Glucose transport activities in erythrocytes and hepatocytes of dogs, cats and cattle.* Comparative Biochemistry and Physiology Part A: Physiology, 1992. **102**(2): p. 285-287.

130. Lindmark, K. and K.G. Engstrom, *D-glucose additive protects against osmotic-induced decrease in erythrocyte filterability.* Scandinavian Journal of Clinical & Laboratory Investigation, 2000. **60**(6): p. 473-81.

131. Engstrom, K.G. and I.B. Taljedal, *Decreased deformability of erythrocytes in hyperglycaemic non-inbred ob/ob mice.* Diabetologia, 1986. **29**(9): p. 661-6.

132. Charles River Laboratories. *Informational Resources: Sprague Dawley Rat*. [cited 2005; Available from: http://www.criver.com/research_models_and_services/research_models/SASCO_Sprague_Dawley.html.

133. McNeill, J.H., ed. *Experimental Models of Diabetes*. 1999, CRC Press: Boca Raton. 418.

134. Hicks, K.K., et al., *Effects of streptozotocin-induced diabetes on heart rate, blood pressure and cardiac autonomic nervous control.* Journal of the Autonomic Nervous System, 1998. **69**(1): p. 21-30.

135. Duke University and Medical Center: Animal Care and Use Program. *Guidelines for Rodent Analgesia*. [cited 2005]; Available from: http://vetmed.duhs.duke.edu/guidelines_for_rodent_analgesia.htm.

136. Noorlander, M.L., et al., *A quantitative method to determine the orientation of collagen fibers in the dermis.* Journal of Histochemistry & Cytochemistry, 2002. **50**(11): p. 1469-74.

137. Ridler, T.W. and S. Calvard, *Picture thresholding using an iterative selection method.* IEEE Transactions on Systems, Man and Cybernetics, 1978. **SMC-8**(8): p. 630-632.

138. Schugens, C., et al., *Biodegradable and macroporous polylactide implants for cell transplantation: 1. Preparation of macroporous polylactide supports by solid-liquid phase separation.* Polymer, 1996. **37**(6): p. 1027-1038.

139. Anderson, J.M., *Inflammatory response to implants.* ASAIO Transactions, 1988. **34**(2): p. 101-7.

140. Anderson, J.M., A. Rodriguez, and D.T. Chang, *Foreign body reaction to biomaterials.* Semin Immunol, 2008. **20**(2): p. 86-100.

141. Babensee, J., et al., *Host response to tissue engineered devices.* Advanced Drug Delivery Reviews, 1998. **33**: p. 111-139.

142. Lam, K.H., et al., *The effect of phagocytosis of poly(L-lactic acid) fragments on cellular morphology and viability.* Journal of Biomedical Materials Research, 1993. **27**(12): p. 1569-77.

143. Xia, Z. and J. Triffitt, *A review on macrophage responses to biomaterials.* Biomed Mater, 2006. **1**: p. R1-R9.

144. Garrigues, G.E., et al., *Gene expression clustering using self-organizing maps: analysis of the macrophage response to particulate biomaterials.* Biomaterials, 2005. **26**(16): p. 2933-45.

145. Blixt, A., et al., *Microscopic studies on the influence of erythrocyte concentration on the post-junctional radial distribution of leukocytes at small venular junctions.* International Journal of Microcirculation: Clinical & Experimental, 1985. **4**(2): p. 141-56.

146. Schmid-Schonbein, G.W., et al., *The interaction of leukocytes and erythrocytes in capillary and postcapillary vessels.* Microvascular Research, 1980. **19**(1): p. 45-70.

147. Nobis, U., A.R. Pries, and P. Gaehtgens, *Rheological mechanisms contributing to WBC-margination.* , in *Microcirculation Reviews I: White Blood Cells - Morphology and Rheology as Related to Function*, U. Bagge, G. Born, and P. Gaehtgens, Editors. 1982, Nijhoff: The Hague. p. 57-65.

148. Goldsmith, H.L. and S. Spain, *Margination of leukocytes in blood flow through small tubes.* Microvascular Research, 1984. **27**(2): p. 204-22.

149. Muller, W., *Migration of leukocytes across the vascular intima. Molecules and mechanism.* Trends Cardiovasc. Med., 1995. **5**: p. 15-20.

150. Theilmeier, G., et al., *Circulating activated platelets assist THP-1 monocytoid/endothelial cell interaction under shear stress.* Blood, 1999. **94**(8): p. 2725-34.

151. Pearson, M.J. and H.H. Lipowsky, *Influence of erythrocyte aggregation on leukocyte margination in postcapillary venules of rat mesentery.* American Journal of Physiology - Heart & Circulatory Physiology, 2000. **279**(4): p. H1460-71.

152. Sacks, M.S. and W. Sun, *Multiaxial mechanical behavior of biological materials.* Annual Review of Biomedical Engineering, 2003. **5**: p. 251-84.

153. Anderson, J. and M. Shive, *Biodegradation and biocompatibility of PLA and PLGA microspheres.* Advanced Drug Delivery Reviews, 1997. **28**: p. 5-24.

154. Lavik, E., et al., *Seeding neural stem cells on scaffolds of PGA, PLA, and their copolymers.* Methods in Molecular Biology, 2002. **198**: p. 89-96.

155. Hudlická, O., M. Brown, and S. Egginton, *The role of hemodynamic and mechanical factors in vascular growth and remodeling*. Endothelium and Mechanical Forces, ed. P. Lelkes. 1999, London: Harwood Academic Publishers. 291-359.

156. Clark, E., *Studies on the growth of blood vessels in the tail of frog larvae.* Am J Anat, 1918. **23**: p. 37-88.

157. Clark, E. and E. Clark, *Microscopic observations on the extraendothelial cells in living mammalian blood vessels.* Am J Anat, 1940. **66**: p. 1-49.

158. Tornling, G., et al., *Proliferative activity of capillary wall cells in skeletal muscle of rats during long-term treatment with dipyridamole.* Arzneimittel-Forschung, 1980. **30**(4): p. 622-3.

159. Mall, G., et al., *Morphometric analysis of the rabbit myocardium after chronic ethanol feeding - early capillary changes.* Basic Research in Cardiology, 1982. **77**(1): p. 57-67.

160. Egginton, S., et al., *Unorthodox angiogenesis in skeletal muscle.* Cardiovascular Research, 2001. **49**: p. 634-646.

161. Zhou, A., et al., *Internal division of capillaries in rat skeletal muscle in response to chronic vasodilator treatment with α1-antagonist prazosin.* Cell Tissue Res, 1998. **293**: p. 293-303.

162. Okazaki, T., et al., *Macrophage colony-stimulating factor induces vascular endothelial growth factor production in skeletal muscle and promotes tumor angiogenesis.* Journal of Immunology, 2005. **174**(12): p. 7531-8.

163. Blair, H.C., et al., *Intravenous Inert Long Chain Polymers Reduce Inflammatory Response to Implants*. 2008.

164. Brant, A.M., *Hemodynamics and mass transfer aspects of arterial disease*. 1985, University of Pittsburgh: Pittsburgh, PA.

165. Transonic Systems, Inc. *Probe Physical Specifications*. 1997 [cited 7-20-08]; Available from: http://www.transonic.com/Research_Home/Products__Laboratory_Research/p._16-17_probe_specs.pdf.